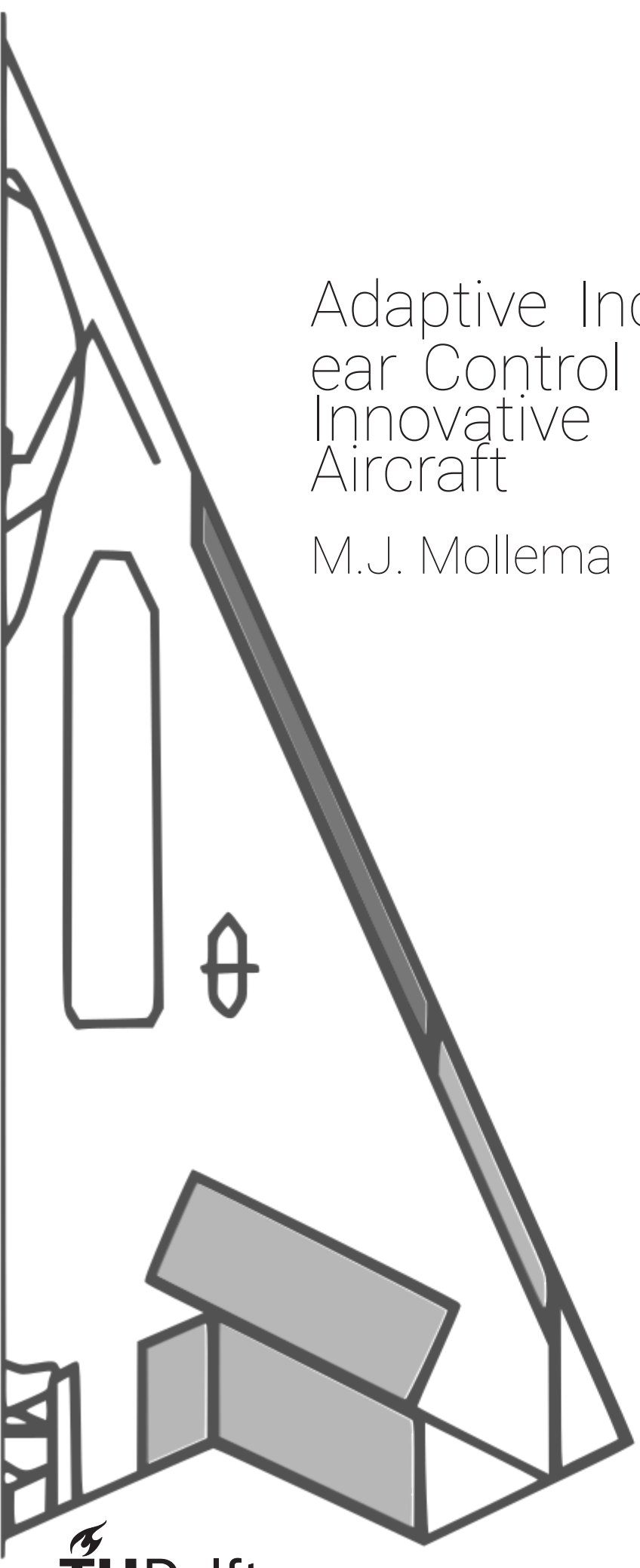

Adaptive Incremental Nonlinear Control Allocation for the Innovative Control Effectors Aircraft

M.J. Mollema

TU Delft

Adaptive Incremental Nonlinear Control Allocation for the Innovative Control Effectors Aircraft

by

M.J. Mollema

to obtain the degree of Master of Science
at the Delft University of Technology,
to be defended publicly on October 11.

Student number: 4284852
Project duration: October 1, 2018 – October 11, 2019
Thesis committee: Dr. ir. C.C. de Visser, Delft University of Technology, Aerospace Engineering, Control & Simulation
Dr. ir. Q.P. Chu, Delft University of Technology, Aerospace Engineering, Control & Simulation

An electronic version of this thesis is available at http://repository.tudelft.nl/.

©2019 | Delft University of Technology | All Rights Reserved

TU Delft

Acknowledgments

I would like to thank Dr. C.C. de Visser, the daily supervisor during my master thesis, for the opportunity to work on this project and for the guidance and insights during the past year. I also wish to thank Dr. Q.P. Chu for his help in steering me to the right research direction.

Secondly I would like to thank the guys from the "UpperHouse": Sven, Stephan, Simon, Peter, Marc, and Joeri. The coffee breaks, WoBos and VriMiBos, techo-sessions, and memes helped immensely in keeping a positive mindset about graduating.

And finally, I would like to deeply thank my parents and sisters for encouraging me to start with the Aerospace Engineering study six years ago and for their support during these past years.

M.J. Mollema
Delft, October 2019

Contents

List of Figures

List of Tables

Nomenclature

Acronyms

ADF	aerodynamic development facility
AMT	all-moving wing tips
AoA	angle of attack
BS	backstepping
CA	control allocation
CAD	computer-aided design
CEJ	control effectiveness Jacobian
CFD	computational fluid dynamics
CG	center of gravity
DATCOM	data compendium
FCS	flight control system
FDI	fault detection and isolation
FTC	fault tolerant control
GTM	general transport model
ICE	innovative control effectors
INCA	incremental nonlinear control allocation
INDI	incremental nonlinear dynamic inversion
LED	leading edge down
LEF	leading edge flap
LMS	least mean squares
LMTAS	Lockheed Martin Tactical Aircraft Systems
LOC	loss of control
MAC	mean aerodynamic chord
MATV	multi-axis thrust vectoring
MoI	moment of inertia
MRAC	model reference adaptive control
NAWCAD	Naval Air Warfare Center
NDI	nonlinear dynamic inversion
PCH	pseudo-control hedging
PF	pitch flap
RCS	radar cross-section
RLS	recursive least squares
RM	reconfiguration mechanism
SSD	spoiler-slot deflector
STC	self-tuning control
TED	trailing edge down
TEU	trailing edge up
VSS-LMS	Variable step size least mean squares
WL/FIGC	Wright Laboratory

Latin symbols

Symbol	Description	Unit
b	Wing span	ft
c	Mean aerodynamic chord	ft
C_l	Dimensionless rolling moment coefficient	-
C_m	Dimensionless pitching moment coefficient	-
C_n	Dimensionless yawing moment coefficient	-
C_X	Dimensionless axial force coefficient	-
C_Y	Dimensionless lateral force coefficient	-
C_Z	Dimensionless vertical force coefficients	-
$\mathbf{d}$	Pseudo-control input	-
I	Moment of inertia	$\text{slug} \cdot \text{ft}^2$
L, M, N	Roll, pitch and yaw moments	$\text{lbf} \cdot \text{ft}$
M	Mach number	-
p, q, r	Roll, pitch and yaw rates	rad/s
S	Surface area	ft^2
$\mathbf{T}$	Thrust vector	lbf
u, v, w	Aircraft velocities in body-frame for x-, y- and z-direction respectively	ft/s
V	True airspeed	ft/s
X, Y, Z	Axial, lateral and normal force components	lbf

Greek symbols

Symbol	Description	Unit
$\boldsymbol{\Delta}$	Increment	-
$\boldsymbol{\Theta}$	Control effectiveness function	-
α	forgetting factor	-
α	Angle of attack	rad
β	Sideslip angle	rad
γ	error scaling factor	-
$\boldsymbol{\delta}$	Control deflection vector	rad
$\boldsymbol{\theta}$	Parameter vector	-
θ	Aircraft pitch angle	rad
$\boldsymbol{\mu}$	Adaptation constant matrix	-
$\boldsymbol{\nu}$	Virtual control vector	-
ρ	Air density	slug/ft^3
$\boldsymbol{\tau}$	Aerodynamic moments around body-axis vector	$\text{lbf} \cdot \text{ft}$
ψ	Aircraft yaw angle	rad
$\boldsymbol{\omega}$	Angular body rates vector	rad/sec
ϕ	Aircraft roll angle	rad

Introduction

In the aviation industry loss of control (LOC) of an aircraft is still one of the leading causes of both fatal and non-fatal accidents [1–3]. This LOC happens when an aircraft is placed outside of its nominal flight envelope and the pilot is not able to control the aircraft using traditional control strategies. An example of such a LOC incident is the crash of a Boeing 747-200 Freighter, El Al Flight 1862, into a residential area in Amsterdam [4]. This accident, known as the “Bijlmer disaster", occurred when the two engines on the right wing separated from the aircraft, thereby also damaging the wing in the process. At first the pilots were able to regain control, however, when attempting to land the aircraft started to roll uncontrollably, mainly due to the extensive damage on the right wing, which resulted in the crash.

Many researches have shown the potential benefit of having FTCs implemented for aircraft safety [5–7]. These FTC systems are a type of flight control system that is able to maintain performance and stability in the event of component failures, structural damage or aerodynamic failures, and can be an important part in preventing LOC accidents. FTC is made possible due to the fact that most airplanes have a redundant set of control surfaces. This means that e.g. when a certain actuator fails or a wing is damaged, the remaining working control surfaces might still be able to generate the required control moments to keep the aircraft inside the safe flight envelope.

Most FTC systems are designed for conventional aircraft and assume a linear relationship between the control forces and moments and the actuator position. Generally speaking this assumption holds when the aircraft is operating under nominal conditions. However, under off-nominal conditions the actuators might deflect to extreme positions where this assumption does not hold any more. But it is exactly in these off-nominal and faulty conditions that a FTC system should be able to generate the correct control forces and moments, which it might not be able to do due to the wrong assumption of linearity in the extreme regions of the actuator positions.

An interesting example of an unconventional, highly nonlinear, overactuated aircraft is the Lockheed-Martin Skunkworks Innovative Control Effectors (ICE) research aircraft concept [8]. This concept was conceived in the 90’s as an effort to design a highly manoeuvrable fighter aircraft with reduced weight and low radar cross-section (RCS). One important aspect of the ICE-aircraft with respect to both the weight reduction as well as low RCS is the removal of the vertical tail. Another result of the low RCS design criterion is that the control surface edges are aligned with external airframe edges. Due to this alignment and the removal of the vertical stabiliser the control suite of the ICE-aircraft exhibits a high degree of coupling between all body axes (roll, pitch and yaw) as well as high nonlinearities between the different control surfaces.

As the ICE-aircraft is overactuated a control allocation (CA) module is required to distribute the required control moments over the redundant set of actuators. Recently such a method for the ICE-aircraft has been proposed in [9], named Incremental Nonlinear Control Allocation (INCA), which is able to make full use of the axis-coupling and nonlinearities of the control suite in real-time. The method relies on an onboard aerodynamic model of the aircraft, known as the Control Effectiveness Jacobian (CEJ). This model depends on different aircraft states and effector positions, and could be identified online to make the aircraft adaptive to model mismatch and failure.

Designing such an adaptive controller is the goal of this master thesis research. This report contains four parts: the first part consists of the preliminary thesis report with a more in depth presentation of the research objective and questions, as well as a literature survey on the ICE-aircraft, existing adaptive control methods, and damage modeling techniques. The next part is a scientific paper presenting the adaptive method used for this research as well as the results of the adaptive controller in different scenarios. This paper is followed by a chapter that gives conclusions and recommendations for the full report. The report concludes with a part containing additional results of the performed simulations.

I

Preliminary report

1

Research objective and questions

This section will discuss the main research objective after which several research questions will be formulated. Answering these questions will first of all help in achieving the research objective, but will also provide a guideline on the work to perform. Following the informally stated goal from the introduction, to design an adaptive controller for the ICE-aircraft, a more formal research objective is defined as follows:

The research objective is to develop a fault-tolerant flight controller, which is capable of compensating for sudden aerodynamic failures and uncertainties, for an overactuated aircraft by extending the current INCA implementation with an adaptive element and investigating its robustness and comparing the results to the current INCA implementation.

In line with this objective, several main and sub-research questions can be formulated:

1. What are the current state-of-the-art fault tolerant control methods which can be implemented alongside the current INCA controller?
2. What are the effects of a structural failure on the ICE-aircraft?
   (a) How does a structural failure affect the aerodynamics of the airframe?
   (b) How does a structural failure affect the effectiveness of the control surfaces in generating control moments?
   (c) How does a structural failure affect the mass of the aircraft?
   (d) How does a structural failure affect the moments of inertia of the aircraft?
   (e) How does a structural failure affect the center of gravity location of the aircraft?
3. How do the current and adaptive INCA implementation compare in case of structural failures?
   (a) How much discrepancy in the control effectiveness Jacobian can both controllers handle?
   (b) How do sudden jumps in the control effectiveness Jacobian affect the stability of both controllers?
   (c) What is the tracking error over an aggressive maneuver for both controllers?
   (d) What is the allocation error over an aggressive maneuver for both controllers?
   (e) What is the control effort over an aggressive maneuver for both controllers?

The main objective can also be divided in smaller parts, resulting in sub-objectives which also can be linked to the research questions. These subgoals are listed below:

- Compare state-of-the-art fault tolerant control methods by performing a literature study on the subject.
- Implement the most promising fault tolerant control method into the current flight control system of the ICE-aircraft.

- Create a model of the damaged/failed ICE-aircraft concerning the aerodynamics and mass properties.
- Evaluate the tracking, allocation and control effort performance of the fault tolerant controller with respect to the nominal controller.

2

The Innovative Control Effectors Aircraft

Increasing survivability in the current and future air combat environments is one of the main concerns in designing the next-generation fighter aircraft. One way to increase the chances of survival is to decrease the observability of the aircraft, which can be achieved by decreasing the radar cross-section (RCS) of the aircraft. A low RCS design can be achieved by specific external shaping, removing vertical control surfaces and aligning control surface edges with airfame edges [8]. Together with this required decrease in observability, new benchmarks for fighter maneuverability made possible by the emergence of multi-axis thrust vectoring (MATV) drive the need for new and innovative control suites for fighter aircraft.

These control suites for low-RCS and highly maneuverable tailless aircraft exhibit a high degree of coupling between the three aircraft axes (roll, pitch and yaw) as well as complex interactions between the different effectors. To investigate the potential for new and innovative methods to stabilize and control such an aircraft, the Innovative Control Effectors (ICE) program was conceived in 1993. This program, which was sponsored by the Wright Laboratory (WL/FIGC) and the Naval Air Warfare Center (NAWCAD), consisted of two phases. In phase I [8] the conceptual design of two baseline aircraft, one land-based and one carrier based, with innovative control effectors was performed. Both concepts can be seen in Figure 2.1. Next to the conceptual design an analytical study was performed to assess the performance of various types and combinations of control effectors. During the second phase [10] the best concepts from phase I were tested in wind tunnels at the Lockheed Martin Tactical Aircraft Systems (LMTAS) Aerodynamic Development Facility (ADF) to gather data to develop accurate aerodynamic and control effector models as well as to identify interactions between control effectors.

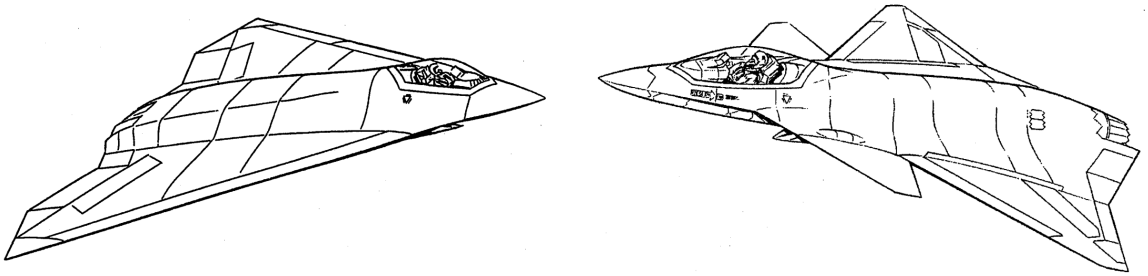

(a) Land-based.

(b) Carrier based.

Figure 2.1: The two baseline concepts for the Innovative Control Effectors program. [8]

The land based model, which will be named the ICE-aircraft for the remainder of this report, was used for the development and assessment of the recently developed Incremental Nonlinear Control Allocation method [9], which will be discussed in Chapter 3. This concept is a high-sweep, tailless flying wing design with a leading edge sweep of 65 degrees and on the trailing edge a 25 degrees chevron shaping. It has a single engine with trust-vectoring capabilities, carries armaments internally and was initially designed to complete high-low-low-high air-to-ground missions with a 1,100 nm radius. The rest of this chapter describes the control

suite employed by the ICE-aircraft, the aerodynamic model and a stability and controllability analysis.

2.1. Control Suite

As the ICE-aircraft has a non-conventional control suite with low RCS characteristics and high angle of attack (AoA) effectiveness the different types of effectors and their application are discussed. The control suite includes leading-edge flaps, all-moving wing tips, multi-axis thrust vectoring, spoiler-slot deflectors, pitch flaps and elevons. With this many effectors, the ICE-aircraft is overactuated: the three aerodynamic moments on the aircraft can be achieved using multiple combinations of effector deflections. A schematic overview of all the effectors and their location on the aircraft can be seen in Figure 2.2.

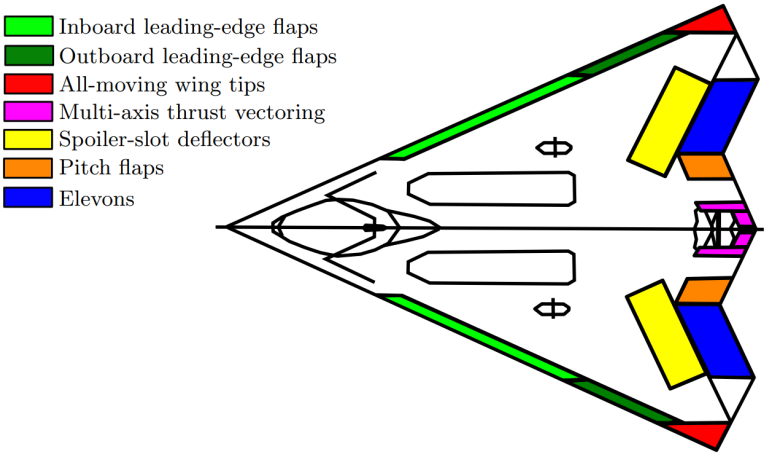

Figure 2.2: The control suite of the ICE-aircraft. [9]

The leading-edge flaps (LEF) can be deflected differentially to provide lateral-directional control at high AoA and are most useful for stability augmentation and roll coordination at high AoA or low speeds. The LEFs were reported to exhibit significant interactions between the inboard and outboard parts, as well as a nonlinear with AoA control effectiveness in roll and yaw [8, 10].

The next innovative control effector are the **all-moving wing tips (AMT)**, which are mainly used to provide yaw control power due to increased profile and induced drag when deflected trailing edge down (TED). The AMT were preferred over more conventional yaw control devices due to a reduced weight, nearly constant yaw with increasing AoA including high AoA, an invariance to sideslip and a more efficient and simpler integration and actuation. This research also found a significant adverse effect of the AMT on the elevons, reducing their effectiveness at low AoA by 15-20% to a 40% reduction at medium AoA. At even higher AoA, above 30 degrees, the adverse effect diminishes. As one of the main design goals was to have a low RCS the AMTs are constrained to only deflect TED, which allows for hingeline sealing which in turn reduces RCS. [11]

Placed in the middle of the wings are the **spoiler-slot deflectors (SSD)**. They differ from conventional spoiler in the way that also a slot is opened between the upper and lower skin when deflecting the spoiler. These SSDs provide lateral-directional control, similar to their conventional counterpart. Their advantage over conventional spoilers however is the increased effectiveness at high AoA and transonic speeds, as well as a linearity in the control moments versus effector deflection. One large drawback of the SSD is their effect of the effectors downstream of the SSD. Deflecting the spoiler can severly degrade the performance of the elevons and pitch flaps. [8]

Right behind the SSDs are the **elevons**, which, as the name does suggest, are a combination of an elevator and an aileron. As such, they are used to provide pitch and roll control power by deflecting symmetrically or asymmetrically, respectively. They can also be deflected independently of each other, causing secondary-axis yawing moments. [9]

On the inboard side of the elevons and behind the SSDs are the **pitch flaps (PF)**. These two surfaces are deflected symmetrically to provide control the pitch direction. Next to this, they are also used to trim the aircraft longitudinal at high AoA. [9].

The final effector of the ICE-aircraft is the **multi-axis thrust vectoring (MATV)** capability of its engine. The thrust vectoring is most powerful at low speeds where it provides yaw and pitch control power. At higher speeds however, the aerodynamic control effectors provide much more control [11]. Next this, MATV is also implemented to enhance the roll capabilities at high AoA, as this could not be achieved with aerodynamic control power alone [12]. The thrust vectoring is achieved by an omnidirectional deflection of 15 degrees [8].

2.2. Simulation model

For the simulation of the dynamics of the ICE-aircraft a high-fidelity aerodynamic model released by Lockheed Martin is used. A summary of this model will be given in this section, as well as a description of its mass properties and control effector properties. A desciption of the tests performed to get the aerodynamic model and its results can be found in [13]. This model is stored in look-up tables and defined in the aerodynamic model body frame, which is not the standard aerospace right-handed axis system. To convert it to this standard, the x- and z-axis are reversed.

2.2.1. Control effector properties

To simulate the physical properties of the effectors on the ICE-aircraft several limit and dynamics are applied to them. The limits consist of both position as well as rate limits for the deflections, whereas the dynamics of the actuators are simulated using either a low-bandwidth or high-bandwidth transfer function Equations (2.1) and (2.2) [9]. The deflection limit for the MATV is a circular constraint in contrast to the other control surfaces, which have a minimum and maximum position limit. A summary of the dynamic properties and the limits can be found in Table 2.1, as well as the notation used to indicate the effectors and how a positive deflection is defined.

$$H_l(s) = \frac{(18)(100)}{(s+18)(s+100)} \tag{2.1}$$

$$H_h(s) = \frac{(40)(100)}{(s+40)(s+100)} \tag{2.2}$$

Table 2.1: Dynamic properties and limits of the ICE-aircraft effectors. [9]

Control effector	Notation	Positive deflection	Position limits [deg]	Rate limits [deg/s]	Dynamics
Inboard LEF	δ_{lfi}, δ_{rfi}	LED	[0, 40]	40	$H_l(s)$
Outboard LEF	δ_{lfo}, δ_{rfo}	LED	[-40, 40]	40	$H_l(s)$
AMT	δ_{la}, δ_{ra}	TED	[0, 60]	150	$H_h(s)$
Elevons	δ_{le}, δ_{re}	TED	[-30, 30]	150	$H_h(s)$
SSD	δ_{ls}, δ_{rs}	TEU	[0, 60]	150	$H_h(s)$
PF	δ_{pf}	TED	[-30, 30]	150	$H_h(s)$
MTV	δ_{ptv}, δ_{ytv}	$\dot{\omega}$	[-15, 15]	150	$H_h(s)$

2.2.2. High fidelity aerodynamic model

The aerodynamic model used in the simulations is provided by Lockheed Martin in the form of dimensionless coefficients for the forces and moments stored in lookup tables. To get the forces acting on the aircraft, the force coefficients (C_X, C_Y and C_Z) have to be denormalized by multiplying them with $\frac{1}{2}\rho V^2 S$, where the density ρ is in slug/ft^3, velocity V is in ft/s and the surface area S in ft^2. The actual moments can be obtained by multiplying the moment coefficients (C_l, C_m and C_n) with either $\frac{1}{2}\rho V^2 Sb$ for the rolling and yawing moment or $\frac{1}{2}\rho V^2 S\bar{c}$ for the pitching moment, where the wingspan b and mean aerodynamic chord (MAC) $\bar{c}$ are in ft. To be able to capture the interactions and nonlinearities of the different effectors, the coefficients are build-up from smaller components, as can be seen in Equations (2.3) to (2.8). Each component depends on either the flight conditions (α, β and M) or control deflections $\boldsymbol{\delta}$ or a combination of these. A more detailed description of each individual component can be found in [13].

$$
\begin{aligned}
-C_X = &+ C_{X_1}(\alpha, M) + C_{X_2}(\alpha, \beta, M) + C_{X_3}(\alpha, \delta_{\text{ls}}, \delta_{\text{le}}, M) + C_{X_4}(\alpha, \delta_{\text{rs}}, \delta_{\text{re}}, M) \\
&+ C_{X_5}(\alpha, \beta, \delta_{1\text{fi}}) + C_{X_6}(\alpha, \beta, \delta_{\text{rfi}}) + C_{X_7}(\alpha, \beta, \delta_{\text{lf}}, \delta_{\text{lfo}}, M) + C_{X_8}(\alpha, \beta, \delta_{\text{rfi}}, \delta_{\text{rfo}}, M) \\
&+ C_{X_9}(\alpha, \delta_{1\text{fo}}, \delta_{\text{la}}) + C_{X_{10}}(\alpha, \delta_{\text{rfo}}, \delta_{\text{ra}}) + C_{X_{11}}(\alpha, \delta_{\text{la}}, \delta_{\text{le}}) + C_{X_{12}}(\alpha, \delta_{\text{ra}}, \delta_{\text{re}}) \\
&+ C_{X_{13}}(\alpha, \delta_{\text{rs}}, \delta_{\text{ls}}, \delta_{\text{pf}}, M) + C_{X_{14}}(\alpha, \beta, \delta_{\text{la}}) + C_{X_{15}}(\alpha, \beta, \delta_{\text{ra}}) + C_{X_{16}}(\alpha, \beta, \delta_{\text{ls}}) \\
&+ C_{X_{17}}(\alpha, \beta, \delta_{\text{rs}})
\end{aligned} \tag{2.3}
$$

$$
\begin{aligned}
C_Y = &+ C_{Y_1}(\alpha, M) + C_{Y_2}(\alpha, \beta, M) + C_{Y_3}(\alpha, \delta_{\text{ls}}, \delta_{\text{le}}, M) - C_{Y_4}(\alpha, \delta_{\text{rs}}, \delta_{\text{rs}}, M) \\
&- C_{Y_5}(\alpha, \beta, \delta_{1\text{fi}}) + C_{Y_6}(\alpha, \beta, \delta_{\text{rfi}}) - C_{Y_7}(\alpha, \beta, \delta_{1\text{f}}, \delta_{\text{lfo}}, M) + C_{Y_8}(\alpha, \beta, \delta_{\text{rfi}}, \delta_{\text{rfo}}, M) \\
&+ C_{Y_9}(\alpha, \delta_{\text{lfo}}, \delta_{\text{la}}) - C_{Y_{10}}(\alpha, \delta_{\text{rfo}}, \delta_{\text{ra}}) + C_{Y_{11}}(\alpha, \delta_{\text{la}}, \delta_{\text{le}}) - C_{Y_{12}}(\alpha, \delta_{\text{ra}}, \delta_{\text{re}}) \\
&+ C_{Y_{13}}(\alpha, \delta_{\text{rs}}, \delta_{\text{ls}}, \delta_{\text{pf}}, M) + C_{Y_{14}}(\alpha, \beta, \delta_{\text{la}}) - C_{Y_{15}}(\alpha, \beta, \delta_{\text{ra}}) + C_{Y_{16}}(\alpha, \beta, \delta_{\text{ls}}) \\
&- C_{Y_{17}}(\alpha, \beta, \delta_{\text{rs}})
\end{aligned} \tag{2.4}
$$

$$
\begin{aligned}
-C_Z = &+ C_{Z_1}(\alpha, M) + C_{Z_2}(\alpha, \beta, M) + C_{Z_3}(\alpha, \delta_{\text{ls}}, \delta_{\text{le}}, M) + C_{Z_4}(\alpha, \delta_{\text{rs}}, \delta_{\text{re}}, M) \\
&+ C_{Z_5}(\alpha, \beta, \delta_{\text{li}}) + C_{Z_6}(\alpha, \beta, \delta_{\text{rfi}}) + C_{Z_7}(\alpha, \beta, \delta_{\text{lfi}}, \delta_{\text{lfo}}, M) + C_{Z_8}(\alpha, \beta, \delta_{\text{rfi}}, \delta_{\text{rfo}}, M) \\
&+ C_{Z_9}(\alpha, \delta_{\text{lfo}}, \delta_{1a}) + C_{Z_{10}}(\alpha, \delta_{\text{rfo}}, \delta_{\text{ra}}) + C_{Z_{11}}(\alpha, \delta_{\text{la}}, \delta_{\text{le}}) + C_{Z_{12}}(\alpha, \delta_{\text{re}}, \delta_{\text{re}}) \\
&+ C_{Z_{13}}(\alpha, \delta_{\text{rs}}, \delta_{\text{ls}}, \delta_{\text{pf}}, M) + C_{Z_{14}}(\alpha, \beta, \delta_{\text{la}}) + C_{Z_{15}}(\alpha, \beta, \delta_{\text{ra}}) + C_{Z_{16}}(\alpha, \beta, \delta_{\text{ls}}) \\
&+ C_{Z_{17}}(\alpha, \beta, \delta_{\text{rs}}) + \frac{q\bar{c}}{2V} C_{Z_{18}}(\alpha, M)
\end{aligned} \tag{2.5}
$$

$$
\begin{aligned}
C_l = &+ C_{l_1}(\alpha, M) + C_{l_2}(\alpha, \beta, M) + C_{l_3}(\alpha, \delta_{\text{ls}}, \delta_{\text{le}}, M) - C_{l_4}(\alpha, \delta_{\text{rs}}, \delta_{\text{re}}, M) \\
&- C_{l_5}(\alpha, \beta, \delta_{\text{lfi}}) + C_{l_6}(\alpha, \beta, \delta_{\text{rfi}}) - C_{l_7}(\alpha, \beta, \delta_{\text{lfi}}, \delta_{\text{lfo}}, M) + C_{l_8}(\alpha, \beta, \delta_{\text{rfi}}, \delta_{\text{rfo}}, M) \\
&+ C_{l_9}(\alpha, \delta_{\text{lfo}}, \delta_{\text{la}}) - C_{l_{10}}(\alpha, \delta_{\text{rfo}}, \delta_{\text{ra}}) + C_{l_{11}}(\alpha, \delta_{\text{la}}, \delta_{\text{le}}) - C_{l_{12}}(\alpha, \delta_{\text{ra}}, \delta_{\text{re}}) \\
&+ C_{l_{13}}(\alpha, \delta_{\text{rs}}, \delta_{\text{ls}}, \delta_{\text{pf}}, M) + C_{l_{14}}(\alpha, \beta, \delta_{\text{la}}) - C_{l_{15}}(\alpha, \beta, \delta_{\text{ra}}) + C_{l_{16}}(\alpha, \beta, \delta_{\text{ls}}) \\
&- C_{l_{17}}(\alpha, \beta, \delta_{\text{rs}}) + \frac{pb}{2V} C_{l_{18}}(\alpha, M) + \frac{rb}{2V} C_{l_{19}}(\alpha, M)
\end{aligned} \tag{2.6}
$$

$$
\begin{aligned}
C_m = &+ C_{m_1}(\alpha, M) + C_{m_2}(\alpha, \beta, M) + C_{m_3}(\alpha, \delta_{\text{ls}}, \delta_{\text{le}}, M) + C_{m_4}(\alpha, \delta_{\text{rs}}, \delta_{\text{re}}, M) \\
&+ C_{m_5}(\alpha, \beta, \delta_{\text{lfi}}) + C_{m_6}(\alpha, \beta, \delta_{\text{rfi}}) + C_{m_7}(\alpha, \beta, \delta_{\text{lf}}, \delta_{\text{lfo}}, M) + C_{m_8}(\alpha, \beta, \delta_{\text{rf}}, \delta_{\text{rfo}}, M) \\
&+ C_{m_9}(\alpha, \delta_{\text{lfo}}, \delta_{\text{la}}) + C_{m_{10}}(\alpha, \delta_{\text{ro}}, \delta_{\text{ra}}) + C_{m_{11}}(\alpha, \delta_{\text{la}}, \delta_{\text{le}}) + C_{m_{12}}(\alpha, \delta_{\text{ra}}, \delta_{\text{re}}) \\
&+ C_{m_{13}}(\alpha, \delta_{\text{rs}}, \delta_{\text{ls}}, \delta_{\text{pf}}, M) + C_{m_{14}}(\alpha, \beta, \delta_{\text{la}}) + C_{m_{15}}(\alpha, \beta, \delta_{\text{ra}}) + C_{m_{16}}(\alpha, \beta_{\text{ls}}) \\
&+ C_{m_{17}}(\alpha, \beta, \delta_{\text{rs}}) + \frac{q\bar{c}}{2V} C_{m_{18}}(\alpha, M)
\end{aligned} \tag{2.7}
$$

$$
\begin{aligned}
C_n = &+ C_{n_1}(\alpha, M) + C_{n_2}(\alpha, \beta, M) + C_{n_3}(\alpha, \delta_{\text{ls}}, \delta_{\text{le}}, M) - C_{n_4}(\alpha, \delta_{\text{rs}}, \delta_{\text{re}}, M) \\
&- C_{n_5}(\alpha, \beta, \delta_{\text{lfi}}) + C_{n_6}(\alpha, \beta, \delta_{\text{rfi}}) - C_{n_7}(\alpha, \beta, \delta_{\text{lf}}, \delta_{\text{lfo}}, M) + C_{n_8}(\alpha, \beta, \delta_{\text{rfi}}, \delta_{\text{rfo}}, M) \\
&+ C_{n_9}(\alpha, \delta_{\text{lfo}}, \delta_{\text{la}}) - C_{n_{10}}(\alpha, \delta_{\text{rfo}}, \delta_{\text{ra}}) + C_{n_{11}}(\alpha, \delta_{\text{la}}, \delta_{\text{le}}) - C_{n_{12}}(\alpha, \delta_{\text{ra}}, \delta_{\text{re}}) \\
&+ C_{n_{13}}(\alpha, \delta_{\text{rs}}, \delta_{\text{ls}}, \delta_{\text{pf}}, M) + C_{n_{14}}(\alpha, \beta, \delta_{\text{la}}) - C_{n_{15}}(\alpha, \beta, \delta_{\text{ra}}) + C_{n_{16}}(\alpha, \beta, \delta_{\text{ls}}) \\
&- C_{n_{17}}(\alpha, \beta, \delta_{\text{rs}}) + \frac{pb}{2V} C_{n_{18}}(\alpha, M) + \frac{rb}{2V} C_{n_{19}}(\alpha, M)
\end{aligned} \tag{2.8}
$$

2.2.3. Multi-axis thrust vectoring

Next to these aerodynamic force and moment coefficients, the MATV also has an influence on the body forces and moments. It is defined that a positive MATV deflection results in negative pitching and yawing moments.

With this convention, the effect of thrust vectoring on the body forces can be seen in Equation (2.9) and the effect on the moments in Equation (2.10). In these equations T is the total thrust force, d_n is the moment arm which is equal to 18.75 ft and δ_{ptv} and δ_{ytv} are the vectoring deflections in pitch and yaw direction. This 3D projection of the thrust vector was proposed in [9] as an extension to the model provided by Lockheed Martin and will be included in the next ICE-model release.

$$\mathbf{T} = T \begin{bmatrix} \cos(\delta_{\text{ptv}}) / \cos(\delta_{\text{ytv}}) \\ \cos(\delta_{\text{ptv}}) \tan(\delta_{\text{ytv}}) \\ \sin(\delta_{\text{ptv}}) \end{bmatrix} \tag{2.9}$$

$$\tau_{\text{T}} = -\text{T} d_n \begin{bmatrix} 0 \\ \sin(\delta_{\text{ptv}}) \\ \cos(\delta_{\text{ptv}}) \tan(\delta_{\text{ytv}}) \end{bmatrix} \tag{2.10}$$

2.2.4. Mass properties

To finish off the simulation model, the mass properties are defined. These properties are defined for a nominal configuration with 50% internal fuel and some missiles and other expendables, a lightweight and a heavyweight configuration and can be found in Table 2.2.

Table 2.2: Mass properties for the three different configurations. [13]

	Configuration			
	Nominal	Lightweight	Heavyweight	
Weight	32,750	25,989	37,084	lbf
x_{cg}	38.84	40	36	% MAC
y_{cg}	0	0	0	in
z_{cg}	88.97	88.97	88.97	in
I_{xx}	35,479	35,479	42,576	slug $\cdot$ ft^2
I_{yy}	78,451	67,500	81,903	slug$\cdot$ ft^2
I_{zz}	110,627	83,800	118,379	slug$\cdot$ ft^2
I_{xz}	-525	-250	-525	slug$\cdot$ ft^2

The MAC is located at 160.84 inch measured from the nose of the aircraft and has a length of 345 inch [13]. This results in an x_{cg} of 294.8 inch for the nominal configuration, 298.8 inch for the lightweight and 285.0 inch for the heavyweight configuration. The vertical location of the center of gravity is measured from the ground when the aircraft is standing on its landing gear.

3

INCA-based Flight Control System

For the ICE-aircraft described in the previous chapter a flight control system (FCS) has been designed in [9]. This FCS is able to take advantage of the full control effector suite and can handle the nonlinearities between effectors in real-time. At the heart of the FCS is a novel control allocation (CA) method known as Incremental Nonlinear Control Allocation (INCA). This chapter first discusses this CA method, after which the outer loops of the FCS are presented. These parts of the FCS system presented here are the ones that need to become fault tolerant.

3.1. Incremental Nonlinear Control Allocation

As the ICE-aircraft is over-actuated a CA method is required to distribute the control moments over the effectors. The INCA method presented in [9] is based on the Incremental Nonlinear Dynamic Inversion (INDI) method [14, 15]. In this INDI method increments in the required control positions are determined instead of absolute deflections. Due to this formulation and application of the time-scale separation principle the model dependency of the controller is reduced in a way that only the control derivatives are needed, whereas for the non-incremental method the stability derivatives are also needed. The time-scale separation principle can be applied to systems where the control deflections have a significantly higher influence than the states on the derivatives of the states, which has been proven true for several aerospace applications [15–17], and states that the influence of these states can be neglected at sufficiently high sampling rates.

3.1.1. INDI derivation

For the derivation of the concept of INDI consider the following general nonlinear system:

$$\dot{\boldsymbol{x}} = \boldsymbol{f}(\boldsymbol{x}, \boldsymbol{u}) \tag{3.1}$$

This system can be linearized around the current state using a first-order Taylor series expansion, see Equation (3.2), where the subscript '0' denotes that parameter is of the current time and no subscript are future values.

$$\begin{aligned} \dot{\boldsymbol{x}} &\approx \boldsymbol{f}(\boldsymbol{x}_0, \boldsymbol{u}_0) + \left.\frac{\partial \boldsymbol{f}(\boldsymbol{x}, \boldsymbol{u})}{\partial \boldsymbol{x}}\right|_{\boldsymbol{x}=\boldsymbol{x}_0, \boldsymbol{u}=\boldsymbol{u}_0} (\boldsymbol{x} - \boldsymbol{x}_0) + \left.\frac{\partial \boldsymbol{f}(\boldsymbol{x}, \boldsymbol{u})}{\partial \boldsymbol{u}}\right|_{\boldsymbol{x}=\boldsymbol{x}_0, \boldsymbol{u}=\boldsymbol{u}_0} (\boldsymbol{u} - \boldsymbol{u}_0) \\ \dot{\boldsymbol{x}} &\approx \dot{\boldsymbol{x}}_0 + F(\boldsymbol{x}_0, \boldsymbol{u}_0)\,(\boldsymbol{x} - \boldsymbol{x}_0) + G(\boldsymbol{x}_0, \boldsymbol{u}_0)\,(\boldsymbol{u} - \boldsymbol{u}_0) \end{aligned} \tag{3.2}$$

where the parts related to the system dynamics are presented by F and the control effectiveness by G. It is assumed in this equation that the sampling time is small and the control effectors are instantaneous, such that the time-scale separation principle can be applied, which leads to ignoring the second term containing F in the equation:

$$\begin{aligned}\dot{\boldsymbol{x}} &\approx \dot{\boldsymbol{x}}_0 + G(\boldsymbol{x}_0, \boldsymbol{u}_0)\,(\boldsymbol{u} - \boldsymbol{u}_0) \\ &\approx \dot{\boldsymbol{x}}_0 + G(\boldsymbol{x}_0, \boldsymbol{u}_0)\Delta\boldsymbol{u}\end{aligned} \tag{3.3}$$

By setting the derivative of the state vector as virtual-input, $\boldsymbol{\nu} = \dot{\boldsymbol{x}}$, in this equation the control input increment can be determined from the latest measurements and the required virtual control:

$$\Delta\boldsymbol{u} = G^{-1}(\boldsymbol{x}_0, \boldsymbol{u}_0)(\boldsymbol{\nu} - \dot{\boldsymbol{x}}_0) \tag{3.4}$$

3.1.2. INCA derivation

The INDI method works for systems that are not over-actuated, if a system is over-actuated the INCA method is required to solve for the required increments in actuator position. The INCA derivation starts from Equation (3.3), and by writing the G matrix differently, as well as setting the input to the system to be actuator deflections:

$$\boldsymbol{\nu}(\mathbf{x}) = \dot{\mathbf{x}} \approx \dot{\mathbf{x}}_0 + \mathbf{g}(\mathbf{x}_0)\,\frac{\partial \boldsymbol{\Phi}(\mathbf{x}_0, \boldsymbol{\delta}_0)}{\partial \boldsymbol{\delta}}\Delta\boldsymbol{\delta} \tag{3.5}$$

where $\boldsymbol{\nu}(\mathbf{x})$ is the virtual control input used to linearize the system, $\dot{\mathbf{x}}$ is the time-derivative of the state vector, $\partial\boldsymbol{\Phi}(\mathbf{x}_0, \boldsymbol{\delta}_0)/\partial\boldsymbol{\delta}$ a control effectiveness Jacobian (CEJ) and $\Delta\boldsymbol{\delta}$ an increment in control deflections. Solving for the required control deflections is possible if the CEJ is a square matrix as it requires inverting this matrix. However, for over-actuated systems such as the ICE-aircraft this matrix is non-square and therefore cannot be inverted. By implementing a control allocation scheme based on the relationship presented in Equation (3.5) this problem can be overcome. First the notation is a bit simplified using Equations (3.6) and (3.7):

$$\nabla_{\boldsymbol{\delta}}\boldsymbol{\Phi}(\mathbf{x}, \boldsymbol{\delta}) = \frac{\partial \boldsymbol{\Phi}(\mathbf{x}, \boldsymbol{\delta})}{\partial \boldsymbol{\delta}} \tag{3.6}$$

$$\mathbf{d}_c = \mathbf{g}(\mathbf{x})^{-1}\left[\boldsymbol{\nu}(\mathbf{x}) - \dot{\mathbf{x}}_0\right] \tag{3.7}$$

where $\mathbf{d}_c$ is the pseudo-control input. The INCA problem is then defined as follows: given this pseudo-control input $\mathbf{d}_c$, the current state $\mathbf{x}_0$, current control positions $\boldsymbol{\delta}_0$ and acceleration measurements $\dot{\mathbf{x}}_0$, determine an increment in control deflections $\Delta\boldsymbol{\delta}$ such that

$$\begin{aligned}&\nabla_{\boldsymbol{\delta}}\boldsymbol{\Phi}(\mathbf{x}_0, \boldsymbol{\delta}_0)\,\Delta\boldsymbol{\delta} = \mathbf{d}_c \\ &\text{subject to} \quad \underline{\Delta\boldsymbol{\delta}} \le \Delta\boldsymbol{\delta} \le \overline{\Delta\boldsymbol{\delta}}\end{aligned} \tag{3.8}$$

In this equation $\underline{\Delta\boldsymbol{\delta}}$ and $\overline{\Delta\boldsymbol{\delta}}$ are upper and lower bands of local incremental constraints for the position and rate of the actuator. A visual representation of the INCA method can be seen in Figure 3.1.

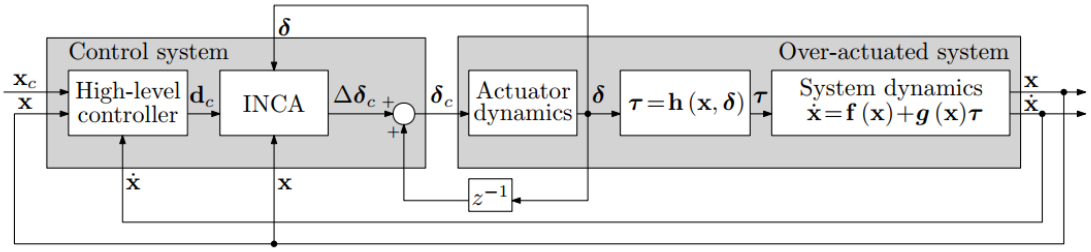

Figure 3.1: Schematic of the INCA method. [9]

Due to the incremental formulation of the control allocation problem INCA is linear in the increments of the effector positions, allowing it to be solved using efficient linear control allocations solvers (e.g. recursive weighted pseudo-inverse or quadratic programming methods [18]). Next to that, the CEJ can be updated at every time-step for the current states $\mathbf{x}$ and deflections $\boldsymbol{\delta}$ which allows for capturing of the nonlinearities and

interactions of the effectors. A final advantage of the INCA method is the mitigation of negative actuator dynamics effects due to the feedback of actual actuator positions $\boldsymbol{\delta}_0$. A more in depth derivation and discussion of the INCA method can be found in [9].

3.1.3. INCA applied to ICE-aircraft

The INCA method has been applied to the inner angular rate control loop of the ICE-aircraft. For this application the required increments in control-induced moments $\Delta\boldsymbol{\tau}_c$ are used as the pseudo-control input $\mathbf{d}_c$. These required moment increments can be calculated using Equation (3.9):

$$\Delta\boldsymbol{\tau}_c = \mathbf{I}\left[\boldsymbol{\nu}_\omega(\mathbf{x}) - \dot{\boldsymbol{\omega}}_0\right] \tag{3.9}$$

where $\mathbf{I}$ is the mass moment of inertia matrix, $\dot{\boldsymbol{\omega}}_0$ are measured angular accelerations and $\boldsymbol{\nu}_\omega(\mathbf{x})$ is the virtual control input coming from a PID-controller on the angular rate, as specified in Equation (3.10).

$$\boldsymbol{\nu}_\omega(\mathbf{x}) = \mathbf{K}_{\omega_P}(\boldsymbol{\omega} - \boldsymbol{\omega}_c) + \mathbf{K}_{\omega_I}\int(\boldsymbol{\omega} - \boldsymbol{\omega}_c)\,dt + \mathbf{K}_{\omega_D}(\dot{\boldsymbol{\omega}} - \dot{\boldsymbol{\omega}}_c) \tag{3.10}$$

To prevent actuator saturation, which can happen when physically unachievable commands are given to the controller, pseudo-control hedging (PCH) is applied to this angular rate loop. First proposed in [19], PCH hedges the reference signal to the control system by subtracting the difference between the commanded and achieved virtual command. These commands can be determined by looking at the commanded and achieved actuator positions, resulting in a difference and thus a hedge signal if an actuator is saturated and the achieved position is not equal to the commanded position. The hedge signal is fed back into a first-order reference model which behaves as a low-pass filter and can be used as a feedforward term to improve tracking performance [16]. An overview of the inner angular rate control loop with INCA and PCH for the ICE-aircraft can be seen in Figure 3.2, where the hedge signal is denoted as $\boldsymbol{\nu}_h$ and the reference model can be found on the left side with the 'rm' subscripts.

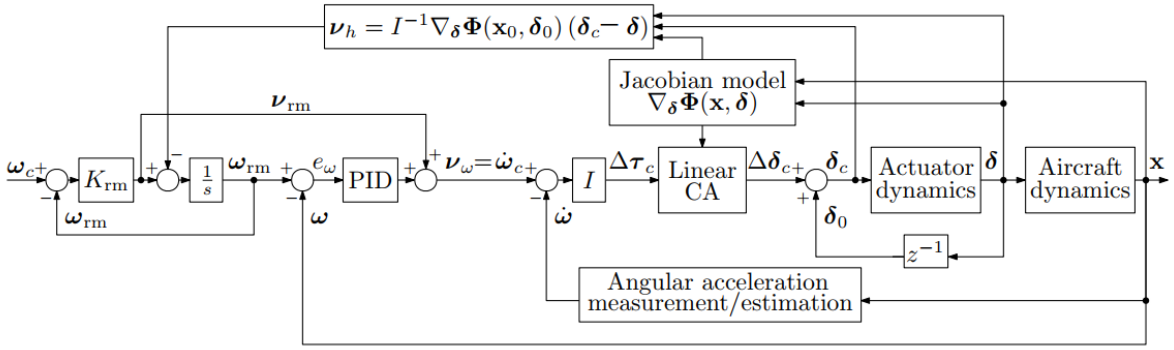

Figure 3.2: Schematic of the angular rate control loop with INCA and PCH. [9]

As mentioned previously, INCA requires an estimation of the control effectiveness of the effectors, the CEJ. This CEJ is derived from a multivariate simplex spline model of the aerodynamic characteristics of the ICE-aircraft, which was first identified as a 0^{th} order continuity model in [20]. To get the partial derivatives with respect to the effectors out of this model the methods presented in [21]. As the model has 0^{th} order continuity on the spline edges some discontinuity or jumps are present in the Jacobian, increasing the continuity order could therefore also improve the INCA method [9]. A spline model was chosen as it can provide a lightweight and accurate representation of the aerodynamic model and is really well suited for online system identification purposes.

3.2. Outer control loops

With the INCA method applied to the inner angular rate loop, several outer loops are designed in [9] to be able to track different reference trajectories. These loops are designed using the Nonlinear Dynamic Inversion (NDI) method [22]. The first loop is the sideslip inversion outer loop, designed to perform coordinated

turns by compensating the sideslip. In this loop the sideslip β is used as a reference signal, which is dynamically inverted to control the yaw rate r. A schematic representing the sideslip outer loop can be seen in Figure 3.3.

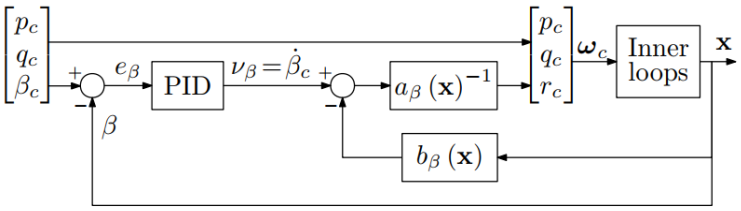

Figure 3.3: Sideslip inversion outer loop schematic. [9]

The second designed loop is used to control the aerodynamic angles for bank angle ϕ, angle of attack α and angle of sideslip β. In this loop these angles are inverted to obtain required values for the angular rates p, q and r. The schematic representation of this loop is found in Figure 3.4.

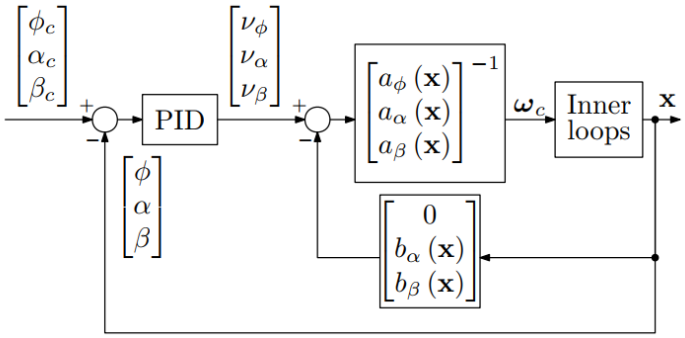

Figure 3.4: Aerodyanmic inversion outer loop schematic. [9]

The last inversion loop is the flight path guidance loop, which is similar to the aerodynamic angle inversion loop, but instead of the AoA the flight path angle γ is controlled. The schematic for this loop can be seen in Figure 3.5.

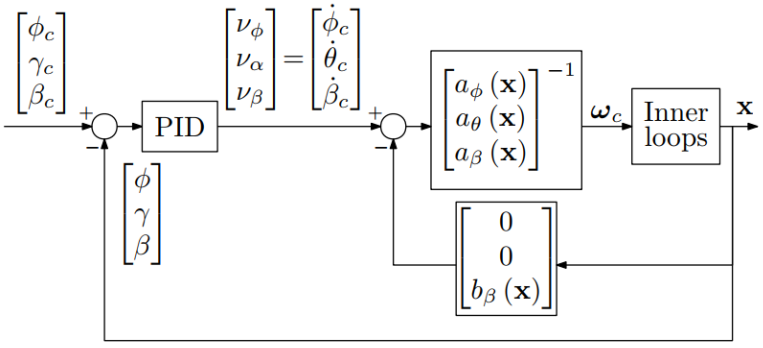

Figure 3.5: Flight path guidance outer loop schematic. [9]

In all these outer loop schematics, the block “Inner loops" contains the INCA-based angular rate loop with PCH as presented in Figure 3.2. For a more in-depth discussion on what the a and b in the inversion loops represent please refer to [9]. To make the ICE-aircraft fault tolerant it is these control loops that should be able to handle suddenly changing aerodynamics and model mismatches.

4

Damage modeling

To be able to develop and test a fault tolerant controller a model of a damaged aircraft is necessary. For this damaged model the mass properties and aerodynamic characteristics have to be defined to be able to use it in the simulation. This chapter investigates several methods to perform both mass modeling and aerodynamic modeling. Next to this, it also provides a small discussion on the effect of asymmetrical damage on the standard equations of motion for an aircraft.

4.1. Mass properties

Modeling the mass properties such as the mass moments of inertia (MoI), location of the center of gravity (CG) and the mass itself is required to perform a structural failure simulation as they govern the reaction of the aircraft to applied moments and forces. The mass properties for three configurations were already specified in Section 2.2, but these will obviously change if e.g. part of the wing falls off. In the literature several methods for the estimation of the mass properties can be found. In [23] a loss of the vertical tail of a Cessna Citation II aircraft is modeled by assuming the mass of the vertical tail to be 2.5% of the total empty mass of the aircraft, uniformly distributed over the span. A vertical tail loss of e.g. 50% is then modeled by subtracting half of the mass of the vertical tail from the nominal mass. The change in location of CG is assumed to be proportional to the loss in mass for the x- and z-location. The y-location is unchanged as it is a symmetrical damage. The last mass property to model is the mass moment of inertia, which will change due to both the decreased mass as well as changed CG location. It is estimated using the following equation:

$$I_{i_{\text{damaged}}} = I_{i_{\text{original}}} + m_{\text{damaged}}\Delta_j^2 - \left(I_{i_{\text{LostPart}}} + m_{\text{LostPart}}d_j^2\right) \quad \text{where} \quad i = xx, yy, zz \quad \text{and} \quad j = z, y, x \tag{4.1}$$

In this equation the part $m_{\text{damaged}}\Delta_j^2$ is due to the change in CG, while the part being subtracted is due to the lost part.

A different way of estimation the mass properties can be found in [24], where a small UAV is modeled as a combination of several simpler geometric shapes. As the volumes and MoIs of these simple shapes (such as slender rods, cylinders and rectangular cuboids) are easily calculated, the total mass and MoI can also be easily determined. The results of the estimation using these simple shapes are compared to experimental results and an estimation based on different point masses. It was found that the simple shapes estimation almost perfectly predicts the MoI, whereas the point mass approach greatly underestimates the values, indicating the the simple shape approach is valid for small UAVs for determining mass properties. One clear drawback of this method however, is the fact that the body of which the mass properties are to be estimated needs to consist of these simple shapes.

Another method of estimating the mass properties is to use CAD models. If a full CAD model of the aircraft is available the mass properties can be estimated by adding a material to the different parts, after which the

CAD software (such as SolidWorks or CATIA) will be able to determine the mass properties. At the moment only a surface model of the ICE-aircraft is available, but this model could still potentially be used by adding thicknesses and densities to the surfaces and model the mass properties is that way.

4.2. Changed equations of motion

One consequence of a change in the CG location is an extra coupling between rotational and translational accelerations, since the force and moment equations are still taken at the old CG location. Also, if the damage is asymmetrical about the x-z plane the products of inertia I_{xy} and I_{yz} are not zero anymore. The force (Equations (4.2) to (4.4)) and moment (Equations (4.5) to (4.7)) equations presented in [25] provide the equations of motion of an aircraft referenced to an arbitrary body-fixed point A (indicated by the subscript). This point A can be the CG, however, after a shift in CG due to damage, the CG will be at a new location while the equations of motion are still referenced around the old one at point A. Thus these equations can describe the aircraft's motion after a shift in CG.

$$\sum F_X = m\left(\dot{u}_A + q w_A - r v_A - \left(q^2 + r^2\right)\Delta x + \left(qp - \dot{r}\right)\Delta y + \left(rp + \dot{q}\right)\Delta z + g\sin\theta\right) \tag{4.2}$$

$$\sum F_Y = m\left(\dot{v}_A + r u_A - p w_A + \left(pq + \dot{r}\right)\Delta x - \left(p^2 + r^2\right)\Delta y + \left(qr - \dot{p}\right)\Delta z - g\cos\theta\sin\phi\right) \tag{4.3}$$

$$\sum F_Z = m\left(\dot{w}_A + p v_A - q u_A + \left(pr - \dot{q}\right)\Delta x + \left(qr + \dot{p}\right)\Delta y - \left(p^2 + q^2\right)\Delta z - g\cos\theta\cos\phi\right) \tag{4.4}$$

$$\begin{aligned}\sum M_{A_X} =& I_{xx}\dot{p} - I_{xy}\dot{q} - I_{xz}\dot{r} + I_{xy}pr - I_{xz}pq + \left(I_{zz} - I_{yy}\right)qr + \left(r^2 - q^2\right)I_{yz} \\ &+ m\left(\left(p v_A - q u_A + \dot{w}_A - g\cos\theta\cos\phi\right)\Delta y + \left(p w_A - r u_A - \dot{v}_A + g\cos\theta\sin\phi\right)\Delta z\right)\end{aligned} \tag{4.5}$$

$$\begin{aligned}\sum M_{A_Y} =& -I_{xy}\dot{p} + I_{yy}\dot{q} - I_{yz}\dot{r} + I_{yz}pq - I_{xy}qr + \left(I_{xx} - I_{zz}\right)pr + \left(p^2 - r^2\right)I_{xz} \\ &+ m\left(\left(q u_A - p v_A - \dot{w}_A + g\cos\theta\cos\phi\right)\Delta x + \left(q w_A - r v_A + \dot{u}_A + g\sin\theta\right)\Delta z\right)\end{aligned} \tag{4.6}$$

$$\begin{aligned}\sum M_{A_Z} =& -I_{xz}\dot{p} - I_{yz}\dot{q} + I_{zz}\dot{r} + I_{xz}qr - I_{yz}pr + \left(I_{yy} - I_{xx}\right)pq + \left(q^2 - p^2\right)I_{xy} \\ &+ m\left(\left(r u_A - p w_A + \dot{v}_A - g\cos\theta\sin\phi\right)\Delta x + \left(r v_A - q w_A - \dot{u}_A - g\sin\theta\right)\Delta y\right)\end{aligned} \tag{4.7}$$

where m is the mass, u, v and w are velocity components in x-, y- and z-direction respectively, p, q and r are the rotational velocities around the three axes, $\Delta(x, y, z)$ are the differences in location between point A and the CG, g is the gravitational constant and θ and ϕ are the roll and pitch Euler angles. As can be seen from these equations, when the point A is in the CG the equations can be greatly simplified.

The same paper presenting these equations also presents an example of a shift in CG for the NASA General Transport Model (GTM) due to a 24% wing loss. For the 209 cm wingspan model the CG shifted 0.10 cm forwards, 1.8 cm towards the undamaged wing and 0.13 cm up [25], which is quite an insignificant change. This conclusion was also made in [26] where a large asymmetric mass change in the form of the physical separation of an engine of the NASA GTM did not result in a substantial change in the CG location. These conclusions would indicate that the equations of motion used in the simulation do not necessarily have to incorporate the change in CG location due to structural damage.

4.3. Aerodynamic properties

Next to the changed mass properties, the aerodynamic properties of the aircraft will also change due to structural damage. To simulate these changes, the coefficients presented in Section 2.2 need to be adapted. This can be done in several ways of which four will be mentioned in this section. The most simple way is to just scale the nominal coefficients with a scaling factor a as done in [7] or apply an additive term. The scaling factor can be used to simulate e.g. reduced lift or increased drag over the entire envelope, while the additive term can e.g. be used to simulate asymmetric damage in the rolling coefficient. The damaged coefficients can then be calculated according to Equation (4.8):

$$C_{\text{damaged}}(\mathbf{x}) = (1 + a)\, C_{\text{nominal}}(\mathbf{x}) + C_{\text{additive}}(\mathbf{x}) \tag{4.8}$$

A second way to model the damaged aerodynamic properties is to make use of the Digital DATCOM method [27]. This is a digital implementation of the U.S. Air Force's Stability and Control Data Compendium [28], which provides methods to predict the stability and control derivatives of symmetrical aircraft based on basic aircraft geometry. This way of estimating the aerodynamic coefficients is being used in [23]. However, as also mentioned in [23], this method has some limitations, such as e.g. an assumed attached flow making the predictions only valid for low angles of attack or assuming a constant airfoil section across the entire wingspan. Next to that, the program only accepts symmetrical airplanes as input, thus making it less useful for determining the aerodynamic properties of an aircraft with damage to one wing.

These two previous methods are relatively simple, but there are of course more sophisticated methods as well. Using CFD-programs is one of these options. In [29] the program "AVL" is used to determine the aerodynamic forces and moments on the NASA GTM aircraft. As CFD-programs are based on aerodynamics theory they could potentially provide better results than just scaling values or using Digital DATCOM. However, CFD-programs still make use of several assumptions, again limiting their credibility, which was also observed in [29]: estimation results depending on dynamic states (e.g. the pitch rate) are less accurate. Next to that, performing a proper CFD simulations is not that simple and will therefore not be considered as a feasible method for estimating the damaged parameters.

A final method to model the effects of structural damage on the aerodynamics of an aircraft is to use wind tunnel testing. In [26, 30] a scaled version of the NASA GTM with four different types of structural damage is tested in a wind tunnel. The damage cases include a missing outboard trailing-edge flap, loss of a leading-edge slat, partial loss of a wing and a large hole in the outboard section of a wing. As the air actually flows around the model and is not simulated, the assumptions required for CFD-methods or the Digital DATCOM do not apply anymore, resulting in a better estimation. However, it is also the least simple and least practical method to perform, thus will again not be considererd.

5

Fault tolerant control

Making a flight control system fault tolerant can be done in a lot of ways. This chapter first discusses a classification for the different methods and describes the general ideas. This is followed by a discussion on one of the classes of fault-tolerant control, adaptive control. At the end also a small overview of previous methods of designing a fault-tolerant flight controller for the ICE-aircraft are discussed.

5.1. Classifications

As there are quite a few different methods to implement a fault tolerant controller, each with its own advantages and disadvantages, specifying some classifications can provide some structure. First of all the methods can be classified as either a passive or an active method. The active methods can further be divided into methods that use an online redesign approach and methods using a projection based approach. And finally, both the active and passive methods can again be divided into methods that are solved using optimization techniques and methods based on Lyapunov's theorem. An overview of these possible classifications can be seen in Figure 5.1 [31] and an explanation of the differences between each category are discussed in the rest of this section.

5.1.1. Passive versus active

The first classification can be made based on if a system is fixed or reconfigurable. Passive methods are fixed and provide fault tolerance by being robust inside a predefined uncertainty region around a nominal model. Only when the system is inside this robust stability radius of the controller stability and performance can be guaranteed. An advantage of passive methods is the immediate control action taken after fault occurrence: it does not have to wait for the controller reconfiguration. Next to that, it is easier to implement compared to active methods However, it also has some major drawbacks. Because of the large stability radius, the controller is more conservative than needed in many cases, resulting in decreased performance. Next to that, any failure that was not anticipated in the control design can fall outside the stability region, possible resulting in loss of control. [32]

In contrast to this are the active fault tolerant methods. These methods are characterized by the ability to take fault information into account to reconfigure the controller. This information is provided by a what is generally called a Fault Detection and Isolation (FDI) module. Because the controller can be reconfigured based on the current situation it does not have to be as conservative in its control as passive methods and generally can account for more types of failures. Active fault tolerant methods however also have disadvantages. Because of it dependency of the FDI module no immediate action is taken after a fault occurs, the fault first has to be detected after which the controller has to be reconfigured. If this takes too long, the aircraft might already be in an unrecoverable state. Next to this, the switching between controllers or reconfiguring of the controller might introduce undesired transients which potentially could worsen the situation. [32]

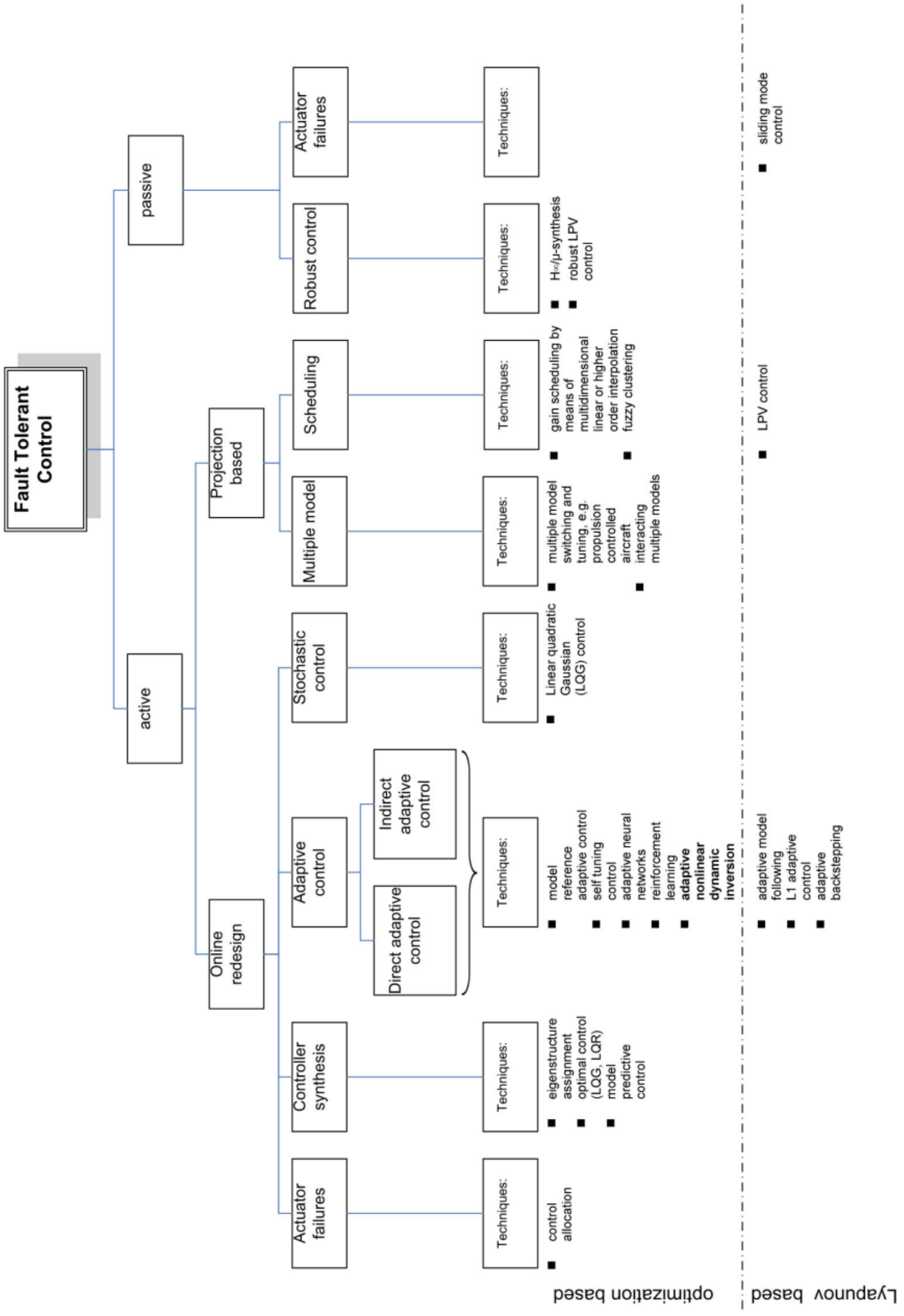

Figure 5.1: Possible classifications of fault tolerant control methods. [31]

5.1.2. Online redesign versus projection based

Active fault controllers can be subdivided again into two categories based on how the controller will be formed after a fault has occurred. The first category are the projection-based methods. As the name already suggests, after a fault a controller is selected from a predefined and offline designed controllers, which can each be designed for a specific fault case. This switching is done by a reconfiguration mechanism (RM) which uses the information supplied by the FDI module to select the best controller for the current situation. As the projection based methods are still based on offline designed controllers it has the same disadvantage, although to a lesser extend, as passive fault tolerant methods in the sense that only a predefined set of faults can be accounted for [31]. A certain type of projection method which aims to reduce this limitation is the Interacting Multiple Model (IMM) method. In this method the resulting controller can also be a combination of several of the predefined offline controllers, thereby increasing the amount of faults or combinations of faults it can account for [33]. The online redesign methods does not rely on predefined offline controllers but actively changes the controller in real-time. Due to this property it is superior to both the passive and projection based methods in terms of types of failures it can account for. However, it also requires the most computational power due to its online property.

5.1.3. Optimization versus Lyapunov based

A final classification for fault tolerant control methods is the way the control methods are designed. This can be done according to Lyapunov's theorem or based on optimization methods. Examples of Lyapunov designed control methods are Sliding Mode Control and Backstepping. It can be proven for these Lyapunov based methods that they are global asymptotically stable, which can be a great advantage for the certification of fault tolerant controllers. A drawback of the Lyapunov method is the fact that they rely on a Control Lyapunov Function (CLF) in their design, and finding such a CLF for nonlinear systems can be complex [34]. Control methods based on optimization procedures is the other class. Control allocation, model predictive control and $\mathcal{H}_\infty$ and μ-synthesis are several examples. The optimization procedure in these methods minimizes a certain cost function and ensures maximal performance, but a guarantee for global asymptotic stabilty is not easily obtained. [31]

5.2. Adaptive fault tolerant control

A very promising active and online redesign based method to achieve fault tolerant control is adaptive control. This approach is based on an accurate onboard aerodynamic model of the plant, which can be adapted online to compensate for inaccuracies in the nominal model and (sudden) changes in the plant parameters. Adaptive control can generally generally be classified into either direct or indirect adaptive control. Next to that there are two main design approaches, Model Reference Adaptive Control (MRAC) and Self-Tuning Control (STC).

5.2.1. Direct versus indirect adaptive control

The difference between the direct and indirect adaptive control is how the controller parameters are estimated: with direct adaptive control the controller parameters (θ_c) are estimated directly, while for the indirect approach first the plant parameters (θ_m) are estimated after which these are used to determine the control parameters. A schematic with both approaches can be seen in Figure 5.2. Direct adaptive control is also called implicit or integrated adaptive control, as the plant parameters are only implicitly considered in the control law and the adaptation algorithm is integrated in the controller [31]. The parameter update laws are often designed using Lyapunov's theorem, allowing for proof of stability. An example of a direct adaptive controller can be found in [35], where an Adaptive Incremental Backstepping controller with three different parameter estimators is designed and tested for a high-performance aircaft.

The indirect adaptive control approach, also called modular or explicit adaptive control due to a separate system identification module which explicitly estimates plant parameters [31], is not based on Lyapunov's theorem but makes use of the *certainty equivalence principle* [36]. This principle allows for the actual model parameters to be replaced by their estimates from the identification module. From these estimated model parameters the required control parameters can subsequently be derived. An example of an indirect adaptive control method can be found in [7], where the model parameters used in the Nonlinear Dynamic Inversion are estimated as a multivariate spline model.

For adaptive control it is important that the estimated parameters converge to the correct values and do so

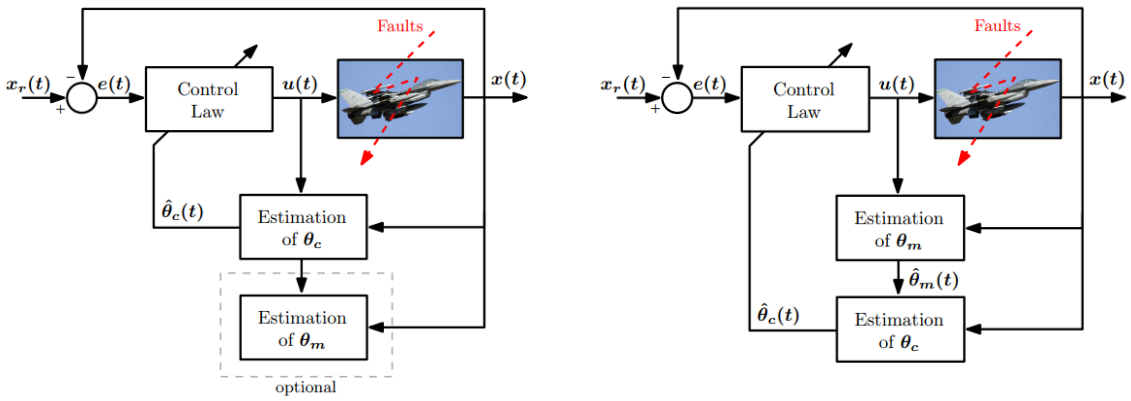

(a) Direct adaptive control.

(b) Indirect adaptive control.

Figure 5.2: Schematic overview of direct and indirect adaptive control. [35]

in a reasonable amount of time. As the identification module requires data regarding the inputs and output of the system, one way of ensuring enough data is available is to perform certain maneuvers containing sufficient frequencies such that all relevant system dynamics are excited. Performing such a maneuver however could be undesirable, e.g. in the case of a structurally damaged aircraft it might not be possible to fly the maneuver. A different way of approaching this requirement of persistent excitation is to apply a *dither* to the control signal: adding small variations on top of the required control deflections. However, if the dither is added directly to the required control deflections unwanted system dynamics could be excited which could deteriorate the performance of the plant. A smarter method to perform dither is discussed in both [37] and [38]. These papers suggest slowly changing the weights specifying the preference for different controls used in the control allocation module. by doing this no moments other than the required control moments are generated, while still making sure different actuators are active at all time. A similar method to this dither can be found in [39], where a dither to the control signal is added that is in the "null-space" of the control effectors. Because the added signal lies in the null-space, no additional moment in generated.

5.2.2. Model reference adaptive control versus self-tuning control

Two other design approaches, which could both be designed in a direct and indirect adaptive fashion, are the Model Reference Adaptive Control (MRAC) and Self-Tuning Control (STC) approaches. Schematics depicting both approaches can be seen in Figure 5.3. As can be seen from the MRAC schematic this approach features a reference model (as is also suggested in the name). This reference model specifies the desired output of the plant to the input commands. The difference between this desired output and the actual plant output then drives an adaptation law which in turn adapts the controller parameters. The goal of the adaptation is to have the actual plant follow the desired dynamics of the reference model. This is the basic form of MRAC, but there are of course more advanced implementations which all try to improve on the basis. An example of these is the composite MRAC reviewed in [40], which makes use of both direct and indirect MRAC to improve the transient performance of the controller. The effectiveness is validated on a simulation of an F-16 model which becomes more unstable and less controllable at a certain time in the simulation. Another example of a more advanced MRAC scheme is found in [41]. In this paper a new virtual-command-based approach to MRAC is presented, which has the advantage of having less oscillations in the transient period while still keeping a high learning rate allowing for fast adaptation. It is validated on a simulation of the NASA GTM with a broken left wing tip. As these methods show fast adaptation to certain errors and still keeping the aircraft flyable and able to track reference inputs, MRAC is considered as a viable option for making INCA fault tolerant.

The second design approach are the self-tuning controllers. These controllers are coupled with an online parameter estimator, which first identifies plant parameters after which a control law is designed based on these parameters. The new control law is then sent to the controller and implemented. The design of the new control law can be done in several ways, such as for example pole placement or according to the rules form Ziegler-Nichols [42].[31]

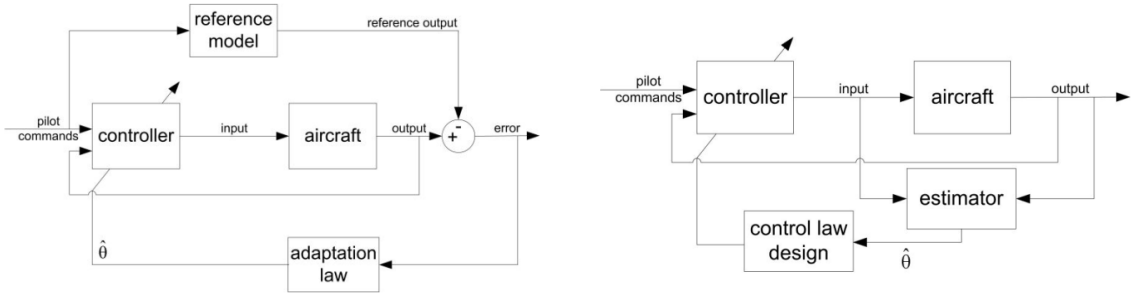

(a) Model reference adaptive control.

(b) Self-tuning control.

Figure 5.3: Schematic overview of MRAC and STC control. [31]

5.3. Incremental fault tolerant control

A sort of fault tolerant controller which can not be found yet in the classification in Figure 5.1 are the incremental controllers. These approaches are improvements on the NDI and Backstepping (BS) methods. NDI and BS are two types of nonlinear flight control which have several advantages over conventional linear flight control, such as no need for gain scheduling and a better performance over the entire flight envelope, even in nonlinear regions [43, 44]. The main idea of NDI is to cancel aircraft nonlinearities, such that the combination of aircraft and NDI controller can be controlled as if it were a linear system. Backstepping on the other hand is a recursive design method based on Lyapunov's theorem. Using this method a controller is designed in a recursive way where some state variables are considered as "virtual controls", after which intermediate control laws are designed for these variables up until the control vector shows up in a control law. An advantage of Backstepping compared to NDI is the fact that nonlinearities can be selectively canceled. As it is Lyapunov based, the advantages and disadvantages presented in Section 5.1 also apply. These two nonlinear controllers can also be designed in an incremental way, which reduces their model dependency and makes it more robust. A small explanation on these incremental methods is presented in the following subsections.

5.3.1. Incremental Nonlinear Dynamic Inversion

The derivation of the INDI method has already been presented in Section 3.1.1. The final equation of that derivation is shown again here for clarity:

$$\Delta \boldsymbol{u} = G^{-1}(\boldsymbol{x}_0, \boldsymbol{u}_0)(\boldsymbol{\nu} - \dot{\boldsymbol{x}}_0) \tag{5.1}$$

where $\Delta \boldsymbol{u}$ are the required increments of the input, G is a control effectiveness matrix, $\boldsymbol{\nu}$ is the virtual control, and $\dot{\boldsymbol{x}}_0$ are the derivatives of certain states.

As can be seen from this last equation, no knowledge of a model of the system dynamics is required as the state derivatives are used instead. Thus this incremental version of NDI has an increased robustness against model mismatch and model uncertainty. However, it does rely more on measurements and sensor and therefore the sensitivity for errors and delays in these is increased. In [45] an analysis is performed to see the effect of sensor bias, noise and delay on the stability of an incremental controller, showing that these phenomena are indeed present but can be prevented. An INDI controller is applied to an MAV in [46]. In this research not only the inner attitude loop is designed using INDI, but also the outer loop for linear accelerations is designed in an incremental way. This results in greatly improved disturbance rejection properties.

Similarly to the regular NDI controllers, the incremental version can also be made adaptive. An example of this is presented in [17], where the control effectiveness matrix of a drone is estimated online using a least-mean squares approach. This way the controller is more robust to changes in the control effectiveness due to for example changes in flight velocity, battery voltage or actuator failures.

5.3.2. Incremental Backstepping

A short description of the final step in the recursive design of an Incremental Backstepping controller is presented here, for a more in depth explanation see [35, pages 97-100]. The derivation starts of similar to INDI up

until Equation (3.3), where the nonlinear system is described in an incremental way. From this point onwards, the standard Backstepping procedure continues: first the system description is inserted into an equation for the tracking error z. After this, a control Lyapunov function $\mathcal{V}$ is defined in terms of the tracking error. The time derivative of this control Lyapunov function needs to be negative definite for the system to be asymptotically stable, so a incremental control vector can be determined to achieve this. As any knowledge of the system dynamics was already excluded in the incremental form of the system description, no system dynamics will show up in the final incremental control vector determined using the Backstepping approach.

5.4. Fault tolerant control for the ICE-aircraft

In the past there have already been several attempts at designing a fault tolerant controller for the ICE-aircraft. This section discusses a few of these attempts. The first attempt was in 1999 and comprised of five modules to control the ICE-aircraft [38]. The first module was the Command Shaping and Limiting module, which shapes and limits the pilot input based on control saturation and failure information. The Online-Control Design module generates pseudo-effector commands based on stability derivatives and pseudo-control estimates (estimated by the Parameter Identification module), full-state feedback, information from the Output Compensation and Estimation module and the desired rates coming from the Command Shaping and Limiting module. The Receding Horizon Optimal (RHO) control method is used to determine the pseudo-commands, which are subsequently sent to the Control Allocation and Optimization module to generate the actual physical effector deflections. The fault tolerant capabilities come from the combination of the RHO control method with the online parameter identification module. During simulations it was found that the proposed control system could indeed reconfigure itself to account for failures, however, this simulation was not run in real-time. Next to that, as only recently a control allocation method has been developed that can take full advantage of the nonlinear and coupled control suite of the ICE-aircraft in real-time [9], the control system does not take this into account. This last remark is a general remark though for all fault tolerant control systems discussed next.

Another fault tolerant controller for the ICE-aircraft was designed in [14]. The method proposed here is basically a version of incremental nonlinear dynamic inversion (INDI), thus the model dependency is reduced by using acceleration measurements instead of a full onboard model. This way, only a model of the control effectiveness is required, which is also updated online. It is also pared with a control allocation module which can take faulty effectors into account by setting their weighting to zero.

The next fault tolerant controller is presented in [47]. This approach is mainly focused on actuator failures as it provides a method for adaptive control allocation. This control allocation module uses fault information supplied by a FDI module to redistribute the required moments over the remaining healthy actuators. An attempt to model the nonlinearities and interactions in the control effectors has also been made. This is done by not only looking at the linear control effectiveness, but also adding terms for the absolute control deflections of the all-moving tips and spoiler-slot deflectors, and interactions based on a predefined table with effectiveness parameters. Not all interactions are modeled though, only the reduced control effectiveness of downstream surfaces due to deflections of the spoiler-slot deflector.

In [48] another method can be found. This is an extension of the INDI method discussed earlier and aims to reduce the likelihood of actuator position/rate saturation. This is achieved by having the control allocator minimize these positions and rates, which can be done by adapting the cost function to include both. Another improvement made in this paper compared to the original is a multi-pass strategy in the allocation module. This strategy aims to mitigate the negative effects of having saturated actuators by restoring lost control power using the remaining unsaturated effectors.

6

Preliminary methodology

This chapter will discus the preliminary method that is chosen to perform the research. First of all the general idea to achieve fault tolerant performance is described, after which two possible implementations are explained.

6.1. Fault tolerant control method

The chosen method to make the current Incremental Nonlinear Control Allocation (INCA) controller fault tolerant is to make it adaptive such that the Control Effectiveness Jacobian (CEJ) can be adapted in real-time to account for changes in the effectiveness of the control surfaces. This method was chosen because adaptive controllers have already shown to be effective in achieving fault tolerance, e.g. in [7] where a spline-based controller for an F-16 aircraft is adapted to aerodynamic uncertainties using a recursive least squares approach, or in [17] where an the control effectiveness matrix of an incremental controller for a drone is estimated at every time-step using a least mean squares approach.

There are however some differences between these two examples and the ICE-aircraft. For example, compared to the F-16 the onboard model of the ICE-aircraft is a lot bigger: 20 spline models for the F-16 compared to 216 for ICE. Because of this, adapting these spline models in real-time online is impossible. The control effectiveness of the drone is not based on splines but is just a single matrix that is updated every time-step. This approach would make real-time implementation for the ICE-aircraft possible, however, because of the highly nonlinear and coupled nature of the ICE-aircraft, spline models are needed to capture these nonlinearities. As such, estimating the complete CEJ completely at every time-step is also not possible.

The chosen approach for the ICE-aircraft is a combination of the two methods discussed above: the base spline model will be kept intact, but a 'delta CEJ' is estimated at every time-step and added on top of this base model, as can be seen in Equation (6.1). A updated schematic overview of the inner loop rate control including this adapting factor can be seen in Figure 6.1.

$$\text{CEJ}\left(\mathbf{x}_0, \boldsymbol{\delta}_0, \Delta\mathbf{x}, \Delta\boldsymbol{\delta}\right) = \text{CEJ}_{\text{spline}}\left(\mathbf{x}_0, \boldsymbol{\delta}_0\right) + \boldsymbol{\Delta}\text{CEJ}\left(\Delta\mathbf{x}, \Delta\boldsymbol{\delta}\right) \tag{6.1}$$

Using this approach, the controller can be made adaptive in real-time while also keeping the splines capturing the nonlinearities and couplings. A concern could be that this $\boldsymbol{\Delta}$CEJ is not a constant matrix and that therefore the estimation algorithm will never converge to the required value to get the correct failed CEJ in a single time-step. However, convergence to the real parameter is not required, as the INCA method has already been shown to be robust to mismatches in the CEJ in [9]. So as long as this $\boldsymbol{\Delta}$CEJ gets the total CEJ inside these robustness bounds the controller should be able to handle the failures. For the estimation of this $\boldsymbol{\Delta}$CEJ two methods can be used and are discussed next.

6.1.1. Least mean squares

The first estimation technique that can be used to estimate the $\boldsymbol{\Delta}$CEJ is a least mean squares (LMS) adaptive filter [49], which was also used in [17] for the drone. This filter works by looking at the error between a pre-

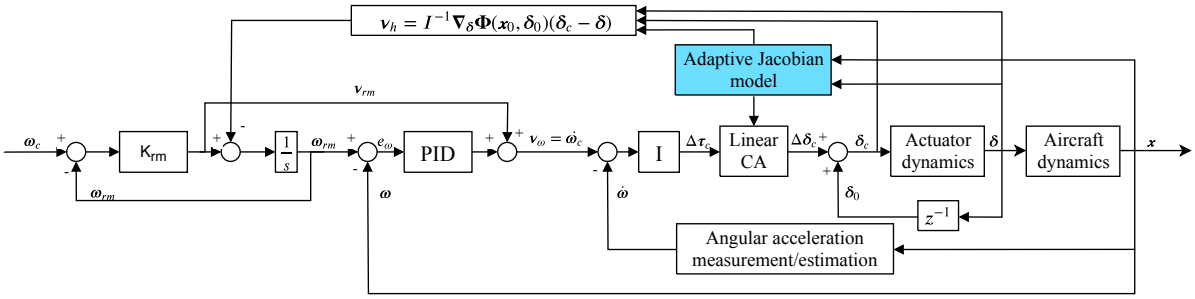

Figure 6.1: Schematic of the adaptive INCA-based angular rate control system.

dicted and the actual response and then updating the matrix or parameters of interest based on this error. If the goal was to estimate the full control effectiveness this error signal would be the calculated according to Equation (6.2):

$$\begin{aligned} \text{error} &= \Delta\boldsymbol{\tau}_{\text{pred}} - \Delta\boldsymbol{\tau}_{\text{act}} \\ &= \text{CEJ} \cdot \Delta\boldsymbol{\delta} - \mathbf{I} \cdot \Delta\dot{\boldsymbol{\omega}} \end{aligned} \tag{6.2}$$

where $\Delta\boldsymbol{\tau}_{\text{pred}} \in \mathbb{R}^{3\times 1}$ are the predicted changes in moments around the aircraft which can be calculated by multiplying the CEJ $\in \mathbb{R}^{3\times 13}$ with the change in effector position $\Delta\boldsymbol{\delta} \in \mathbb{R}^{13\times 1}$, and $\Delta\boldsymbol{\tau}_{\text{act}} \in \mathbb{R}^{3\times 1}$ are the actual changes in moments determined by multiplying the moment of inertia tensor $\mathbf{I} \in \mathbb{R}^{3\times 3}$ with the change in measured rotational accelerations $\Delta\dot{\boldsymbol{\omega}} \in \mathbb{R}^{3\times 1}$. In this equation it is assumed the time-scale separation principle applies, meaning that the rotational accelerations measured are mainly caused by effector deflections and not by airframe contributions. However, the goal is not to estimate the full CEJ but only the ΔCEJ. By substituting Equation (6.1) into Equation (6.2) an error equation containing ΔCEJ is obtained:

$$\text{error}(k) = \left(\text{CEJ}_{\text{spline}}(k) + \Delta\text{CEJ}(k)\right) \cdot \Delta\boldsymbol{\delta} - \mathbf{I} \cdot \Delta\dot{\boldsymbol{\omega}} \tag{6.3}$$

With the error for the least mean square filter defined the full equation for the filter is as follows:

$$\Delta\text{CEJ}(k) = \Delta\text{CEJ}(k-1) - \boldsymbol{\mu}_2 \cdot \left(\left[\text{CEJ}_{\text{spline}}(k-1) + \Delta\text{CEJ}(k-1)\right] \cdot \Delta\boldsymbol{\delta} - \mathbf{I} \cdot \Delta\dot{\boldsymbol{\omega}}\right) \cdot \Delta\boldsymbol{\delta}^T \cdot \boldsymbol{\mu}_1 \tag{6.4}$$

where the new symbols $\boldsymbol{\mu}_1 \in \text{R}^{13\times 13}$ and $\boldsymbol{\mu}_2 \in \text{R}^{3\times 3}$ are diagonal matrices containing adaptation constants for the 13 effectors and 3 axes respectively. Any knowledge about damage can be incorporated into these matrices. For the scope of this research it is assumed a Fault Detection and Isolation (FDI) module is in place which can provide accurate damage information. So for example when it is known that only a certain effector is damaged the adaptation constant for this effector can be set to a non-zero value while keeping the rest of the constants at zero, thereby making sure only the effectiveness of the damaged effector is updated.

From the equation it is also clear that when there is no discrepancy between the expected and actual moments no update takes place. This is useful since this adaptation only needs to take place when there is a mismatch. Another thing that can be noted is that when there is no input there is also no adaptation, or, when there is a lot of input there is faster adaptation. As was mentioned in [50], after a failure occurs the inputs given by the control system to counteract the induced motion creates sufficient inputs for identification.

An schematic of how the 'Adaptive Jacobian model' in Figure 6.1 would look like for this LMS-estimator can be seen in Figure 6.2. This will first be implemented in a 'perfect' environment without sensor noise and disturbances. If the LMS-estimator is found to be able to adapt the controller to certain failures and keep the aircraft flyable, sensor noise and disturbances will be added. As these disturbances will add noise to the angular acceleration measurements, a filter is required to make sure it does not adapt to the disturbances. This filter however will also introduce a delay in the angular acceleration measurement, so to make sure the input and output of the estimation algorithm are synchronized the filter is also applied to the actuator input. It was shown in [17] that this approach works for the estimation of the control effectiveness of a drone.

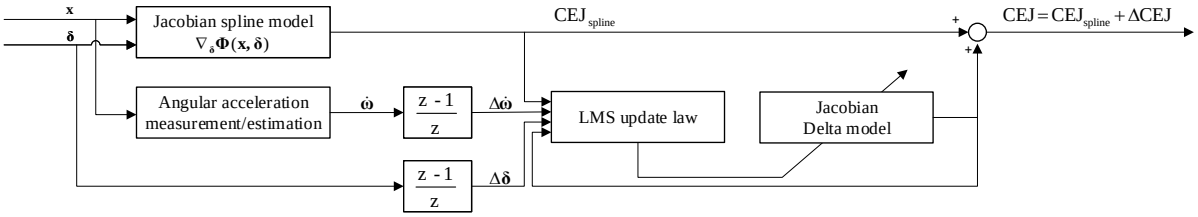

Figure 6.2: Schematic of the LMS-estimator.

6.1.2. Recursive least squares

A second estimation technique which can be used is the Recursive Least Squares (RLS) method. This is a modification of the ordinary/weighted least squares estimation algorithm which allows new data to be efficiently used to update a model in real-time. Compared to the LMS estimator it has a higher computational complexity as there are more matrix inversions and the covariance matrix needs to be determined at every step, but it has excellent convergence properties.

An advantage of the RLS compared to LMS is that it can estimate modeling functions instead of just single values. This way the ΔCEJ can be estimated using for example several polynomial functions. In [7] the RLS estimator is used to estimate aerodynamic uncertainties of an F-16 aircraft.

To make sure the RLS estimator does not saturate and will not adapt to new incoming data anymore the covariance matrix can be reset when a fault is detected. This way the algorithm will be unfrozen and start the estimation again. Another way this saturation can be prevented is by using a variable forgetting factor, such as the one proposed in [51]. This variable forgetting factor was again used in [7].

References

[1] Boeing Commercial Airplanes. Statistical Summary of Commercial Jet Airplane Accidents: Worldwide Operations | 1959-2017. Technical report, Aviation Safety, Boeing Commercial Airplanes, 2018.

[2] European Aviation Safety Agency. Annual Safety Review. Technical report, European Aviation Safety Agency, 2011.

[3] Civil Aviation Authority of the Netherlands (CAA-NL). Civil aviation safety data: 1993 - 2007. Technical report, Civil Aviation Authority of the Netherlands (CAA-NL), 2008.

[4] Netherlands Aviation Safety Board. Aircraft accident report 92-11: El Al Flight 1862. Technical report, Netherlands Aviation Safety Board, 1992.

[5] J. M. Maciejowski and C. N. Jones. MPC fault-tolerant flight control case study: flight 1862. *IFAC Proceedings Volumes*, 36(5):119–124, jun 2003.

[6] R. J. Montoya, W. E. Howell, W. T. Bundick, A. J. Ostroff, R. M. Hueschen, and C. M. Belcastro. Restructurable Controls. Technical report, NASA Langley Research Center, Hampton, VA, 1982.

[7] H. J. Tol, C. C. de Visser, L. G. Sun, E. van Kampen, and Q. P. Chu. Multivariate Spline-Based Adaptive Control of High-Performance Aircraft with Aerodynamic Uncertainties. *Journal of Guidance, Control, and Dynamics*, 39(4):781–800, 2016.

[8] K. M. Dorsett and D. R. Mehl. Innovative Control Effectors (ICE). Technical report, Lockheed Martin Tactical Aircraft Systems, Fort Worth, TX, 1996.

[9] I. Matamoros and C. C. de Visser. Incremental Nonlinear Control Allocation for a Tailless Aircraft with Innovative Control Effectors. In *2018 AIAA Guidance, Navigation, and Control Conference*, Reston, Virginia, jan 2018. American Institute of Aeronautics and Astronautics.

[10] K. M. Dorsett, H. P. Houlden, and S. P. Fears. Innovative Control Effectors (ICE) Phase II. Technical report, Lockheed Martin Tactical Aircraft Systems, Fort Worth, TX, 1997.

[11] W. J. Gillard and K. M. Dorsett. Directional control for tailless aircraft using all moving wing tips. *22nd Atmospheric Flight Mechanics Conference*, 1997.

[12] J. A. Bowlus, D. Multhopp, and S. S. Banda. Challenges and opportunities in tailless aircraft stability and control. *Guidance, Navigation, and Control Conference*, pages 1713–1718, 1997.

[13] M. A. Niestroy, K. M. Dorsett, and K. Markstein. A Tailless Fighter Aircraft Model for Control-Related Research and Development. In *AIAA Modeling and Simulation Technologies Conference*, pages 1–18, Reston, Virginia, jan 2017. American Institute of Aeronautics and Astronautics.

[14] B. J. Bacon and A. J. Ostroff. Reconfigurable flight control using nonlinear dynamic inversion with a special accelerometer implementation. In *AIAA Guidance, Navigation, and Control Conference and Exhibit*, pages 748–756, Reston, Virigina, aug 2000. American Institute of Aeronautics and Astronautics.

[15] S. Sieberling, Q. P. Chu, and J. A. Mulder. Robust Flight Control Using Incremental Nonlinear Dynamic Inversion and Angular Acceleration Prediction. *Journal of Guidance, Control, and Dynamics*, 33(6):1732–1742, 2010.

[16] P. Simplício, M. D. Pavel, E. van Kampen, and Q. P. Chu. An acceleration measurements-based approach for helicopter nonlinear flight control using incremental nonlinear dynamic inversion. *Control Engineering Practice*, 21(8):1065–1077, 2013.

[17] E. J. J. Smeur, Q. P. Chu, and G. C. H. E. de Croon. Adaptive Incremental Nonlinear Dynamic Inversion for Attitude Control of Micro Air Vehicles. *Journal of Guidance, Control, and Dynamics*, 39(3):450–461, 2016.

[18] T. A. Johansen and T. I. Fossen. Control allocation - A survey. *Automatica*, 49(5):1087–1103, 2013.

[19] E. N. Johnson and A. J. Calise. Pseudo Control Hedging: a New Method for Adaptive Control. In *Advances in Navigation Guidance and Control Technology Workshop*, Redstone Arsenal. AL, 2000.

[20] I. V. van der Peijl, C. C. de Visser, and M. A. Niestroy. *Physical Splines for Aerodynamic Modelling of Innovative Control Effectors*. Master's thesis, Delft University of Technology, 2017.

[21] H. J. Tol, C. C. de Visser, E. van Kampen, and Q. P. Chu. Nonlinear Multivariate Spline-Based Control Allocation for High-Performance Aircraft. *Journal of Guidance, Control, and Dynamics*, 37(6):1840–1862, nov 2014.

[22] J. Slotine and W. Li. *Applied Nonlinear Control*. Prentice-Hall, Englewood Cliffs, NJ, 1991.

[23] H. N. Nabi, T. J. J. Lombaerts, Y. Zhang, E. van Kampen, Q. P. Chu, and C. C. de Visser. Effects of Structural Failure on the Safe Flight Envelope of Aircraft. *Journal of Guidance, Control, and Dynamics*, 41(6):1–19, 2018.

[24] A. Mendes, E. van Kampen, B. Remes, and Q. P. Chu. Determining moments of inertia of small UAVs: A comparative analysis of an experimental method versus theoretical approaches. In *AIAA Guidance, Navigation, and Control Conference*, number August, pages 1–14, Reston, Virigina, aug 2012. American Institute of Aeronautics and Astronautics.

[25] B. J. Bacon and I. M. Gregory. General Equations of Motion for a Damaged Asymmetric Aircraft. In *AIAA Atmospheric Flight Mechanics Conference and Exhibit*, pages 1–13, Reston, Virigina, aug 2007. American Institute of Aeronautics and Astronautics.

[26] G. H. Shah and M. A. Hill. Flight Dynamics Modeling and Simulation of a Damaged Transport Aircraft. *AIAA Modeling and Simulation Technologies Conference*, (August):1–12, 2012.

[27] United States Air Force. The USAF Stability And Control Digital Datcom Volume 1: Users Manual. *Technical Report*, 1979.

[28] R. D. Finck. USAF Stability and Control DATCOM. *Flight Dynamics Labaratory*, 1978.

[29] J. A. Ouellette, B. Raghavan, M. J. Patil, and R. K. Kapania. Flight Dynamics and Structural Load Distribution for a Damaged Aircraft. *AIAA Atmospheric Flight Mechanics Conference*, (August):1–20, 2009.

[30] G. H. Shah. Aerodynamic Effects and Modeling of Damage to Transport Aircraft. In *AIAA Atmospheric Flight Mechanics Conference and Exhibit*, number August, pages 1–13, Reston, Virigina, aug 2008. American Institute of Aeronautics and Astronautics.

[31] T. J. J. Lombaerts. *Fault Tolerant Flight Control - a physical model approach*. PhD thesis, Delft University of Technology, 2010.

[32] J. Jiang and X. Yu. Fault-tolerant control systems: A comparative study between active and passive approaches. *Annual Reviews in Control*, 36(1):60–72, apr 2012.

[33] P. S. Maybeck and R. D. Stevens. Reconfigurable flight control via multiple model adaptive control methods. *IEEE Transactions on Aerospace and Electronic Systems*, 27(3):470–480, 1991.

[34] E. Van Oort. *Adaptive Backstepping Control and Safety Analysis for Modern Fighter Aircraft*. PhD thesis, Delft University of Technology, apr 2011.

[35] P. van Gils, E. van Kampen, C. C. de Visser, and Q. P. Chu. *Adaptive Incremental Backstepping Flight Control for a High-Performance Aircraft with Uncertainties*. PhD thesis, Delft University of Technology, Reston, Virginia, jan 2015.

[36] M. Krstic, P. V. Kokotovic, and I. Kanellakopoulos. *Nonlinear and Adaptive Control Design*. John Wiley & Sons, Inc., New York, NY, USA, 1 edition, 1995.

[37] A. Casavola and E. Garone. Fault-tolerant adaptive control allocation schemes for overactuated systems. *International Journal of Robust and Nonlinear Control*, 20(17):1958–1980, nov 2010.

[38] R. L. Eberhardt and D. G. Ward. Indirect adaptive flight control of a tailless fighter aircraft. *Guidance, Navigation, and Control Conference and Exhibit*, (c), 1999.

[39] D. B. Doman and A. D. Ngo. Dynamic Inversion-Based Adaptive/Reconfigurable Control of the X-33 on Ascent. *Journal of Guidance, Control, and Dynamics*, 25(2):275–284, 2002.

[40] E. Lavretsky. Combined/Composite Model Reference Adaptive Control. *IEEE Transactions on Automatic Control*, 54(11):2692–2697, nov 2009.

[41] J. Zhang, X. Yang, and L. Yang. Virtual-command-based model reference adaptive control for abrupt structurally damaged aircraft. *Aerospace Science and Technology*, 78:452–460, 2018.

[42] J. G. Ziegler and N. B. Nichols. Optimum Settings for Automatic Controllers. *Journal of Dynamic Systems, Measurement, and Control*, 115(2B):220–222, jun 1993.

[43] L. Sonneveldt, Q. P. Chu, and J. A. Mulder. *Adaptive Backstepping Flight Control for Modern Fighter Aircraft*. PhD thesis, Delft University of Technology, jul 2011.

[44] W. Falkena. *Investigation of Practical Flight Control Systems for Small Aircraft*. PhD thesis, Delft University of Technology, dec 2012.

[45] R. C. van 't Veld, E. van Kampen, and Q. P. Chu. Stability and Robustness Analysis and Improvements for Incremental Nonlinear Dynamic Inversion Control. *2018 AIAA Guidance, Navigation, and Control Conference*, (January), 2018.

[46] E. J. J. Smeur, G. C. H. E. de Croon, and Q. P. Chu. Cascaded incremental nonlinear dynamic inversion for MAV disturbance rejection. *Control Engineering Practice*, 73(January):79–90, 2018.

[47] J. B. Davidson, F. J. Lallman, and W. T. Bundick. Real-time adaptive control allocation applied to a high performance aircraft. In *5th SIAM Conference on Control and its Applications*, pages 1–11, 2001.

[48] A. J. Ostroff and B. J. Bacon. Enhanced NDI strategies for reconfigurable flight control. *Proceedings of the 2002 American Control Conference*, pages 3631–3636, 2002.

[49] S. Haykin and B. Widrow. *Least-mean-square Adaptive Filters*. Wiley, Hoboken, NJ, 2003.

[50] Y. Zhang, C. C. de Visser, and Q. P. Chu. Aircraft Damage Identification and Classification for Database-Driven Online Flight-Envelope Prediction. *Journal of Guidance, Control, and Dynamics*, pages 1–12, 2017.

[51] T. Fortescue, L. Kershenbaum, and B. Ydstie. Implementation of self-tuning regulators with variable forgetting factors. *Automatica*, 17(6):831–835, nov 1981.

[52] H. Mehmood, H. J. Tol, and C. C. de Visser. Multivariate Spline-Based Adaptive Control for High Performance Aircraft in the Presence of Atmospheric Turbulence. (January), 2018.

II

Scientific paper

Adaptive Incremental Nonlinear Control Allocation for the Innovative Control Effectors aircraft

M.J. Mollema[1] and C.C. de Visser[2]
Delft University of Technology, 2629 HS Delft, The Netherlands

In this paper an adaptive version of the incremental nonlinear control allocation (INCA), which is able to account for sudden changes in the aerodynamic configuration of an aircraft, is investigated. The controller is designed for the highly maneuverable and tailless innovative control effectors (ICE) aircraft, which has a control suite of 13 nonlinear, interacting and axis-coupled effectors. The least mean squares (LMS) method is used to estimate a delta control effectiveness Jacobian (CEJ) based on the difference between the expected and measured accelerations of the aircraft. This delta CEJ model is then added to the onboard spline CEJ model to achieve fault tolerance. By keeping the nominal spline model intact the nonlinearities and interactions of the effectors remain modeled, while the LMS estimator allows for fast adaptation. Simulations for four different maneuvers and failure cases showed that the estimator is able to stabilize the aircraft for the most demanding maneuver. For two less demanding maneuvers the adaptive controller greatly reduced the control effort while keeping the tracking error similar to the non-adaptive controller. For the remaining fourth maneuver, which operates in a flight region with the most significant interactions and nonlinearities, the adaptive controller had a reduced performance compared to the non-adaptive controller. A sensitivity analysis showed that the choice of design parameters greatly influences the results, and no general set of best performing parameters was found.

---

[1] MSc student, Control and Simulation Division, Faculty of Aerospace Engineering, Kluyverweg 1, 2629HS, Delft, The Netherlands
[2] Assistant Professor, Control and Simulation Division, Faculty of Aerospace Engineering, Kluyverweg 1, 2629HS, Delft, The Netherlands, AIAA member

I. Introduction

Many researches have demonstrated the potential benefit of having fault tolerant control (FTC) implemented for safety [1–3]. These FTC systems are a type of flight control system that is able to maintain performance and stability in the event of component failures, structural damage or aerodynamic failures. FTC is made possible due to the fact that most airplanes have a redundant set of control surfaces.

Most FTC systems are designed for conventional aircraft and assume a linear relationship between the control forces and moments and the actuator position. Generally speaking this assumption holds when the aircraft is operating under nominal conditions. However, under off-nominal conditions the actuators might deflect to extreme positions where this assumption does not hold any more. But it is exactly in these off-nominal and faulty conditions that a FTC system should be able to generate the correct control forces and moments, which it might not be able to do due to the wrong assumption of linearity in the extreme regions of the actuator positions.

An interesting example of an unconventional, highly nonlinear, overactuated aircraft is the Lockheed-Martin innovative control effectors (ICE) research aircraft concept [4]. Designed in the 90's as a highly maneuverable fighter aircraft with reduced weight and low radar cross-section (RCS), resulting in a tailless design with the control surface and external airframe edges aligned. Due to this alignment and the removal of the vertical stabiliser the control suite of the ICE-aircraft exhibits a high degree of coupling between all body axes (roll, pitch and yaw) as well as high nonlinearities between the different control surfaces.

As the ICE-aircraft is overactuated a control allocation (CA) module is required to distribute the required control moments over the redundant set of actuators. Recently such a method for the ICE-aircraft has been proposed in [5], named incremental nonlinear control allocation (INCA), which is able to make full use of the axis-coupling and nonlinearities of the control suite in real-time. The method relies on an onboard aerodynamic spline model of the aircraft [6], known as the control effectiveness Jacobian (CEJ). This multivariate spline model depends on different aircraft states and

effector positions, and could be identified online to make the aircraft adaptive to model mismatch and failures. This approach has been investigated before for an F-16 aircraft [3], where the spline models were estimated online using recursive least squares (RLS). Another possible approach is to directly estimate the error in the CEJ, which is the approach used in this research. The estimation is done using a least mean squares (LMS) estimator, similar to the one used for a quadcopter in [7]. The results presented in this paper investigate the performance of two adaptive controllers in the presence of aerodynamic model mismatch for different failure cases and maneuvers and compare the results to the current non-adaptive INCA controller. The main contribution of this paper is the design of an adaptive component for the INCA controller which is able to account per axis for reduced control effectiveness using a LMS-estimator.

II. The Innovative Control Effectors aircraft

The aircraft under consideration for this research is the ICE aircraft designed by Lockheed Martin in the 1990's [4, 8]. The goal of the program was to develop an aircraft which would meet new requirements for improved stealth characteristics, high maneuverability and a reduction in airframe weight [9]. This concept is a supersonic tailless flying wing design with a leading edge sweep of 65 degrees, a single engine capable of thrust-vectoring and an unconventional set of innovative control effectors. This section will first discuss this control suite, after which the aerodynamic model used to simulate the aircraft is described.

A. Control Suite

The control suite of the ICE aircraft consists of 13 control effectors and is therefore overactuated. A schematic overview of all the effectors and their location on the aircraft can be seen in Fig. 1.

Each of these effectors provide a different type of control power: both the inboard and outboard leading edge flaps (LEFs) provide lateral directional control at high angle of attack (AoA) and exhibit significant interactions between the inboard and outboard parts, the all-moving wing tips (AMT) are used to provide yaw control power, however, they have a significant adverse effect on the elevons, reducing their effectiveness at low to medium AoA. These elevons are able to generate pitch and roll moments by deflecting symmetrically or asymmetrically. Another option is to deflect

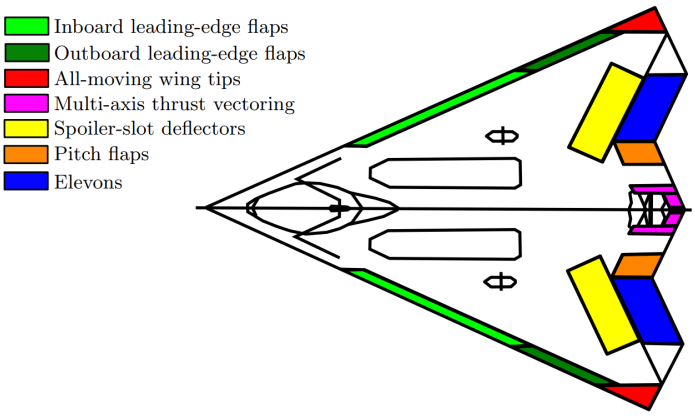

Fig. 1 The control suite of the ICE-aircraft. [5]

them independently causing secondary-axis yawing moments. Next to the elevons are the pitch flaps (PFs), which are deflected symmetrically to provide pitch control. The final control surfaces are the spoiler-slot deflectors (SSDs). Unlike conventional spoilers, the SSDs have a slot that is opened between the upper and lower skin when deflecting. They provide lateral-directional control even at high AoA and transonic speeds. When deflecting the SSD the effectiveness of the downstream PF and elevon can be degraded severely. [4, 5, 8, 10]

Next to these control surfaces, the ICE aircraft also has multi-axis thrust vectoring (MATV) capabilities, which is most powerful at low speeds where it provides yaw an pitch control power. It can also be used to enhance roll capabilities and high AoA. [9, 10]

The position and rate limits of the effectors can be seen in Table 1, next to how a positive deflection is defined and how the dynamics are described. These dynamics are modeled as the second-order transfer function in Equations (1) and (2).

$$H_l(s) = \frac{(18)(100)}{(s+18)(s+100)} \qquad (1) \qquad\qquad H_h(s) = \frac{(40)(100)}{(s+40)(s+100)} \qquad (2)$$

B. High fidelity aerodynamic model

The aerodynamic model of the ICE-aircraft is provided by Lockheed Martin in the form of dimensionless coefficients for the forces and moments stored in lookup tables. To be able to capture the interactions and nonlinearities of the different effectors, the coefficients are a summation of nonlinear smaller components, as can be seen in Eq. (3). A more detailed description of each

Table 1 Dynamic properties and limits of the ICE-aircraft effectors. [5]

Control effector	Notation	Positive deflection	Position limits [deg]	Rate limits [deg/s]	Dynamics
Inboard LEF	$\delta_{\text{lfi}},\ \delta_{\text{rfi}}$	LED	[0, 40]	40	$H_l(s)$
Outboard LEF	$\delta_{\text{lfo}},\ \delta_{\text{rfo}}$	LED	[-40, 40]	40	$H_l(s)$
AMT	$\delta_{\text{la}},\ \delta_{\text{ra}}$	TED	[0, 60]	150	$H_h(s)$
Elevons	$\delta_{\text{le}},\ \delta_{\text{re}}$	TED	[-30, 30]	150	$H_h(s)$
SSD	$\delta_{\text{ls}},\ \delta_{\text{rs}}$	TEU	[0, 60]	150	$H_h(s)$
PF	δ_{pf}	TED	[-30, 30]	150	$H_h(s)$
MTV	$\delta_{\text{ptv}},\ \delta_{\text{ytv}}$	$\dot{\omega}$	[-15, 15]	150	$H_h(s)$

individual component and how this data was obtained can be found in [11].

$$C_i = \sum_{j=1}^{19} C_{ij}\left(\boldsymbol{\delta}, \alpha, \beta, M, \omega\right) \tag{3}$$

where $i = l, m, n, X, Y, Z$ and the components $C_{ij}\left(\boldsymbol{\delta}, \alpha, \beta, M, \omega\right)$ are stored in lookup tables.

C. Multi-axis thrust vectoring

The MATV also has an influence on the body forces and moments. It is defined that a positive MATV deflection results in negative pitching and yawing moments. With this convention, the effect of thrust vectoring on the body forces can be seen in Eq. (4) and the effect on the moments in Eq. (5). In these equations T is the total thrust force, d_n is the moment arm which is equal to 18.75 ft and δ_{ptv} and δ_{ytv} are the vectoring deflections in pitch and yaw direction. This 3D projection of the thrust vector was proposed in [5] as an extension to the model provided by Lockheed Martin and will be included in the next ICE-model release.

$$\mathbf{T} = T \begin{bmatrix} \cos\left(\delta_{\text{ptv}}\right) / \cos\left(\delta_{\text{ytv}}\right) \\ \cos\left(\delta_{\text{ptv}}\right) \tan\left(\delta_{\text{ytv}}\right) \\ \sin\left(\delta_{\text{ptv}}\right) \end{bmatrix} \tag{4}$$

$$\boldsymbol{\tau}_{\text{T}} = -\text{T} d_n \begin{bmatrix} 0 \\ \sin\left(\delta_{\text{ptv}}\right) \\ \cos\left(\delta_{\text{ptv}}\right) \tan\left(\delta_{\text{ytv}}\right) \end{bmatrix} \tag{5}$$

D. Mass properties

The mass properties of the ICE-aircraft are defined for a nominal configuration with 50% internal fuel and some missiles and other expendables, a lightweight, and a heavyweight configuration and can be found in Table 2.

Table 2 Mass properties for the three different configurations. [11]

	Configuration			
	Nominal	Lightweight	Heavyweight	
Weight	32,750	25,989	37,084	lbf
x_{cg}	38.84	40	36	% MAC
y_{cg}	0	0	0	in
z_{cg}	88.97	88.97	88.97	in
I_{xx}	35,479	35,479	42,576	slug $\cdot$ ft^2
I_{yy}	78,451	67,500	81,903	slug$\cdot$ ft^2
I_{zz}	110,627	83,800	118,379	slug$\cdot$ ft^2
I_{xz}	-525	-250	-525	slug$\cdot$ ft^2

The mean aerodynamic chord (MAC) is located at 160.84 inch measured from the nose of the aircraft and has a length of 345 inch [11]. This results in an x_{cg} of 294.8 inch for the nominal configuration, 298.8 inch for the lightweight and 285.0 inch for the heavyweight configuration. The vertical location of the center of gravity is measured from the ground when the aircraft is standing on its landing gear.

III. INCA-based Flight Control System

A flight control system (FCS) for the ICE-aircraft has been designed in [5], which is able to take advantage of the full control effector suite and can handle the nonlinearities between effectors in real-time. At the heart of the FCS is a novel control allocation (CA) method known as INCA [5]. This method is based on the incremental nonlinear dynamic inversion (INDI) method [12, 13]. Due to the incremental formulation and application of the time-scale separation principle the model dependency of the controller is reduced in a way that only the control derivatives are needed, whereas for the non-incremental method the stability derivatives are also needed. The time-scale separation principle can be applied to systems where the control deflections have a significantly higher influence than the states on the derivatives of the states, which has been proven true for several aerospace applications [7, 13, 14], and states that the influence of these states can be neglected at sufficiently high sampling rates. In this section the INDI and INCA method are derived and the application of INCA to the ICE-aircraft is discussed.

A. INDI derivation

For the derivation of the concept of INDI consider the following general nonlinear system:

$$\dot{\boldsymbol{x}} = \boldsymbol{f}(\boldsymbol{x}, \boldsymbol{u}) \tag{6}$$

This system can be linearized around the current state using a first-order Taylor series expansion, see Eq. (7), where the subscript '0' denotes that parameter is of the current time and no subscript are future values.

$$\begin{aligned} \dot{\boldsymbol{x}} &\approx \boldsymbol{f}(\boldsymbol{x}_0, \boldsymbol{u}_0) + \left.\frac{\partial \boldsymbol{f}(\boldsymbol{x}, \boldsymbol{u})}{\partial \boldsymbol{x}}\right|_{\boldsymbol{x}=\boldsymbol{x}_0, \boldsymbol{u}=\boldsymbol{u}_0} (\boldsymbol{x} - \boldsymbol{x}_0) + \left.\frac{\partial \boldsymbol{f}(\boldsymbol{x}, \boldsymbol{u})}{\partial \boldsymbol{u}}\right|_{\boldsymbol{x}=\boldsymbol{x}_0, \boldsymbol{u}=\boldsymbol{u}_0} (\boldsymbol{u} - \boldsymbol{u}_0) \\ \dot{\boldsymbol{x}} &\approx \dot{\boldsymbol{x}}_0 + F(\boldsymbol{x}_0, \boldsymbol{u}_0)\,(\boldsymbol{x} - \boldsymbol{x}_0) + G(\boldsymbol{x}_0, \boldsymbol{u}_0)\,(\boldsymbol{u} - \boldsymbol{u}_0) \end{aligned} \tag{7}$$

where the parts related to the system dynamics are presented by F and the control effectiveness by G. It is assumed in this equation that the sampling time is small and the control effector deflections are instantaneous, such that the time-scale separation principle can be applied, which leads to ignoring the second term containing F in the equation:

$$\begin{aligned} \dot{\boldsymbol{x}} &\approx \dot{\boldsymbol{x}}_0 + G(\boldsymbol{x}_0, \boldsymbol{u}_0)\,(\boldsymbol{u} - \boldsymbol{u}_0) \\ &\approx \dot{\boldsymbol{x}}_0 + G(\boldsymbol{x}_0, \boldsymbol{u}_0)\Delta\boldsymbol{u} \end{aligned} \tag{8}$$

By setting the derivative of the state vector as virtual-input, $\boldsymbol{\nu} = \dot{\boldsymbol{x}}$, in this equation the control input increment can be determined from the latest measurements and the required virtual control:

$$\Delta\boldsymbol{u} = G^{-1}(\boldsymbol{x}_0, \boldsymbol{u}_0)(\boldsymbol{\nu} - \dot{\boldsymbol{x}}_0) \tag{9}$$

B. INCA derivation

The INDI method works for systems that are not over-actuated, if a system is over-actuated the INCA method is required to solve for the required increments in actuator position. The INCA derivation starts from Eq. (8). In this equation the G matrix is split in a constant part independent

on the partial derivatives and a part that has partial derivatives, as well as setting the input to the system to be actuator deflections:

$$\boldsymbol{\nu}(\mathbf{x}) = \dot{\mathbf{x}} \approx \dot{\mathbf{x}}_0 + \mathbf{g}\left(\mathbf{x}_0\right) \frac{\partial \boldsymbol{\Phi}\left(\mathbf{x}_0, \boldsymbol{\delta}_0\right)}{\partial \boldsymbol{\delta}} \Delta \boldsymbol{\delta} \tag{10}$$

where $\boldsymbol{\nu}(\mathbf{x})$ is the virtual control input used to linearize the system, $\dot{\mathbf{x}}$ is the time-derivative of the state vector, $\mathbf{g}\left(\mathbf{x}_0\right)$ is the constant part of the control effectiveness, $\partial \boldsymbol{\Phi}\left(\mathbf{x}_0, \boldsymbol{\delta}_0\right) / \partial \boldsymbol{\delta}$ a Jacobian model containing the partial derivatives of the control effectiveness, and $\Delta \boldsymbol{\delta}$ an increment in control deflections. Solving for the required control deflections is possible if the CEJ is a square matrix as it requires inverting this matrix. However, for over-actuated systems such as the ICE-aircraft this matrix is non-square and therefore cannot be inverted. By implementing a control allocation scheme based on the relationship presented in Eq. (10) this problem can be overcome. First the notation is simplified using Eqs. (11) and (12):

$$\nabla_{\boldsymbol{\delta}} \boldsymbol{\Phi}\left(\mathbf{x}, \boldsymbol{\delta}\right) = \frac{\partial \boldsymbol{\Phi}\left(\mathbf{x}, \boldsymbol{\delta}\right)}{\partial \boldsymbol{\delta}} \tag{11}$$

$$\mathbf{d}_c = \mathbf{g}(\mathbf{x})^{-1}\left[\boldsymbol{\nu}(\mathbf{x}) - \dot{\mathbf{x}}_0\right] \tag{12}$$

where $\mathbf{d}_c$ is the pseudo-control input. The INCA problem is then defined as follows: given this pseudo-control input $\mathbf{d}_c$, the current state $\mathbf{x}_0$, current control positions $\boldsymbol{\delta}_0$ and acceleration measurements $\dot{\mathbf{x}}_0$, determine an increment in control deflections $\Delta \boldsymbol{\delta}$ such that

$$\begin{aligned} \nabla_{\boldsymbol{\delta}} \boldsymbol{\Phi}\left(\mathbf{x}_0, \boldsymbol{\delta}_0\right) \Delta \boldsymbol{\delta} &= \mathbf{d}_c \\ \text{subject to} \quad \underline{\Delta \boldsymbol{\delta}} \leq \Delta \boldsymbol{\delta} &\leq \overline{\Delta \boldsymbol{\delta}} \end{aligned} \tag{13}$$

In this equation $\underline{\Delta \boldsymbol{\delta}}$ and $\overline{\Delta \boldsymbol{\delta}}$ are upper and lower bands of local incremental constraints for the position and rate of the actuator. A visual representation of the INCA method can be seen in Fig. 2.

Due to the incremental formulation of the control allocation problem INCA is linear in the increments of the effector positions, allowing it to be solved using efficient linear control allocations solvers (e.g. recursive weighted pseudo-inverse or quadratic programming methods [15]). Next to that, the CEJ can be evaluated at every time-step for the current states $\mathbf{x}_0$ and deflections $\boldsymbol{\delta}_0$ which allows for capturing of the nonlinearities and interactions of the effectors. A final advantage of the

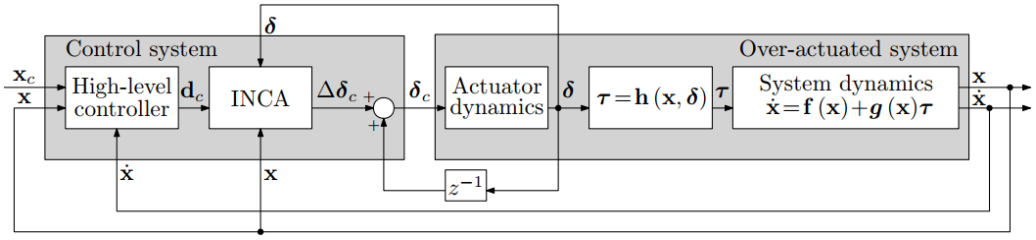

Fig. 2 Schematic of the INCA method. [5]

INCA method is the mitigation of negative actuator dynamics effects due to the feedback of actual actuator positions $\boldsymbol{\delta}_0$. A more in depth derivation and discussion of the INCA method can be found in [5].

C. INCA applied to ICE-aircraft

The INCA method has been applied to the inner angular rate control loop of the ICE-aircraft. For this application the required increments in control-induced moments $\Delta\boldsymbol{\tau}_c$ are used as the pseudo-control input $\mathbf{d}_c$. These required moment increments can be calculated using Eq. (14):

$$\Delta\boldsymbol{\tau}_c = \mathbf{I}\left[\boldsymbol{\nu}_\omega(\mathbf{x}) - \dot{\boldsymbol{\omega}}_0\right] \tag{14}$$

where $\mathbf{I}$ is the mass moment of inertia matrix, $\dot{\boldsymbol{\omega}}_0$ are measured angular accelerations and $\boldsymbol{\nu}_\omega(\mathbf{x})$ is the virtual control input coming from a PID-controller on the angular rate, as specified in Eq. (15).

$$\boldsymbol{\nu}_\omega(\mathbf{x}) = \mathbf{K}_{\omega_P}(\boldsymbol{\omega}-\boldsymbol{\omega}_c) + \mathbf{K}_{\omega_I}\int(\boldsymbol{\omega}-\boldsymbol{\omega}_c)\,dt + \mathbf{K}_{\omega_D}(\dot{\boldsymbol{\omega}}-\dot{\boldsymbol{\omega}}_c) \tag{15}$$

The commanded angular rates are the result of outer-control loops, of which an in depth discussion can be found in [5]. To prevent actuator saturation, which can happen when physically unachievable commands are given to the controller, pseudo-control hedging (PCH) [16] is applied to this angular rate loop. An overview of the inner angular rate control loop with INCA and PCH for the ICE-aircraft can be seen in Fig. 3.

As mentioned previously, INCA requires an estimation of the control effectiveness of the effectors, the CEJ. This CEJ is derived from a multivariate simplex spline model of the aerodynamic

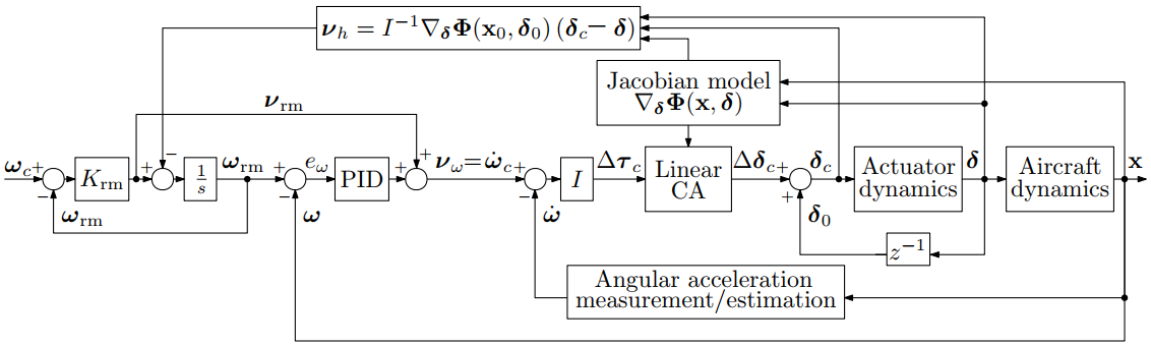

Fig. 3 Schematic of the angular rate control loop with INCA and PCH. [5]

characteristics of the ICE-aircraft, which was first identified as a 0^{th} order continuity model in [6]. To get the partial derivatives with respect to the effectors out of this model the methods presented in [17]. As the model has 0^{th} order continuity on the spline edges some discontinuity or jumps are present in the Jacobian, increasing the continuity order could therefore also improve the INCA method [5]. A spline model was chosen as it can provide a light-weight and accurate representation of the aerodynamic model and is really well suited for online system identification purposes.

IV. Adaptive-INCA using Least Mean Squares

One way to make INCA fault tolerant is to adapt the CEJ in real-time to account for changes in the effectiveness of the control surfaces. It has been shown that such adaptive controllers are effective in achieving fault tolerance, e.g. in [3] where a multivariate spline-based controller for an F-16 aircraft is adapted to aerodynamic uncertainties using a RLS approach, or in [7] where an the control effectiveness matrix of an incremental controller for a drone is estimated at every time-step using a LMS estimator.

There are however some differences between these two examples and the ICE-aircraft. For example, compared to the F-16 in [3] the onboard model of the ICE-aircraft is significantly more complex: 20 spline models for the F-16 compared to 216 for ICE. Because of this, adapting these spline models in real-time online represents a significant challenge. The control effectiveness of the drone in [7] is not based on splines but is a single matrix that is updated every time-step. However, as the CEJ is highly dependent on the aircraft state, an estimation based on a previous state is not necessarily a correct estimation for a new state.

The chosen approach for the ICE-aircraft is a combination of the two methods discussed above: the base spline CEJ model is considered to be static, but a 'delta CEJ' is re-estimated at every time-step and superimposed on the base model, as can be seen in Eq. (16). A updated schematic overview of the inner loop rate control including this adapting factor can be seen in Fig. 4.

$$\mathrm{CEJ}\left(\mathbf{x}_0, \boldsymbol{\delta}_0, \Delta\mathbf{x}, \Delta\boldsymbol{\delta}\right) = \mathrm{CEJ}_{\mathrm{spline}}\left(\mathbf{x}_0, \boldsymbol{\delta}_0\right) + \boldsymbol{\Delta}\mathrm{CEJ}\left(\Delta\mathbf{x}, \Delta\boldsymbol{\delta}\right) \tag{16}$$

With this approach, the controller can be made locally adaptive around the current state in real-time while keeping the global spline model capturing the nonlinearities and couplings intact. A concern could be that the model mismatch the $\boldsymbol{\Delta}$CEJ should approximate is not constant and that therefore the estimation algorithm will never converge to the required value in a single time-step. The INCA method however was already found to be robust to model mismatches up to a scaling factor of $\pm 40\%$ in [5]. For the estimation of this $\boldsymbol{\Delta}$CEJ the LMS approach is used, of which the implementation is discussed next.

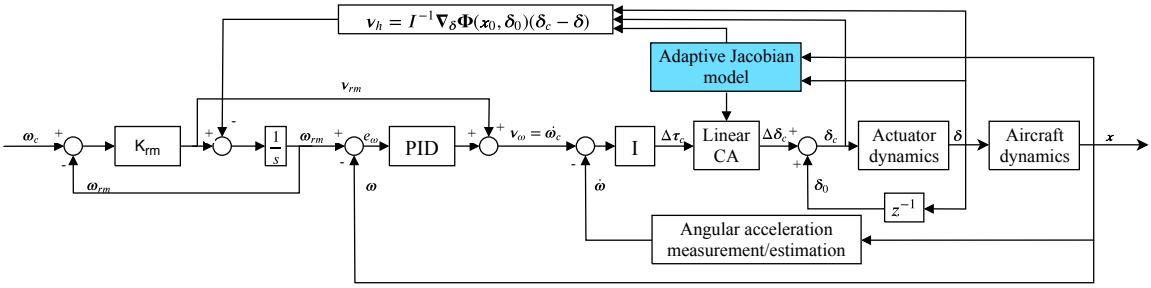

Fig. 4 Schematic of the adaptive INCA-based angular rate control system.

A. Least mean squares

The estimation of $\boldsymbol{\Delta}$CEJ is done using a least mean squares (LMS) adaptive filter [18]. This algorithm was also used in e.g. [7] to estimate the control effectiveness of a drone, or in [19] as a yaw moment controller on a car. The estimator works by determining the error between a predicted and the actual response and then updating the matrix based on this error. If the goal was to estimate

the full control effectiveness this error signal would be calculated according to Eq. (17):

$$\begin{aligned} \text{error} &= \boldsymbol{\Delta\tau_{\text{pred}}} - \boldsymbol{\Delta\tau_{\text{act}}} \\ &= \text{CEJ} \cdot \boldsymbol{\Delta\delta} - \mathbf{I} \cdot \boldsymbol{\Delta\dot{\omega}} \end{aligned} \tag{17}$$

where $\boldsymbol{\Delta\tau_{\text{pred}}} \in \mathbb{R}^{3\times1}$ are the predicted changes in moments around the aircraft which can be calculated by multiplying the CEJ $\in \mathbb{R}^{3\times13}$ with the change in effector position $\boldsymbol{\Delta\delta} \in \mathbb{R}^{13\times1}$, and $\boldsymbol{\Delta\tau_{\text{act}}} \in \mathbb{R}^{3\times1}$ are the actual changes in moments determined by multiplying the moment of inertia tensor $\mathbf{I} \in \mathbb{R}^{3\times3}$ with the change in measured rotational accelerations $\boldsymbol{\Delta\dot{\omega}} \in \mathbb{R}^{3\times1}$. In this equation it is assumed the time-scale separation principle applies, meaning that the rotational accelerations measured are mainly caused by effector deflections and not by airframe contributions. However, the goal is to estimate $\boldsymbol{\Delta}$CEJ. By substituting Eq. (16) into Eq. (17) an error equation containing $\boldsymbol{\Delta}$CEJ is obtained:

$$\text{error}(k) = \left(\text{CEJ}_{\text{spline}}(k) + \boldsymbol{\Delta}\text{CEJ}(k)\right) \cdot \boldsymbol{\Delta\delta} - \mathbf{I} \cdot \boldsymbol{\Delta\dot{\omega}} \tag{18}$$

With the error for the LMS estimator defined the full equation is as follows:

$$\boldsymbol{\Delta}\text{CEJ}(k) = \boldsymbol{\Delta}\text{CEJ}(k-1) - \boldsymbol{\mu}_2 \cdot \Big(\left[\text{CEJ}_{\text{spline}}(k-1) + \boldsymbol{\Delta}\text{CEJ}(k-1)\right] \cdot \boldsymbol{\Delta\delta} - \mathbf{I} \cdot \boldsymbol{\Delta\dot{\omega}}\Big) \cdot \boldsymbol{\Delta\delta}^T \cdot \boldsymbol{\mu}_1 \tag{19}$$

where $\boldsymbol{\mu}_1 \in \text{R}^{13\times13}$ and $\boldsymbol{\mu}_2 \in \text{R}^{3\times3}$ are diagonal matrices containing adaptation constants for the thirteen effectors and three axes respectively. Any knowledge about damage can be incorporated into these matrices. For the scope of this research it is assumed a Fault Detection and Isolation (FDI) module is in place which can provide accurate damage information on the effectors. It was found in the simulations that the best performing values for $\boldsymbol{\mu}_1$, with $\boldsymbol{\mu}_2$ specified to be the identity matrix, differ for each failure case and each maneuver it was tested on. The maximum absolute values for $\boldsymbol{\Delta}$CEJ are limited based on the $\text{CEJ}_{\text{spline}}$ values during nominal operation.

From Eq. (19) it is also clear that when there is no discrepancy between the expected and actual moments no update takes place. This is useful since this adaptation only needs to take place when there is a mismatch. Another thing that can be noted is that when there is no input there is also

no adaptation, or, when there is a lot of input there is faster adaptation. As was mentioned in [20], after a failure occurs the inputs given by the control system to counteract the induced motion creates sufficient inputs for identification. A schematic of how the 'Adaptive Jacobian model' in Fig. 4 would look like for this LMS-estimator can be seen in Fig. 5.

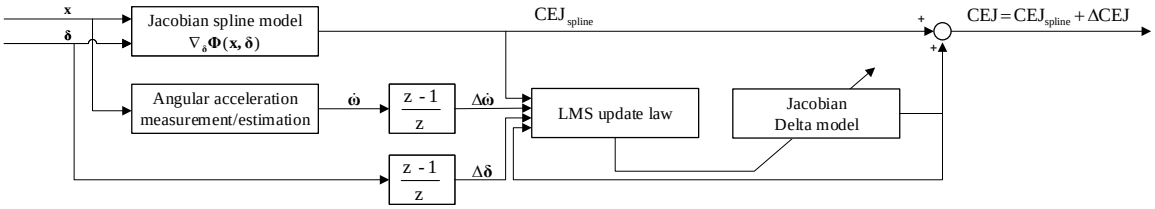

Fig. 5 Schematic of the LMS-estimator.

B. Variable step size least mean squares

Another way in which damage information can be incorporated is by making $\boldsymbol{\mu}_2$ adaptive based on the error signal. This is known as Variable step size least mean squares (VSS-LMS) [21]:

$$\boldsymbol{\mu}_2'(k) = \alpha \cdot \boldsymbol{\mu}_2(k-1) + \gamma \cdot \text{error}^2(k-1) \tag{20}$$

with

$$0 < \alpha < 1, \quad \gamma > 0$$

and

$$\boldsymbol{\mu}_2(k) = \begin{cases} \mu_{\max} & \text{if } \boldsymbol{\mu}_2'(k) > \mu_{\max} \\ \mu_{\min} & \text{if } \boldsymbol{\mu}_2'(k) < \mu_{\min} \\ \boldsymbol{\mu}_2'(k) & \text{otherwise} \end{cases}$$

Using this approach the amount of adaptation per axis can be controlled by the error and the two design parameters α and γ. Next to this, it might provide better convergence after a failure, as right after failure the error is high, so higher adaptation constants are needed. If the error becomes

smaller, the constant also reduces to make sure the estimation does not overshoot the actual value. The maximum value $\mu_{\max}$ was chosen to be 1 and the minimum value to be close to zero.

V. Simulation and results

To assess the performance of the Adaptive-INCA and normal INCA in the presence of sudden aerodynamic changes both controllers were tested in a simulation environment in Matlab and Simulink. The simulation is run in real-time using a sampling rate of 100 Hz. The initial flight conditions of the aircraft are in a trimmed state at an altitude of 20.000 ft and $M = 0.85$. For the scope of this research there is assumed to be no turbulence. The assessment is based on three metrics: the tracking error $\text{RMS}(\boldsymbol{u} - \boldsymbol{u}_C)$ determines the ability to follow commanded reference inputs, the allocation error $\text{RMS}(\boldsymbol{\tau} - \boldsymbol{\tau}_c)$ determines the ability of the inner-loop control allocation algorithm to attain the required control moments, and finally the control effort $\text{RMS}(\boldsymbol{\delta} - \boldsymbol{\delta}_p)$ specifies how much the effectors were deflected. In this section the failure case under consideration is discussed first, after which the maneuvers used for the assessment are presented. Finally the results are presented and discussed.

A. Failure case

For this research a failure case is defined where there is icing on the right inboard LEF, one second into the simulation. As most fighter aircraft do not have an anti-icing system in place for the airframe, a failure case like this can prove to be very dangerous. As the icing occurs on the LEF, its effectivenss will be reduced [22]. Next to this, the air behind the LEF will be disturbed as well, therefore also influencing the effectiveness of the downstream control surfaces: the SSD, elevon and pitch flap[1]. As there is also an interaction between the inboard and outboard LEF the coefficients for the outboard LEF will also be scaled down. It is also assumed that the normal force on the right wing will decrease and the axial force will increase due to the disturbed airflow. This asymmetrical force distribution in turn will result in an induced rolling and yawing moment.

---

[1] As the left and right pitch flaps are considered as a single effector in the look-up tables of Lockheed-Martin, the effectiveness of both are scaled equivalently, which also means no yawing or rolling moments can be introduced by the pitch flaps.

This failure case is simulated by adapting the nominal lookup tables from Lockheed Martin. All the affected surfaces are scaled according to Eq. (21):

$$C_{ij,failed} = a \cdot C_{ij,nominal} \tag{21}$$

with $i = \{l, m, n, X, Y, Z\}$ and j the indices of the affected control surfaces. The airframe aerodynamics are also scaled in this way to account for the reduced normal force and increased axial force, rolling moment and yawing moment. An overview of the applied scaling factors for different intensities of the failure can be seen in Table 3.

	LEF					Forces		Moments	
Failure case	Inboard	Outboard	Elevon	SSD	Pitch flap	Normal	Axial	Roll	Yaw
Light	0.5	0.8	0.6	0.6	0.6	1.0	1.0	1.0	1.0
Medium	0.5	0.8	0.6	0.6	0.6	0.8	1.3	1.3	1.2
Heavy	0.2	0.7	0.45	0.45	0.45	0.8	1.3	1.3	1.2

Table 3 Overview of used scaling factors for different failure cases.

B. Aggressive maneuvers

Since the ICE-aircraft is a highly maneuverable fighter jet it should be able to perform difficult maneuvers. In [5] four aggressive air combat acrobatic maneuvers were designed to test the INCA controller, and these maneuvers will again be used to assess the performance of the Adaptive-INCA. The four maneuvers are defined as follows:

- Maneuver A: a high bank angle coordinated spiral climb with the bank angle ϕ, flight path angle γ and sideslip angle β as control inputs and a load factor of 4.5. As it is a coordinated climb the sideslip angle command is zero, while the flight path angle has a reference of 15 deg and the bank angle is kept at 80 degrees. The maneuver is performed in 100 seconds.

- Maneuver B: consists of two consecutive barrel rolls with constant body pitch and roll rates of 12.75 deg/s, after which straight and level flight should be achieved. During the maneuver the sideslip angle is kept at zero. The duration of this maneuver is 47 seconds.

- Maneuver C: the most demanding move of the four, consisting of an aileron roll of 180 deg/sec for 4 seconds, an asymmetric looping of 18 deg/sec with a sideslip angle of 5 degrees for the first ten seconds of the looping and 0 degrees for the remaining ten, and half an aileron roll with 90 deg/sec input for 2 seconds followed by an Immelman turn to return to straight-and-level flight. The simulation runs for 45 seconds.

- Maneuver D: a high-AoA and high-sideslip maneuver to test the controller in the flight envelope regions where the nonlinearities and interactions of the controller are most significant. The commanded variables are the angle of attack α, sideslip angle β and the bank angle ϕ. The maneuver starts of with a ± 40 deg input doublet for α, followed by a doublet for β of ± 25 deg. The bank angle is kept zero at all times and the simulation is run for 27 seconds.

Fig. 6 shows the flight trajectories of the maneuvers for an undamaged case, and the damaged cases with and without adaptation.

C. Results

The performance of the three controllers (non-adaptive INCA, Adaptive-INCA and VSS-Adaptive-INCA) are presented here for the four maneuvers. For maneuvers A, B and D the simulation were run for the medium and high failure cases. For maneuver C however only the light simulation was run, as the other failure cases proved to be too extreme, even when a spline CEJ model of the failed aerodynamics was used in the simulations.

Figure 7 shows a timeseries plot of the commanded and attained moments together with the control effort for maneuver A with the high failure case, and Fig. 8 shows the control variables. As can be seen from the left plots, the non-adaptive controller is still able to follow the reference trajectory, albeit with a higher control effort. This robustness to a Jacobian model mismatch was also found in [5] and is a result of the incremental control allocation implementation with acceleration feedback in the inner loop. From the moment plots it can however be seen that with an adaptation module the commanded moments are followed slightly better, which can be seen most clearly from the lower peaks. A similar result is observed for maneuver B.

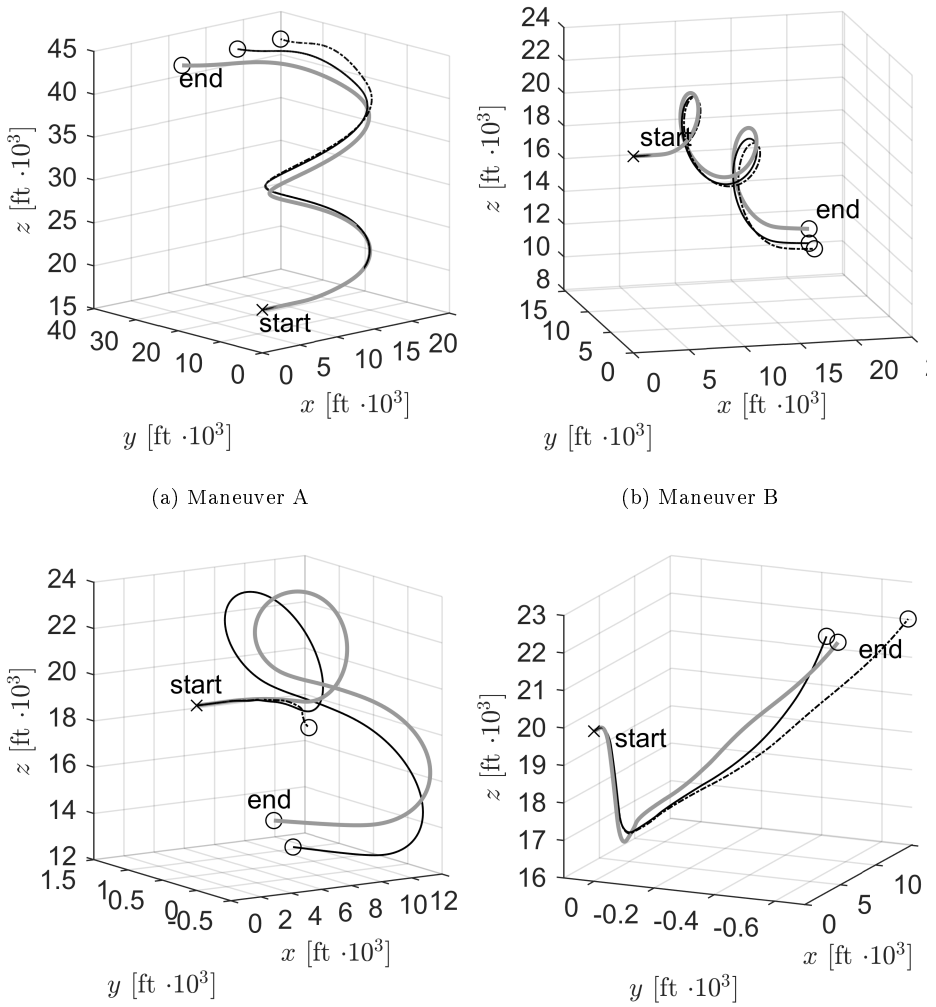

(a) Maneuver A

(b) Maneuver B

(c) Maneuver C

(d) Maneuver D

Fig. 6 Flight trajectories of the four maneuvers for the undamaged case (solid grey), damaged without adaptation (dot-dashed) and with adaptation (solid black).

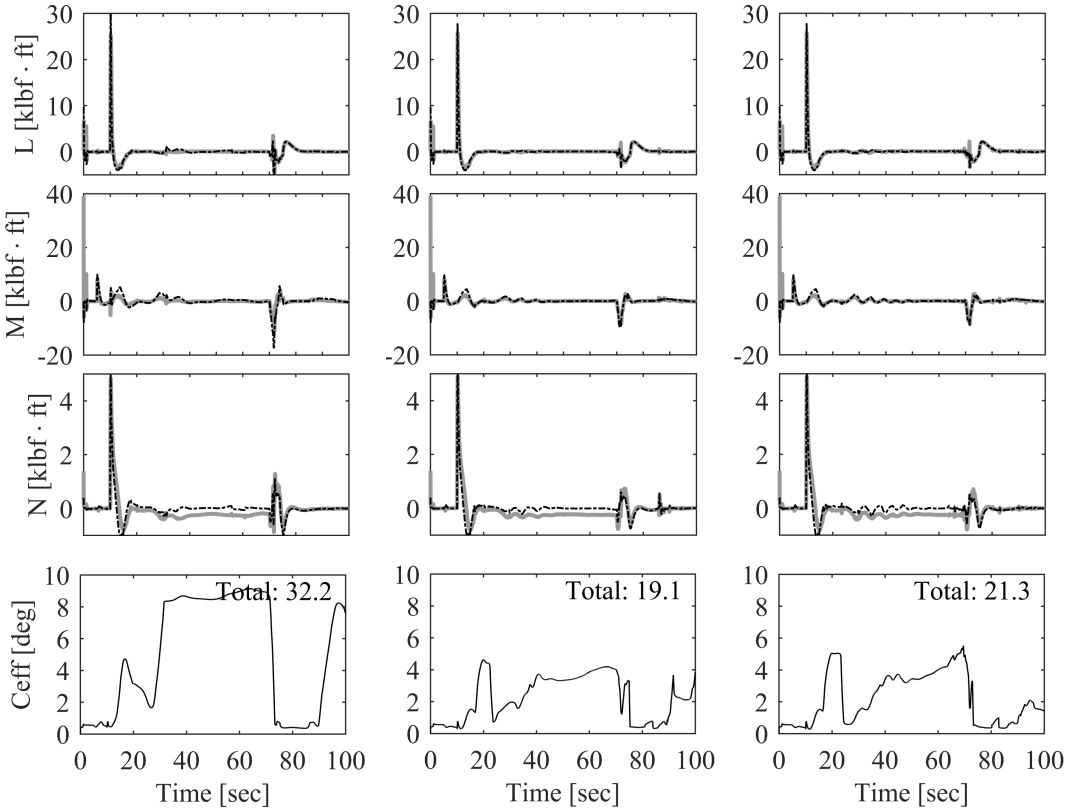

Fig. 7 Commanded (solid grey line) and attained (dot-dashed line) control-induced moments and control effort of maneuver A for INCA (left), Adaptive-INCA (middle) and VSS-Adaptive-INCA (right) for the high failure case.

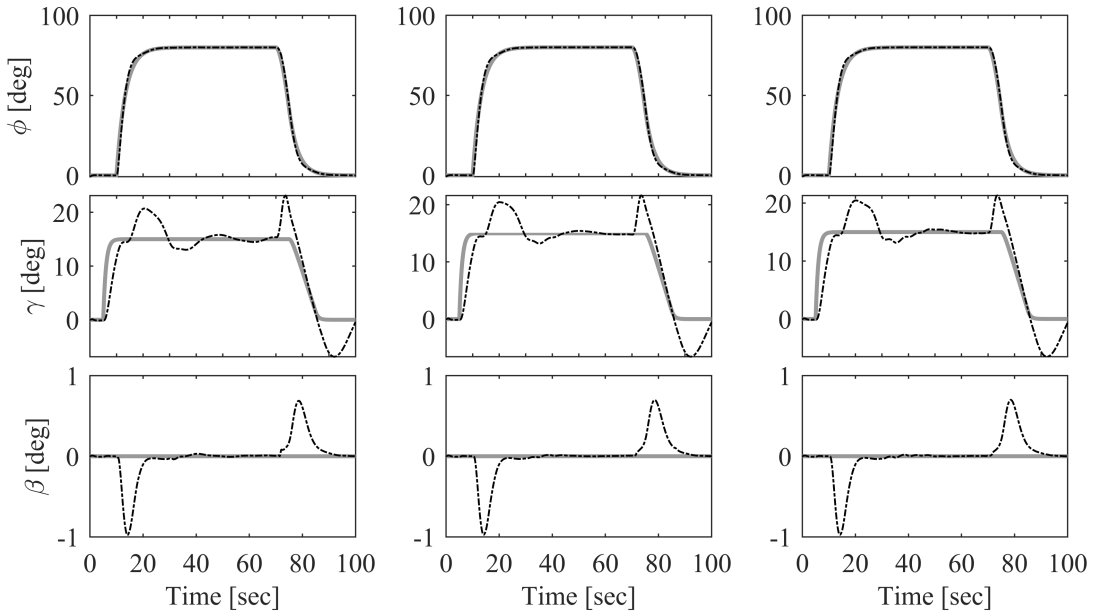

Fig. 8 Commanded (solid grey line) and attained (dot-dashed line) control variables of maneuver A for INCA (left), Adaptive-INCA (middle) and VSS-Adaptive-INCA (right) for the high failure case.

For maneuver C there is a significant difference between the non-adapting and adapting controllers, as can be seen in Figs. 9 and 10. Without adaptation, the aircraft becomes unstable very quickly, whereas with adaptation the controller is able to regain control after a few seconds after which it follows the commanded moments and control variables nicely again. This simulation perfectly shows the capability of an overactuated aircraft to regain control after a failure if an adapting element is in place.

Maneuver D has again a different result: the non-adapting controller has better or similar performance compared to the adapting ones. This can be seen from the RMS scores for the allocation error in Table 4. However, that does not mean that an adaptation module will never increase the performance in this case, as a simulation with a spline CEJ model of the failed aerodynamics shows better results: the total RMS for the high failure case is 30.2 klbf $\cdot$ ft compared to 38.5 for INCA. This decreased performance of the adapting controllers is therefore the result of a poorly performing LMS-estimator. The LMS method does not work in this case because maneuver D operates in the high AoA and sideslip regions where the nonlinearities and interactions are significant, and the

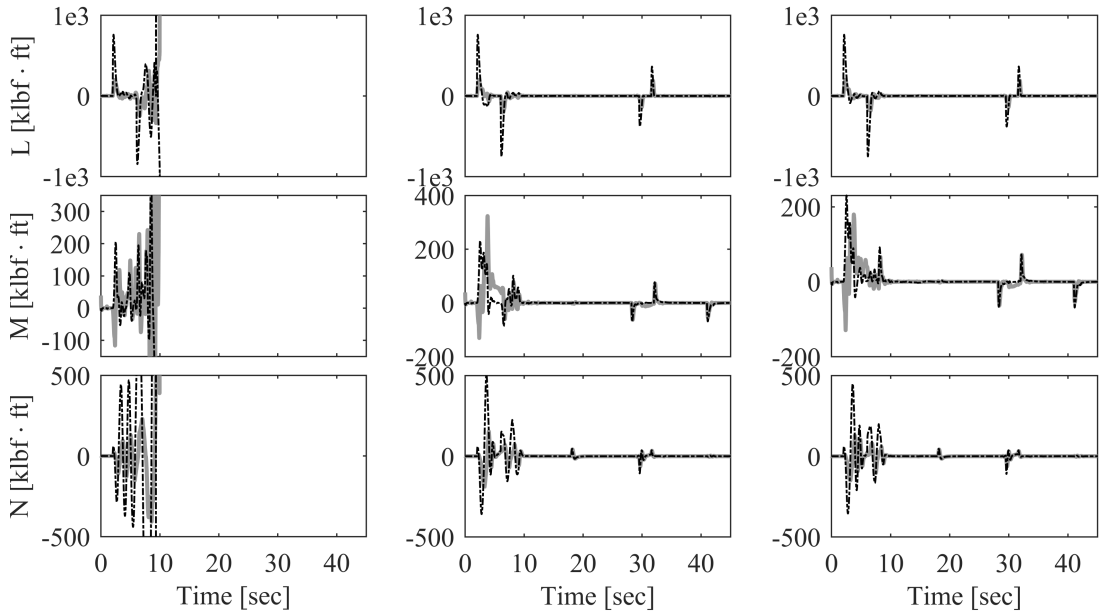

Fig. 9 Commanded (solid grey line) and attained (dot-dashed line) control-induced moments of maneuver C for INCA (left), Adaptive-INCA (middle) and VSS-Adaptive-INCA (right) for the light failure case.

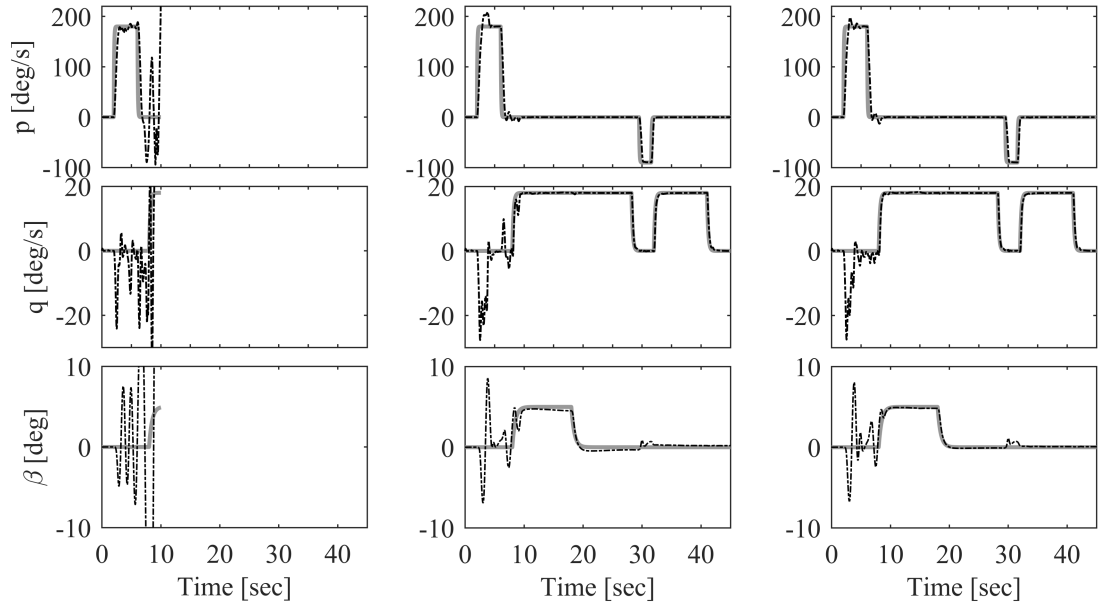

Fig. 10 Commanded (solid grey line) and attained (dot-dashed line) control variables of maneuver C for INCA (left), Adaptive-INCA (middle) and VSS-Adaptive-INCA (right) for the light failure case.

estimator does not take these aircraft states or the interactions between effectors into consideration.

Table 4 Allocation errors for the three controllers for maneuver D.

Controller	INCA		Adaptive-INCA		VSS-Adaptive-INCA	
Failure case	Medium	High	Medium	High	Medium	High
L [klbf · ft]	8.50	20.0	14.6	24.5	13.3	22.7
M [klbf · ft]	29.9	49.2	32.9	50.2	36.3	45.8
N [klbf · ft]	33.9	40.4	40.9	48.4	28.6	35.3
Total	26.6	38.5	31.5	42.7	27.8	35.9

The control effort is also a parameter of high interest and the scores for all four maneuvers are shown in Table 5. In this table the scores for maneuver A and B are especially interesting, as the control effort for the adapting controllers is lower than for INCA. So even though the adapting controllers do not increase the tracking and allocation performance for maneuver A and B, it does reduce the control effort required to follow the maneuvers. This result is important for a fighter jet such as the ICE-aircraft, as this will also keep the RCS at a lower level. The large discrepancy between INCA and the adapting controllers for maneuver C is because the INCA controller is not able to keep a stable trajectory, resulting in a lot of effector deflections. The control effort scores for maneuver D again show the inability of the LMS-estimator to handle nonlinearities and interactions.

Table 5 Total control effort [deg] of the simulated maneuvers with different failure cases for the three controllers.

Controller	INCA			Adaptive-INCA			VSS-Adaptive-INCA		
Failure case	Light	Medium	High	Light	Medium	High	Light	Medium	High
Maneuver A	-	27.5	32.2	-	16.4	23.3	-	16.1	21.3
Maneuver B	-	42.3	47.3	-	31.2	33.7	-	24.6	33.7
Maneuver C	141	-	-	56.2	-	-	56.6	-	-
Maneuver D	-	91.4	92.3	-	77.1	97.2	-	121	166

The convergence of single effectors to their failed values is also of interest. Figure 11 shows that the effectors actually do not converge to their failed value: the solid black line does not converge towards the dot-dashed line, even though the allocation error decreases when an adapting element is in place. This again is a flaw of the LMS estimator as it just distributes the error over all effectors, which can most clearly be seen from the fact that with adaptation the pitch flaps suddenly contribute

to the rolling and yawing moments. Next to the single effectors the total moment contribution also does not converge. Figure 12 however shows a magnitude plot of the CEJ contributions of the adapting and non-adapting controllers, as well as the ±40% scaling robustness bounds of the INCA controller [5]. From these plots it can be seen, especially in the zoomed-in plot, that the adapting controller is inside the robustness bounds more often, showing that the adaptation indeed does not need to converge to the perfect failed value to be able to stabilize the aircraft. The values are not always inside the bounds however, which could indicate that these bounds are not hard limits.

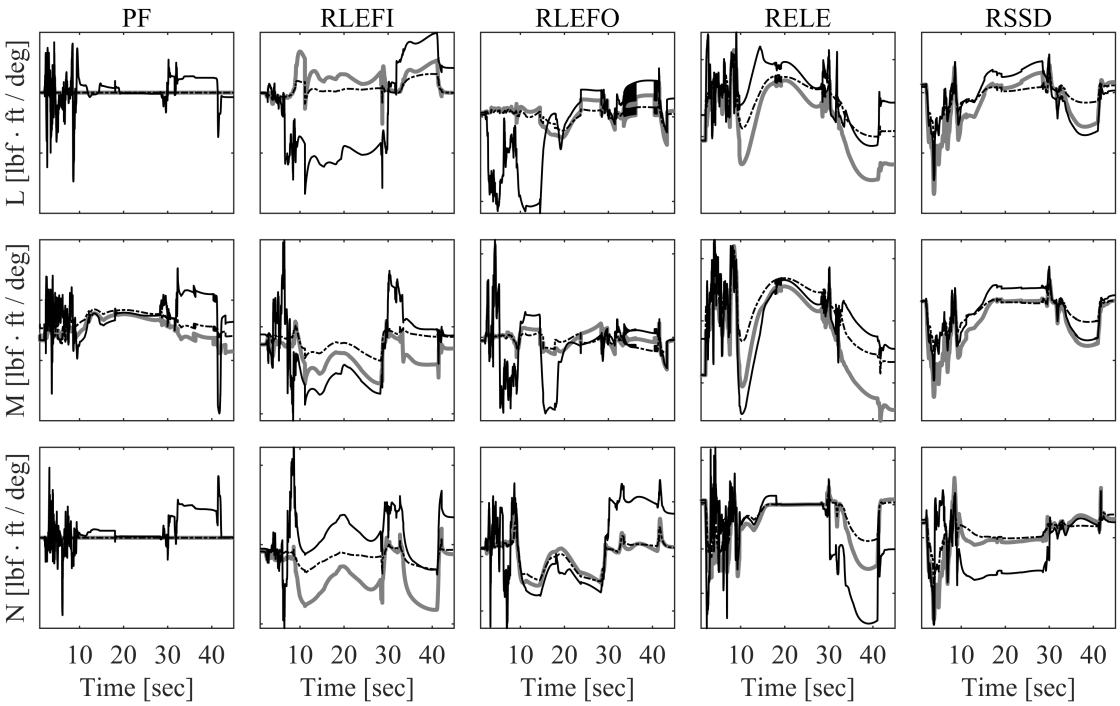

Fig. 11 CEJ contributions of the adapting VSS-LMS controller (solid black line), the original spline (solid grey line) and the failed spline (dot-dashed line) for the five failed effectors for maneuver C in the low failure case.

D. Adaptation parameter sensitivity

The results from the previous section were obtained using optimal values for the adaptation constants and parameters. These values were obtained from a gridsearch on the VSS-LMS parameters $\boldsymbol{\mu}_1$, α and γ, and the LMS parameter $\boldsymbol{\mu}_1$. The tested values for these three parameters are listed in Table 6.

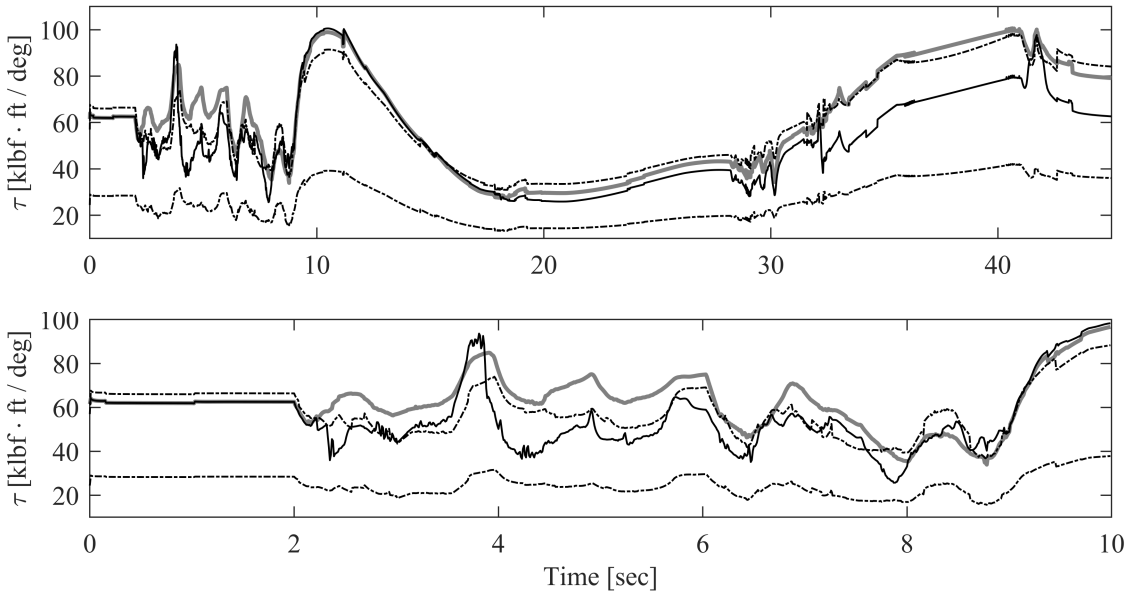

Fig. 12 Magnitude plot of the CEJ contributions of the adapting VSS-LMS controller (solid black line) and the original spline (solid grey line), as well as the ±40% robustness bounds (dot-dashed line) of the INCA controller for maneuver C with low failure case.

Table 6 Values used in the gridsearch for LMS and VSS-LMS.

Parameter	Tested values
$\boldsymbol{\mu}_1$	[1, 2, 5, 10, 15, 20, 25]
α	[0.5, 0.6, 0.7, 0.8, 0.85, 0.9, 0.95]
γ	[1e-6, 1e-5, 1e-4, 1e-3, 1e-2]

As mentioned previously, there is no one value for $\boldsymbol{\mu}_1$ that results in the best performance for all maneuvers and failure cases: e.g. for maneuver A a value of 20 has the best results, whereas this is 15 for B in the medium failure case and 5 for the high failure case. For maneuver D this is even more extreme, as it was already found that no adaptation is better for this maneuver, and a high adaptation constant such as the 20 used for maneuver A can even make the maneuver unstable.

From the gridsearch it was also found that the parameters for α and γ do not influence the results of the VSS-LMS significantly, whereas the maximum value for $\boldsymbol{\mu}_1$ does. This only holds for maneuvers A and B though, since adaptation makes maneuver D worse and maneuver C is such a demanding maneuver that the adaptation only works with the best parameters. To visualize this the boxplots in Fig. 13 were made for maneuver B. Each plot shows the spread of the allocation

error for when one of the parameters is kept constant and the others are varied: e.g. the leftmost plot shows for each tested value of $\boldsymbol{\mu}_1$ the scores of all combinations of the other two parameters.

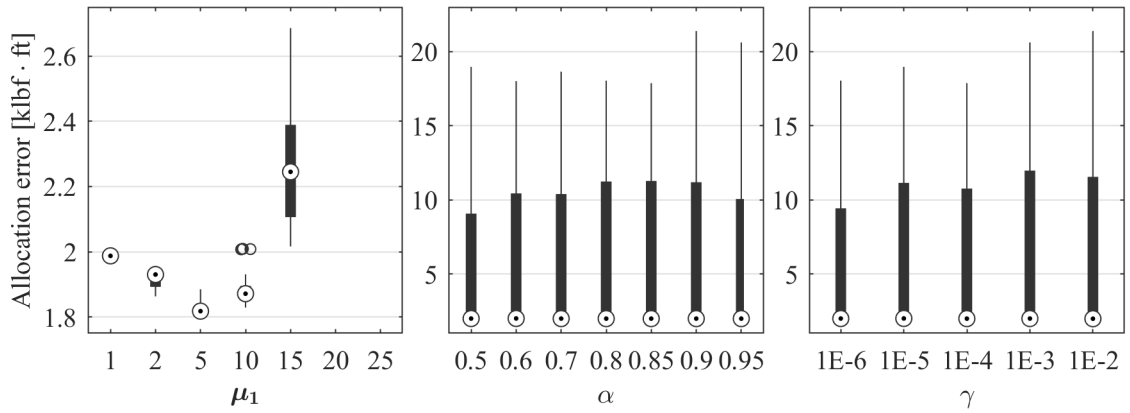

Fig. 13 Boxplots showing allocation error distribution of the gridsearch for maneuver B at the high failure case.

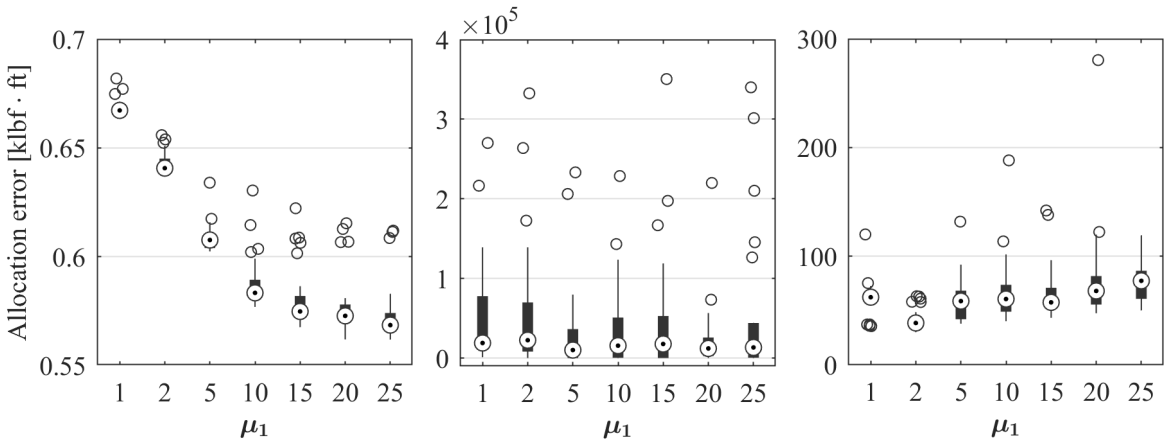

Fig. 14 Boxplots showing allocation error distribution of the μ_1 gridsearch for maneuver A (left), C (middle) and D (right).

As can be seen in these figures, the median, minimum and maximum values change with changing $\boldsymbol{\mu}_1$ with the best scores at a value of 5, while for α and γ these values remain more or less constant. The error for $\boldsymbol{\mu}_1$ equal to 20 and 25 becomes really high and thus does not show in this plot. This best score of 5 is not a general best score for multiple maneuvers however, as can be seen from Fig. 14. These plots show that maneuver A has the best performance for a value of 25, maneuver C does not have a general best performing value, and maneuver D has best performance when the

parameter resulting in the least adaptation is used.

The sensitivity of the adaptation module to the failure information coming from an fault detection and isolation (FDI) module is also important. This analysis is not performed for maneuver C as that maneuver only works with the perfect set of parameters due to the difficulty of it and therefore also only works with perfect FDI. For the other three maneuvers the results of the allocation error can be seen in Table 7. The analysis is performed for four different FDI outputs: the first one is a perfect fault estimation, the second one only detects the faulty LEFs on the right wing, the third one detects an error on the entire right wing, and the final one sets all effectors to faulty. From the scores it becomes clear that a good FDI module is of great importance: in three of the six cases where all effectors are adapted the resulting trajectory becomes unstable. Maneuver A even becomes unstable with the LMS adaptation in the case where the entire right wing is adapted, even though the right AMT is the only false-positive effector that is included in the FDI information. When only the LEFs are classified as faulty, the performance of the controllers is similar to the non-adapting INCA controller for maneuvers A and B. For maneuver D however the results improve when only the LEFs are adapted, which might be because it does not try to estimate the nonlinearities and interactions between the SSD and downstream effectors.

Table 7 Total allocation error [klbf · ft] of maneuvers A, B, and D for different FDI information.

	Perfect	LEFs	Right wing	All
LMS				
A	0.57	0.87	3.93E+5*	0.53
B	1.79	2.85	1.81	1.82
D	42.6	38.6	68.7	9.07E+03*
VSS				
A	0.56	0.87	0.58	1.31E+3*
B	1.79	2.84	1.82	1.85
D	35.9	32.5	59.0	1.65E+4*

* *Unstable trajectory.*

VI. Conclusions and recommendations

In this paper an adaptive version of the state-of-the-art incremental nonlinear control allocation (INCA) controller for the highly nonlinear and overactuated Lockheed-Martin innovative control

effectors (ICE) aircraft is presented. This controller attempts to achieve fault-tolerance by estimating the error between the measured rotational accelerations and the rotational accelerations as predicted from the onboard aerodynamic spline model of the control effectiveness, the control effectiveness Jacobian (CEJ). The error is then used to drive a least mean squares (LMS) update law, which estimates a delta CEJ that is added to the spline CEJ to approximate the failed CEJ. The combination of keeping the spline based CEJ and estimating the error using LMS allows for fast adaptation while keeping the nonlinearities and interactions intact in the spline models.

In this paper several experiments have been performed to test the feasibility of the adaptive controller. Simulations of four different maneuvers with different failure cases have shown that the controller is able to adapt to sudden aerodynamic failures in three cases. In two of the four maneuvers the non-adaptive INCA controller was already able to keep the trajectory due to the inherent robustness of this control allocation method. The adaptive controller however improved on this by reducing the control effort required to follow the trajectory. For the most demanding maneuver the adaptive controllers showed greatly improved performance as they were able to keep the aircraft stable, whereas the INCA controller became unstable very quickly. During the last maneuver, which operates in a flight region where nonlinearities and interactions are most significant, the LMS estimator resulted in a reduced performance, which is due to the inability of the estimator to take aircraft states and actuator interactions into account.

A sensitivity analysis showed that the design parameters of the estimator differed per maneuver, and no general set of parameters performing well in all cases was found. This unfortunately reduces the general applicability of this method as it of course is never known when a failure will occur and what the failure mode is. The results do show the potential of adaptive controllers, and that the adaptation can be done while keeping the time-scale separation principle assumption in place.

Future work on adaptive controllers for the ICE-aircraft can focus on several topics. For example on the effect of disturbances and noise, as these can influence the performance of parameter estimators. Also different estimators such as a RLS estimator can be used which does take aircraft states into account. Another interesting topic is the influence on the pseudo-control hedging (PCH) module, as this module uses the CEJ.

References

[1] Maciejowski, J. M. and Jones, C. N., "MPC fault-tolerant flight control case study: flight 1862," *IFAC Proceedings Volumes*, 10.1016/S1474-6670(17)36480-7.

[2] Montoya, R. J., Howell, W. E., Bundick, W. T., Ostroff, A. J., Hueschen, R. M., and Belcastro, C. M., "Restructurable Controls," Tech. rep., NASA Langley Research Center, Hampton, VA, 1982.

[3] Tol, H. J., de Visser, C. C., Sun, L. G., van Kampen, E., and Chu, Q. P., "Multivariate Spline-Based Adaptive Control of High-Performance Aircraft with Aerodynamic Uncertainties," *Journal of Guidance, Control, and Dynamics*, 10.2514/1.G001079.

[4] Dorsett, K. M. and Mehl, D. R., "Innovative Control Effectors (ICE)," Tech. rep., Lockheed Martin Tactical Aircraft Systems, Fort Worth, TX10.1016/0022-460X(71)90105-2.

[5] Matamoros, I. and de Visser, C. C., "Incremental Nonlinear Control Allocation for a Tailless Aircraft with Innovative Control Effectors," in "2018 AIAA Guidance, Navigation, and Control Conference," American Institute of Aeronautics and Astronautics, Reston, Virginia10.2514/6.2018-1116.

[6] van der Peijl, I. V., de Visser, C. C., and Niestroy, M. A., *Physical Splines for Aerodynamic Modelling of Innovative Control Effectors*, Master's thesis, Delft University of Technology, 2017.

[7] Smeur, E. J. J., Chu, Q. P., and de Croon, G. C. H. E., "Adaptive Incremental Nonlinear Dynamic Inversion for Attitude Control of Micro Air Vehicles," *Journal of Guidance, Control, and Dynamics*, 10.2514/1.G001490.

[8] Dorsett, K. M., Houlden, H. P., and Fears, S. P., "Innovative Control Effectors (ICE) Phase II," Tech. rep., Lockheed Martin Tactical Aircraft Systems, Fort Worth, TX, 1997.

[9] Bowlus, J. A., Multhopp, D., and Banda, S. S., "Challenges and opportunities in tailless aircraft stability and control," *Guidance, Navigation, and Control Conference*, 10.2514/6.1997-3830.

[10] Gillard, W. J. and Dorsett, K. M., "Directional control for tailless aircraft using all moving wing tips," 10.2514/6.1997-3487.

[11] Niestroy, M. A., Dorsett, K. M., and Markstein, K., "A Tailless Fighter Aircraft Model for Control-Related Research and Development," in "AIAA Modeling and Simulation Technologies Conference," American Institute of Aeronautics and Astronautics, Reston, Virginia, 2017, 10.2514/6.2017-1757.

[12] Bacon, B. J. and Ostroff, A. J., "Reconfigurable flight control using nonlinear dynamic inversion with a special accelerometer implementation," in "AIAA Guidance, Navigation, and Control Conference and Exhibit," American Institute of Aeronautics and Astronautics, Reston, Virigina, 2000, 10.2514/6.2000-4565.

[13] Sieberling, S., Chu, Q. P., and Mulder, J. A., "Robust Flight Control Using Incremental Nonlinear

Dynamic Inversion and Angular Acceleration Prediction," *Journal of Guidance, Control, and Dynamics*, 10.2514/1.49978.

[14] Simplício, P., Pavel, M. D., van Kampen, E., and Chu, Q. P., "An acceleration measurements-based approach for helicopter nonlinear flight control using incremental nonlinear dynamic inversion," *Control Engineering Practice*, 10.1016/j.conengprac.2013.03.009.

[15] Johansen, T. A. and Fossen, T. I., "Control allocation - A survey," *Automatica*, 10.1016/j.automatica.2013.01.035.

[16] Johnson, E. N. and Calise, A. J., "Pseudo Control Hedging: a New Method for Adaptive Control," in "Advances in Navigation Guidance and Control Technology Workshop," Redstone Arsenal. AL, 2000.

[17] Tol, H. J., de Visser, C. C., van Kampen, E., and Chu, Q. P., "Nonlinear Multivariate Spline-Based Control Allocation for High-Performance Aircraft," *Journal of Guidance, Control, and Dynamics*, 10.2514/1.G000065.

[18] Haykin, S. and Widrow, B., *Least-mean-square Adaptive Filters*, Wiley, Hoboken, NJ, 2003.

[19] Yim, S., "Integrated chassis control with adaptive algorithms," 10.1177/0954407015605947.

[20] Zhang, Y., de Visser, C. C., and Chu, Q. P., "Aircraft Damage Identification and Classification for Database-Driven Online Flight-Envelope Prediction," *Journal of Guidance, Control, and Dynamics*, 10.2514/1.G002866.

[21] Kwong, R. and Johnston, E., "A Variable Step Size LMS Adaptive Algorithm," , 1992.

[22] Ratvasky, T. P., Barnhart, B. P., and Lee, S., "Current Methods Modeling and Simulating Icing Effects on Aircraft Performance, Stability, Control," *Journal of Aircraft*, 10.2514/1.44650.

III

Conclusions and recommendations

Conclusions and recommendations

The literature survey on fault tolerant control (FTC) resulted in an overview and classification of the different types and implementations. From this overview the most promising category of FTC are the active, online redesign methods. These methods can be reconfigured based on the information supplied by a fault detection and isolation (FDI) module and therefore can be less conservative compared to passive methods and generally can account for more types of failures. Of the online redesign FTC methods adaptive controllers such as Model Reference Adaptive Control (MRAC), Self-Tuning Control (STC) or Adaptive Nonlinear Dynamic Inversion (ANDI) are the most promising. With adaptive controllers the onboard model on which the controllers relies to generate its control commands is adapted to compensate for model inaccuracies and/or changes in the aircraft parameters.

Another interesting type of FTC are the incremental versions of nonlinear dynamic inversion and backstepping. This incremental approach reduces the dependency on the onboard plant model, resulting in a more robust controller. The Incremental Nonlinear Control Allocation (INCA) method is already designed with this incremental approach and therefore has an inherent robustness against model mismatch. As these incremental controllers still rely on a reduced onboard model they can also be made adaptive, similar to the ANDI controller.

The effects of a structural failure on the ICE-aircraft have also been investigated in the literature survey. To model the effect of a structural failure on the mass properties several options are available. The new mass can simply be modeled by subtracting a percentage proportional to the damage from the total mass. The moment of inertia can then also be changed according to the lost mass and its position. A more precise estimation can be made by using CAD models, as the software used to create the models are able to calculate the mass properties of any model. The effect of structural damage on the location of the center of gravity (CG) can be neglected, as research on the NASA General Transport Model (GTM) with either a 24% wing loss or separation of an engine did not result in a substantial change in the CG location. For the remainder of the research the failure case was chosen to be one without any structural damage however, and therefore none of these methods was implemented.

Next to the mass properties, a structural failure also has effect on the aerodynamics. The simplest way, and the only way considered viable for this research, to model the changed aerodynamics is to scale the aerodynamic coefficients or add a constant term. Another option is to use CFD-programs. This method is, if performed correctly, already a lot more credible than the scaling of the coefficients. However, performing the simulations is not straightforward and requires time. A last method is to perform wind tunnel tests with a damaged model. And even though this will provide the best estimation, it is the least simple and least practical method to perform.

With the literature survey concluded, the remainder of the research was performed by implementing a FTC method and comparing it against the current INCA implementation. To make INCA fault tolerant, an adaptive element was superimposed on top of the nominal onboard multivariate spline model used by INCA. This element attempts to achieve fault-tolerance by estimating the error between the measured rotational accelerations and the rotational accelerations as predicted from the onboard aerodynamic spline model of the control effectiveness, the CEJ. The error is then used to drive a LMS update law, which estimates a delta CEJ that is superimposed on top of the spline CEJ to approximate the failed CEJ. The combination of keeping the spline based CEJ and estimating the error using LMS allows for fast adaptation while keeping the nonlinearities and interactions intact in the spline models.

During the research several experiments have been performed to test the feasibility of the adaptive controller. Simulations of four different maneuvers with different failure cases have shown that the controller is able to adapt to sudden aerodynamic failures in three cases. In two of the four maneuvers the non-adaptive INCA controller was already able to keep the trajectory due to the inherent robustness of this control allocation method. The adaptive controller however improved on this by reducing the control effort required to follow

the trajectory. For the most demanding maneuver the adaptive controllers showed greatly improved performance as they were able to keep the aircraft stable, whereas the INCA controller became unstable very quickly. During the last maneuver, which operates in a flight region where nonlinearities and interactions are most significant, the LMS estimator resulted in a reduced performance, which is due to the inability of the estimator to take aircraft states and actuator interactions into account.

A sensitivity analysis showed that the design parameters of the estimator differed per maneuver, and no general set of parameters performing well in all cases was found. This unfortunately reduces the general applicability of this method as it of course is never known when a failure will occur and what the failure mode is. The results do show the potential of adaptive controllers, and that the adaptation can be done while keeping the time-scale separation principle assumption in place.

Future work on adaptive controllers for the ICE-aircraft can focus on several topics. For example on the effect of disturbances and noise, as these can influence the performance of parameter estimators. To minimize these influences a low-pass filter can be implemented on both the angular acceleration measurements and the control deflections, as was done in [17], or the disturbances can be parameterized and included in the estimation algorithm, as done in [52]. Also different estimators such as a RLS estimator can be used which does take aircraft states into account and could result in a more generalizable adaptation module. Another interesting topic is the influence on the PCH module, as this module uses the CEJ to limit actuator saturation. To increase the fidelity of the obtained results a better damage model, e.g. obtained from CFD-simulations or wind tunnel testing, can be used. Further research into the robustness of INCA against model mismatch and sudden jumps in the CEJ can also prove very valuable, as this could make it more clear how well an adapting element should perform.

IV

Additional results

1

Maneuver A: High bank climbing spiral

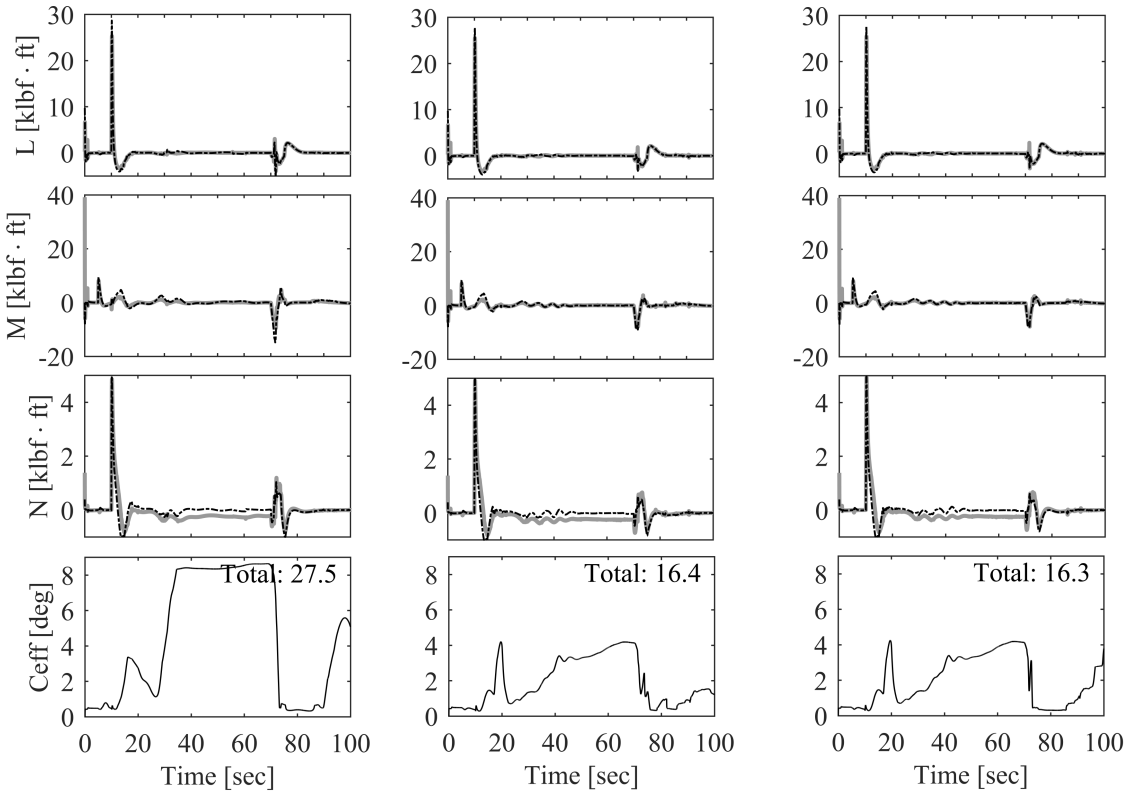

Figure 1.1: Commanded (dot-dashed line) and attained (solid line) control-induced moments and control effort of maneuver A with medium failure case for INCA (left), Adaptive-INCA (middle) and VSS-Adaptive-INCA (right).

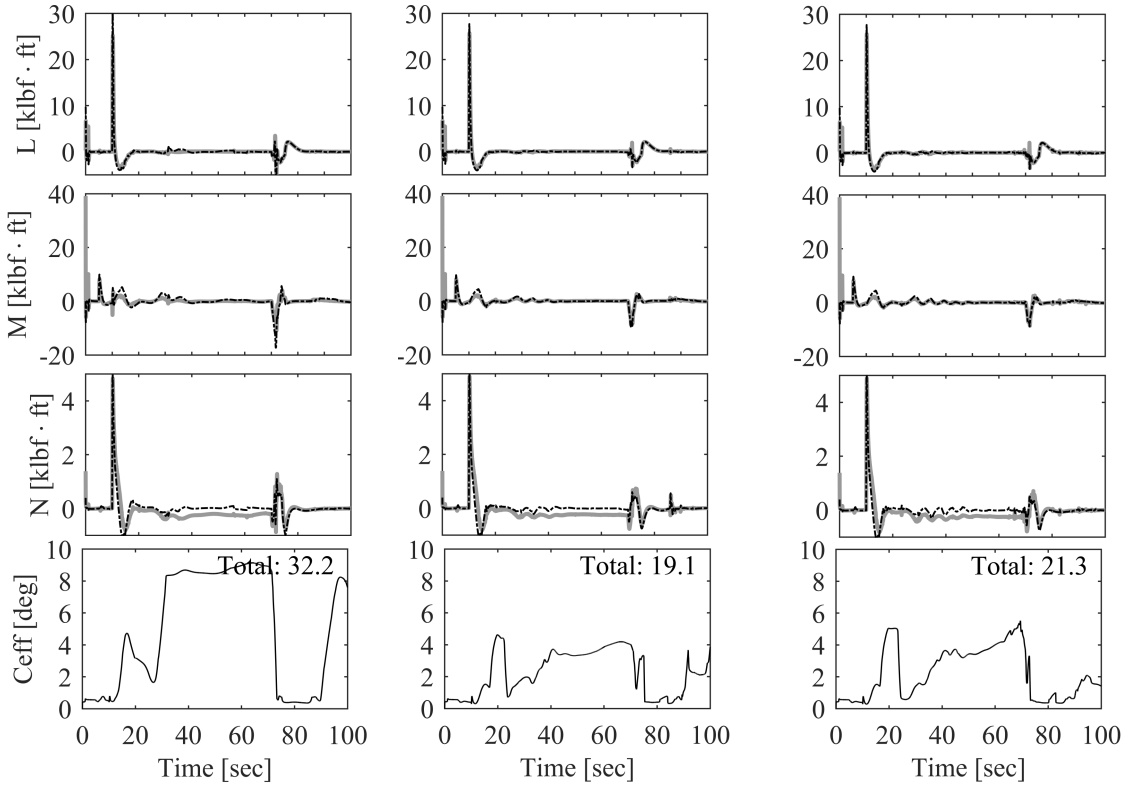

Figure 1.2: Commanded (dot-dashed line) and attained (solid line) control-induced moments and control effort of maneuver A with high failure case for INCA (left), Adaptive-INCA (middle) and VSS-Adaptive-INCA (right).

Table 1.1: Allocation errors for the three controllers for maneuver A.

Controller	INCA		Adaptive-INCA		VSS-Adaptive-INCA	
Failure case	Medium	High	Medium	High	Medium	High
L [klbf · ft]	0.56	0.71	0.45	0.47	0.45	0.47
M [klbf · ft]	1.14	1.37	0.79	0.83	0.79	0.82
N [klbf · ft]	0.24	0.25	0.23	0.24	0.23	0.23
Total	0.75	0.90	0.54	0.57	0.54	0.56

Table 1.2: Tracking errors for the three controllers for maneuver A.

Controller	INCA		Adaptive-INCA		VSS-Adaptive-INCA	
Failure case	Medium	High	Medium	High	Medium	High
ϕ [deg]	1.49	1.49	1.49	1.49	1.49	1.49
γ [deg]	3.37	3.36	3.19	3.20	3.19	3.18
β [deg]	0.24	0.24	0.24	0.24	0.24	0.24
Total	2.13	2.13	2.04	2.04	2.04	2.03

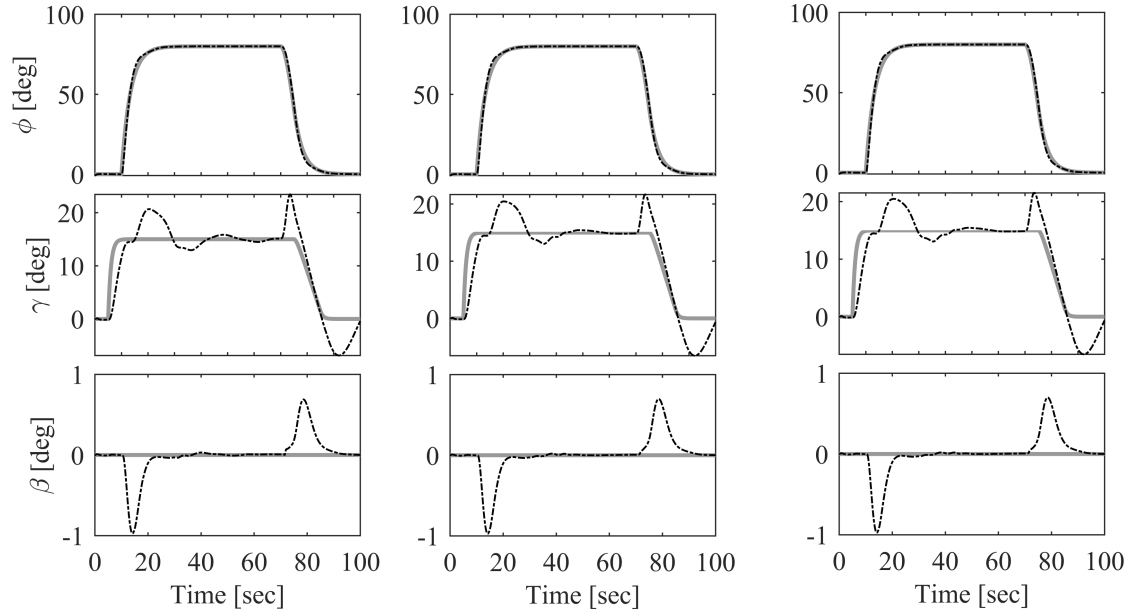

Figure 1.3: Commanded (dot-dashed line) and attained (solid line) control variables of maneuver A with medium failure case for INCA (left), Adaptive-INCA (middle) and VSS-Adaptive-INCA (right).

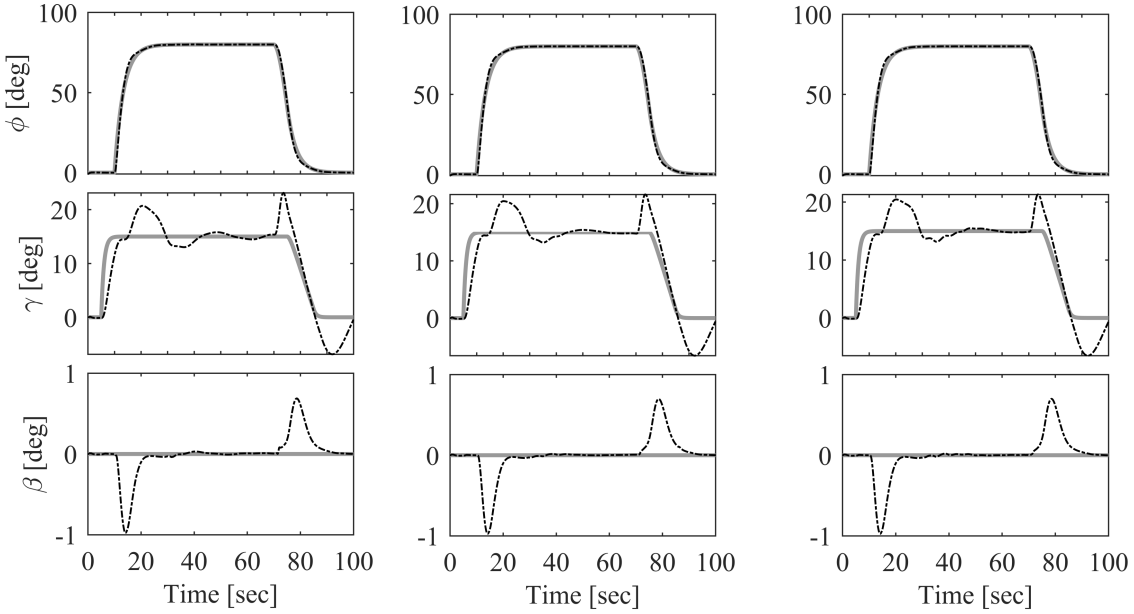

Figure 1.4: Commanded (dot-dashed line) and attained (solid line) control variables of maneuver A with high failure case for INCA (left), Adaptive-INCA (middle) and VSS-Adaptive-INCA (right).

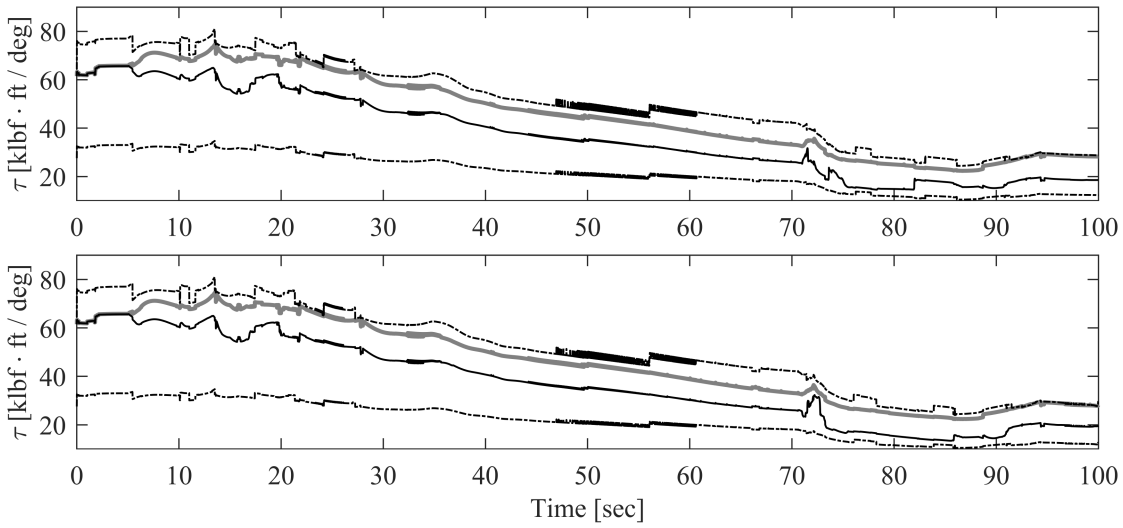

Figure 1.5: Magnitude plot of the CEJ contributions (solid black line) of the Adaptive-INCA (top) and VSS-Adaptive-INCA (bottom) controllers and the original spline (solid grey line), as wel as the ±40% robustness bounds (dot-dashed line) of the INCA controller for maneuver A with medium failure case.

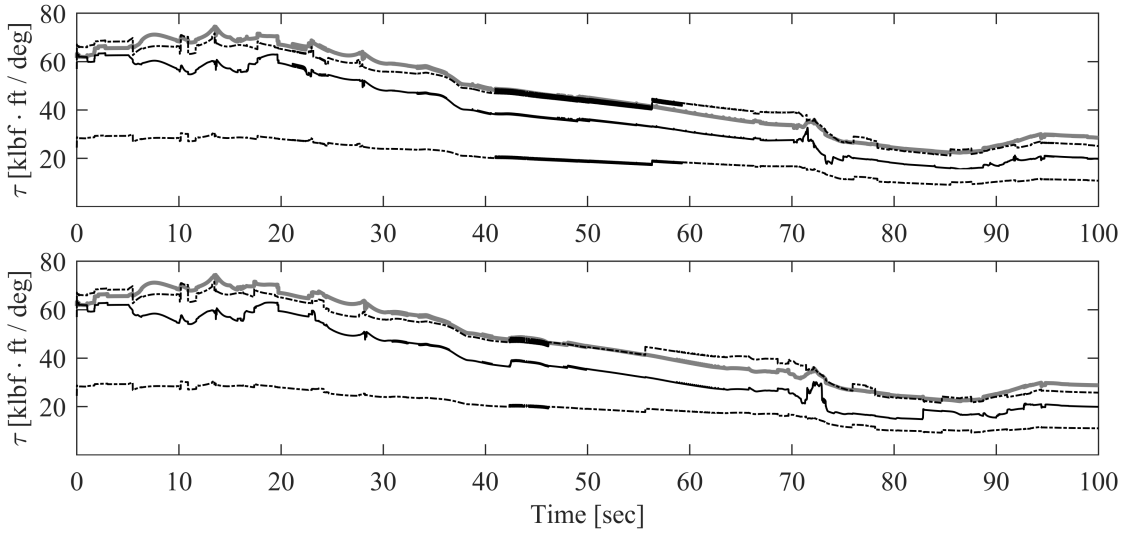

Figure 1.6: Magnitude plot of the CEJ contributions (solid black line) of the Adaptive-INCA (top) and VSS-Adaptive-INCA (bottom) controllers and the original spline (solid grey line), as wel as the ±40% robustness bounds (dot-dashed line) of the INCA controller for maneuver A with high failure case.

2

Maneuver B: Barrel roll

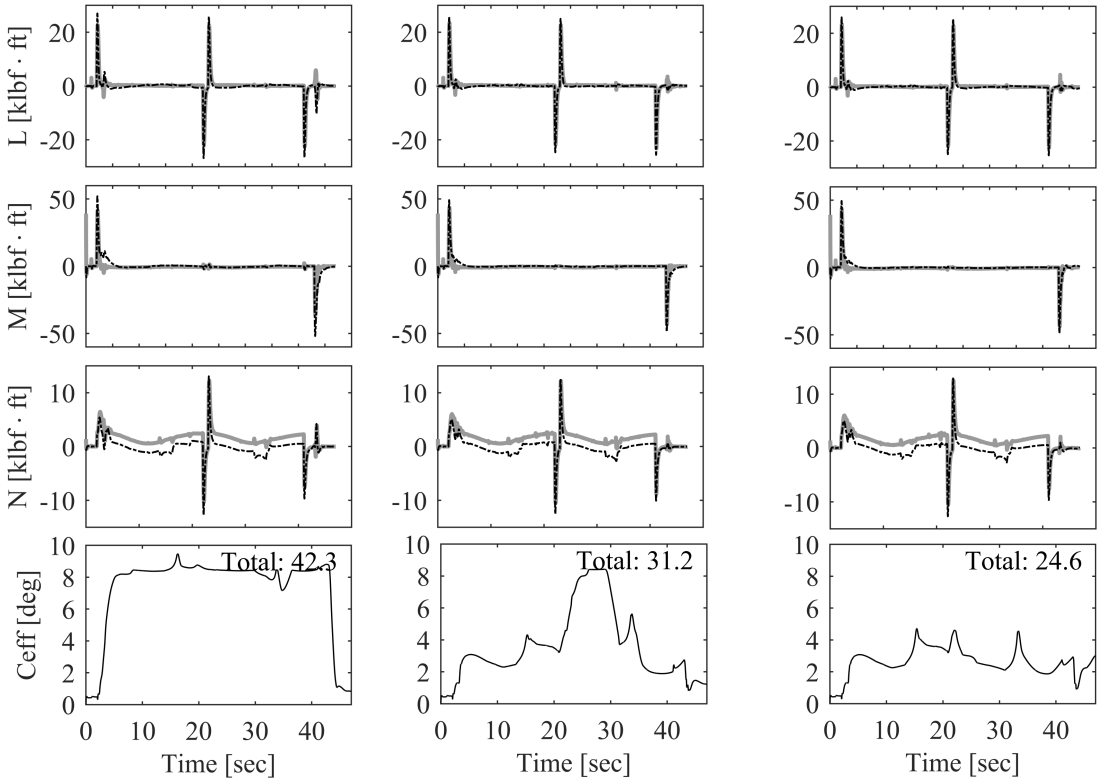

Figure 2.1: Commanded (dot-dashed line) and attained (solid line) control-induced moments and control effort of maneuver B with medium failure case for INCA (left), Adaptive-INCA (middle) and VSS-Adaptive-INCA (right).

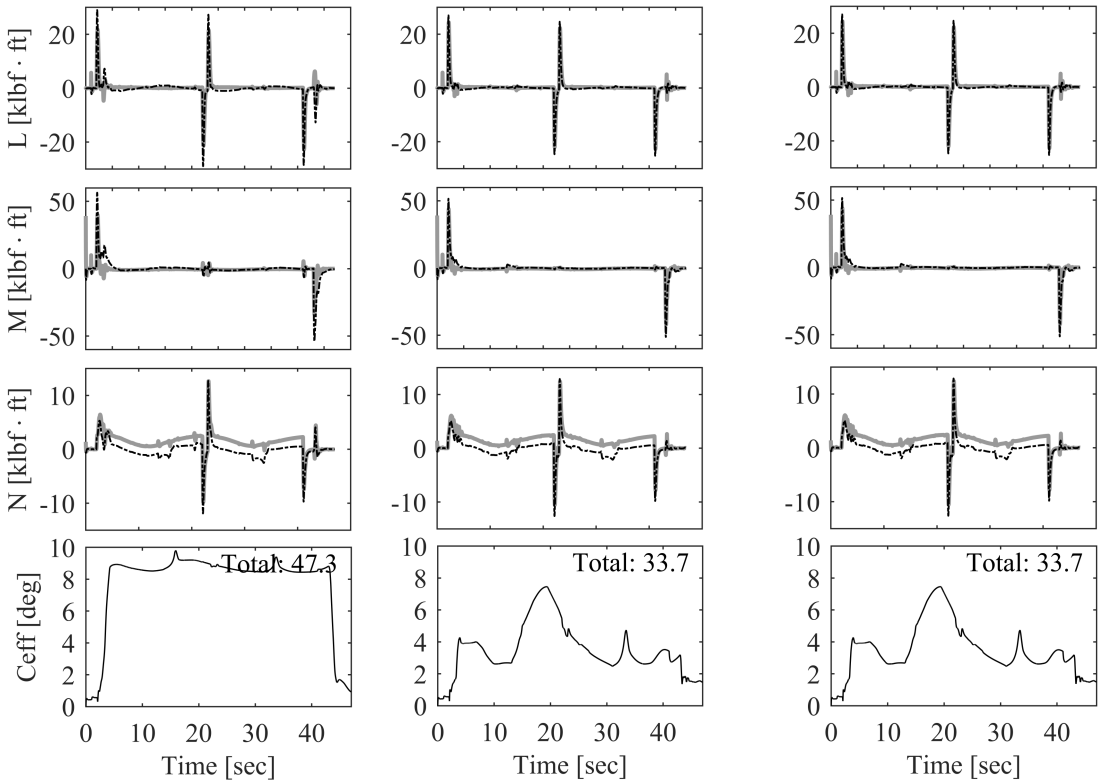

Figure 2.2: Commanded (dot-dashed line) and attained (solid line) control-induced moments and control effort of maneuver B with high failure case for INCA (left), Adaptive-INCA (middle) and VSS-Adaptive-INCA (right).

Table 2.1: Allocation errors for the three controllers for maneuver B.

Controller	INCA		Adaptive-INCA		VSS-Adaptive-INCA	
Failure case	Medium	High	Medium	High	Medium	High
L [klbf · ft]	1.66	2.14	1.15	1.19	1.15	1.19
M [klbf · ft]	3.15	4.15	2.13	2.38	2.05	2.38
N [klbf · ft]	1.72	1.68	1.65	1.60	1.65	1.60
Total	2.28	2.87	1.69	1.79	1.66	1.79

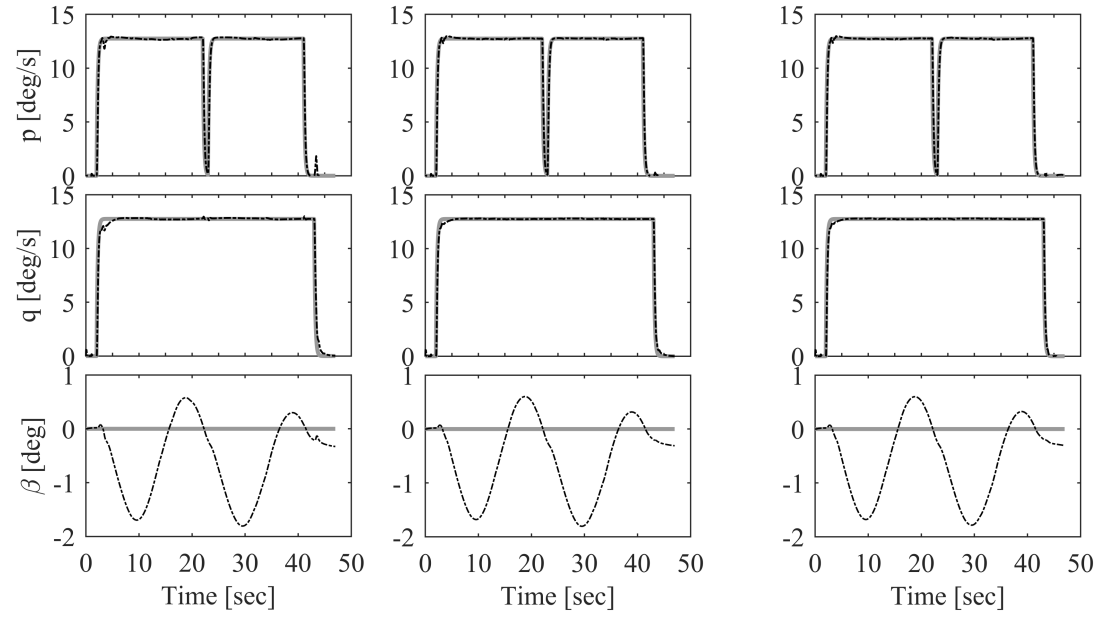

Figure 2.3: Commanded (dot-dashed line) and attained (solid line) control variables of maneuver B with medium failure case for INCA (left), Adaptive-INCA (middle) and VSS-Adaptive-INCA (right).

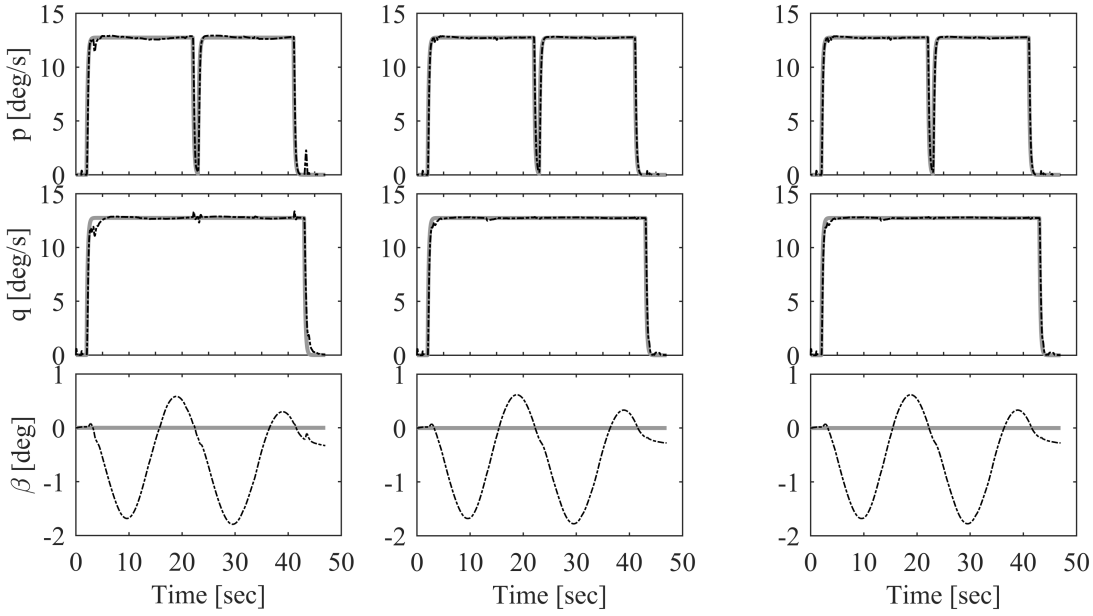

Figure 2.4: Commanded (dot-dashed line) and attained (solid line) control variables of maneuver B with high failure case for INCA (left), Adaptive-INCA (middle) and VSS-Adaptive-INCA (right).

Table 2.2: Tracking errors for the three controllers for maneuver B.

Controller	INCA		Adaptive-INCA		VSS-Adaptive-INCA	
Failure case	Medium	High	Medium	High	Medium	High
p [deg/sec]	0.61	0.68	0.56	0.56	0.57	0.56
q [deg/sec]	0.52	0.60	0.43	0.46	0.43	0.46
r [deg/sec]	0.13	0.12	0.13	0.12	0.13	0.12
Total	0.47	0.53	0.41	0.43	0.42	0.43

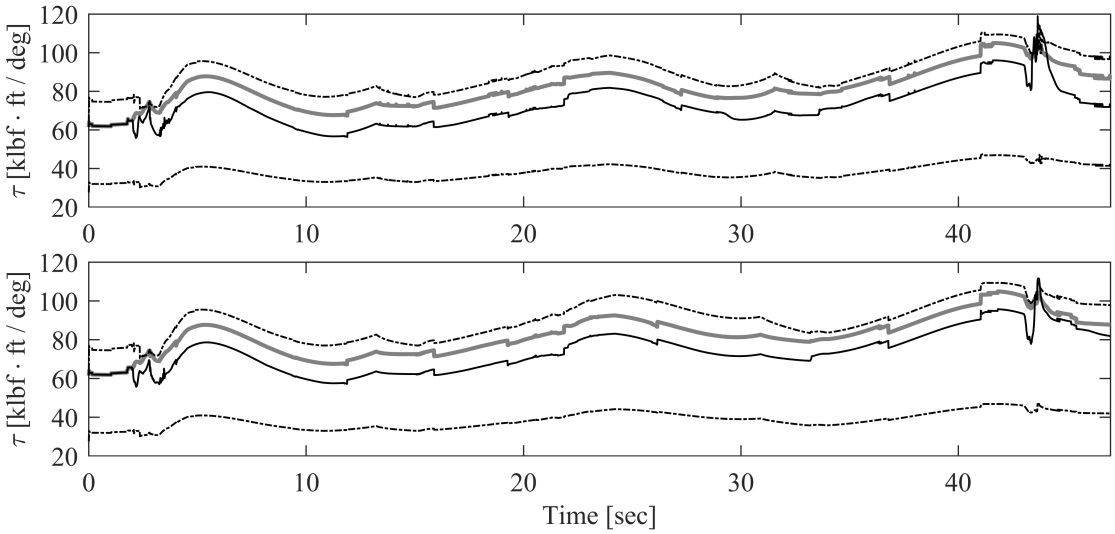

Figure 2.5: Magnitude plot of the CEJ contributions (solid black line) of the Adaptive-INCA (top) and VSS-Adaptive-INCA (bottom) controllers and the original spline (solid grey line), as wel as the ±40% robustness bounds (dot-dashed line) of the INCA controller for maneuver B with medium failure case.

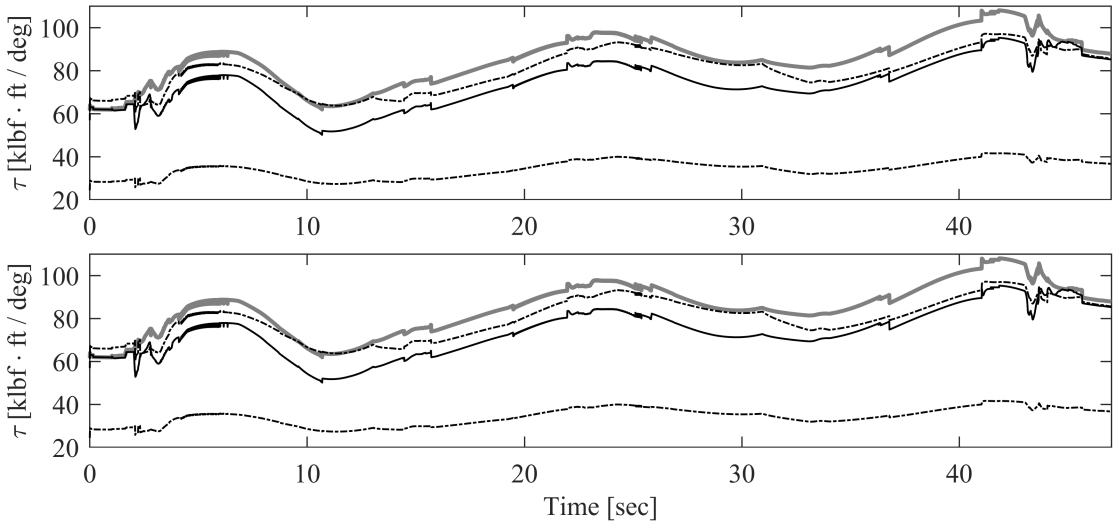

Figure 2.6: Magnitude plot of the CEJ contributions (solid black line) of the Adaptive-INCA (top) and VSS-Adaptive-INCA (bottom) controllers and the original spline (solid grey line), as wel as the ±40% robustness bounds (dot-dashed line) of the INCA controller for maneuver B with high failure case.

3

Maneuver C: Aerobatics sequence

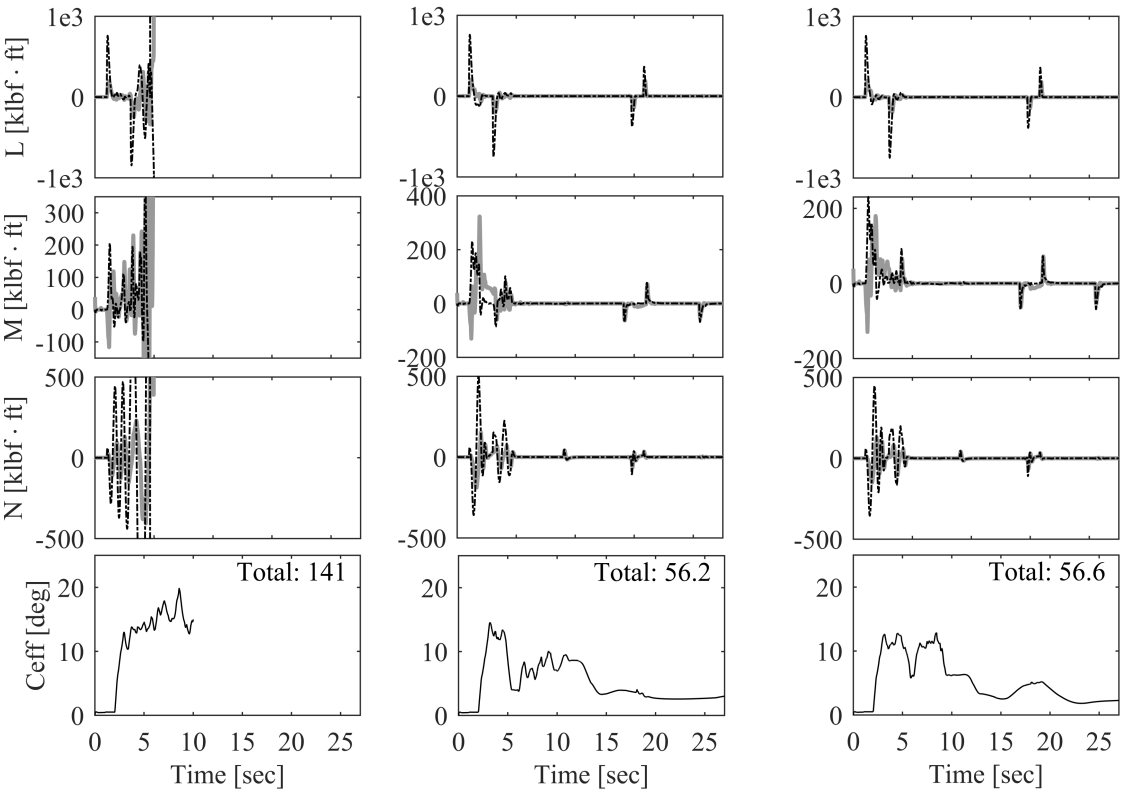

Figure 3.1: Commanded (dot-dashed line) and attained (solid line) control-induced moments and control effort of maneuver C with low failure case for INCA (left), Adaptive-INCA (middle) and VSS-Adaptive-INCA (right).

Table 3.1: Allocation errors for the three controllers for maneuver C.

Controller	INCA*	Adaptive-INCA	VSS-Adaptive-INCA
Failure case	Light	Light	Light
L [klbf · ft]	354	74.9	73.5
M [klbf · ft]	867	38.2	30.3
N [klbf · ft]	1.36E+04	69.0	61.8
Total	7.87E+03	62.8	58.1

* *Unstable trajectory.*

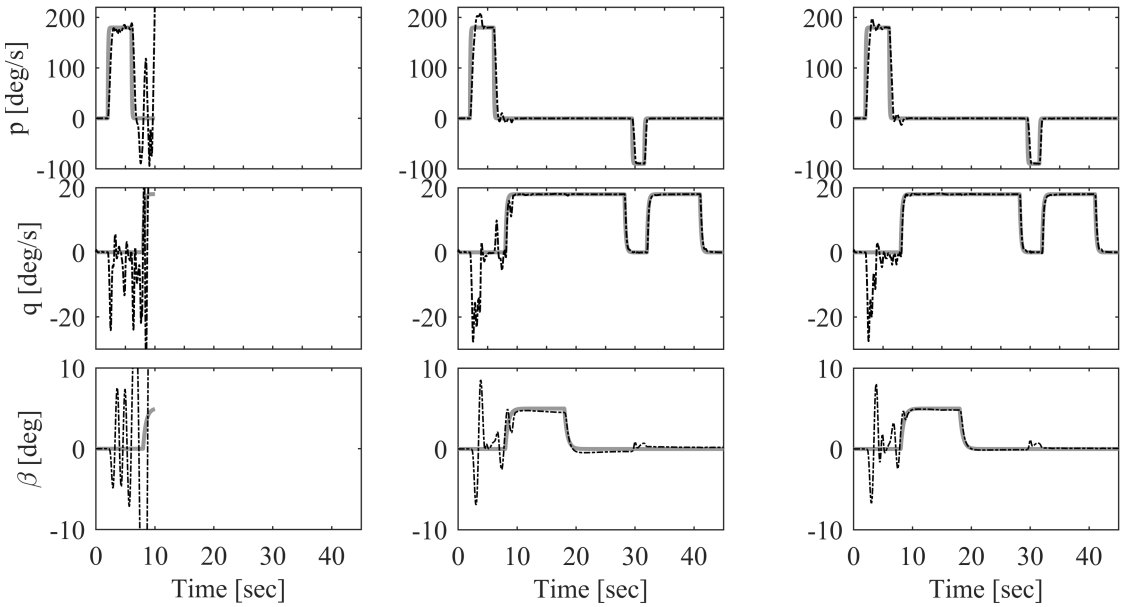

Figure 3.2: Commanded (dot-dashed line) and attained (solid line) control variables of maneuver C with low failure case for INCA (left), Adaptive-INCA (middle) and VSS-Adaptive-INCA (right).

Table 3.2: Tracking errors for the three controllers for maneuver C.

Controller	INCA*	Adaptive-INCA	VSS-Adaptive-INCA
Failure case	Light	Light	Light
p [deg/sec]	60.2	19.6	19.4
q [deg/sec]	48.0	3.87	3.28
r [deg/sec]	922	6.92	6.46
Total	534	12.2	12.0

* *Unstable trajectory.*

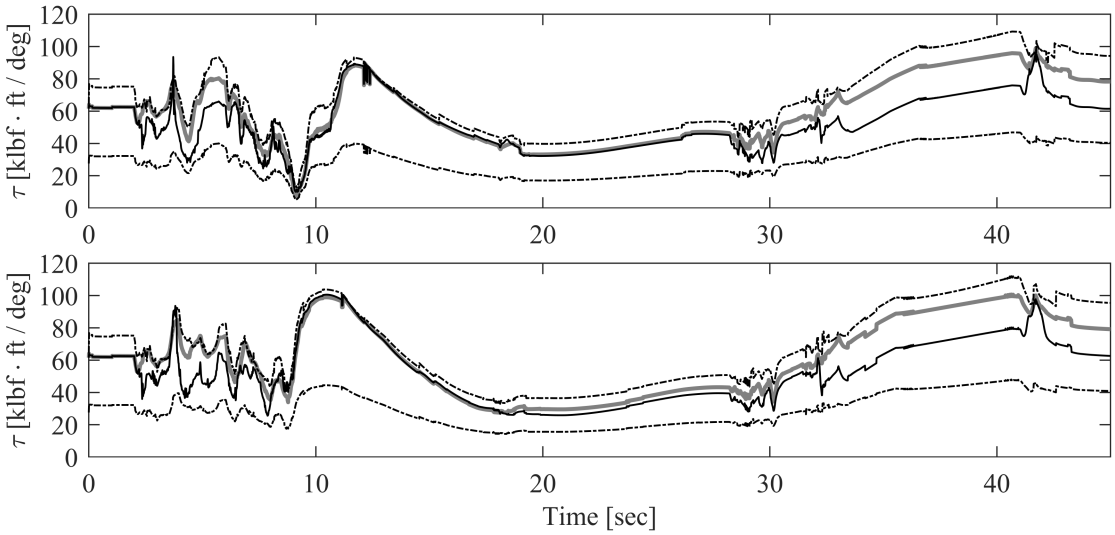

Figure 3.3: Magnitude plot of the CEJ contributions (solid black line) of the Adaptive-INCA (top) and VSS-Adaptive-INCA (bottom) controllers and the original spline (solid grey line), as wel as the ±40% robustness bounds (dot-dashed line) of the INCA controller for maneuver C with light failure case.

4

Maneuver D: High angle of attack and sideslip commands

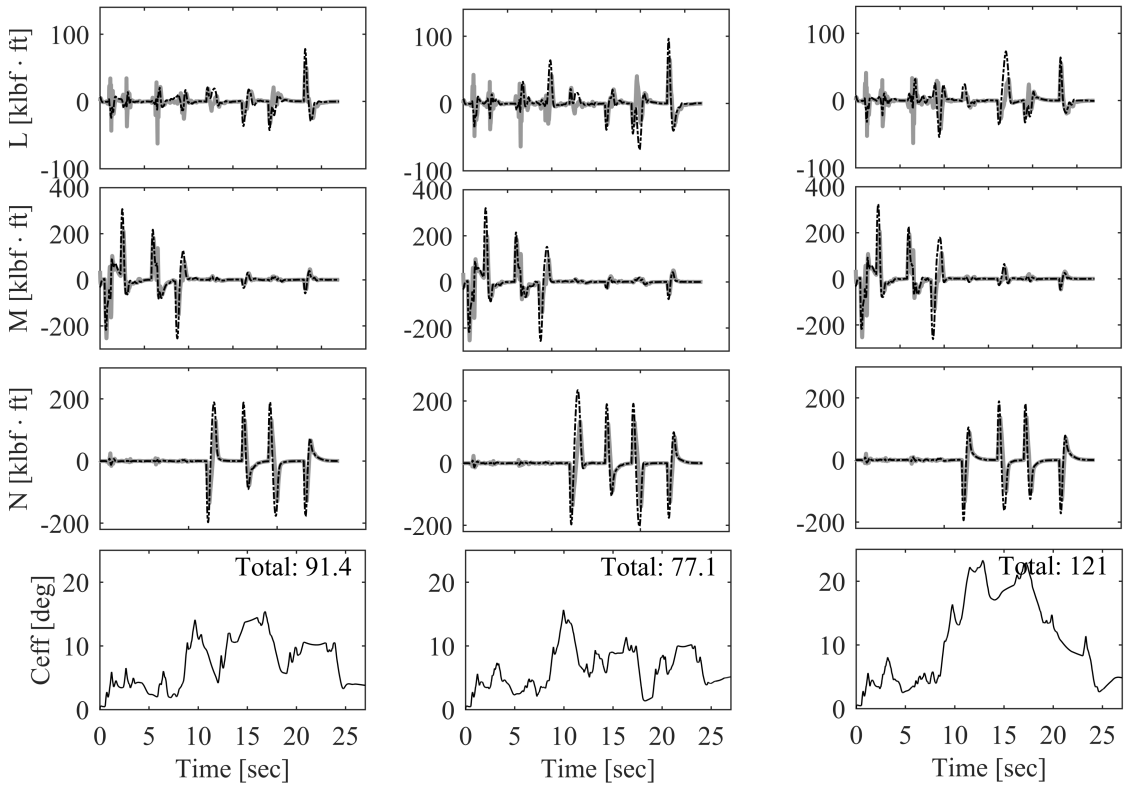

Figure 4.1: Commanded (dot-dashed line) and attained (solid line) control-induced moments of maneuver D with medium failure case for INCA (left), Adaptive-INCA (middle) and VSS-Adaptive-INCA (right).

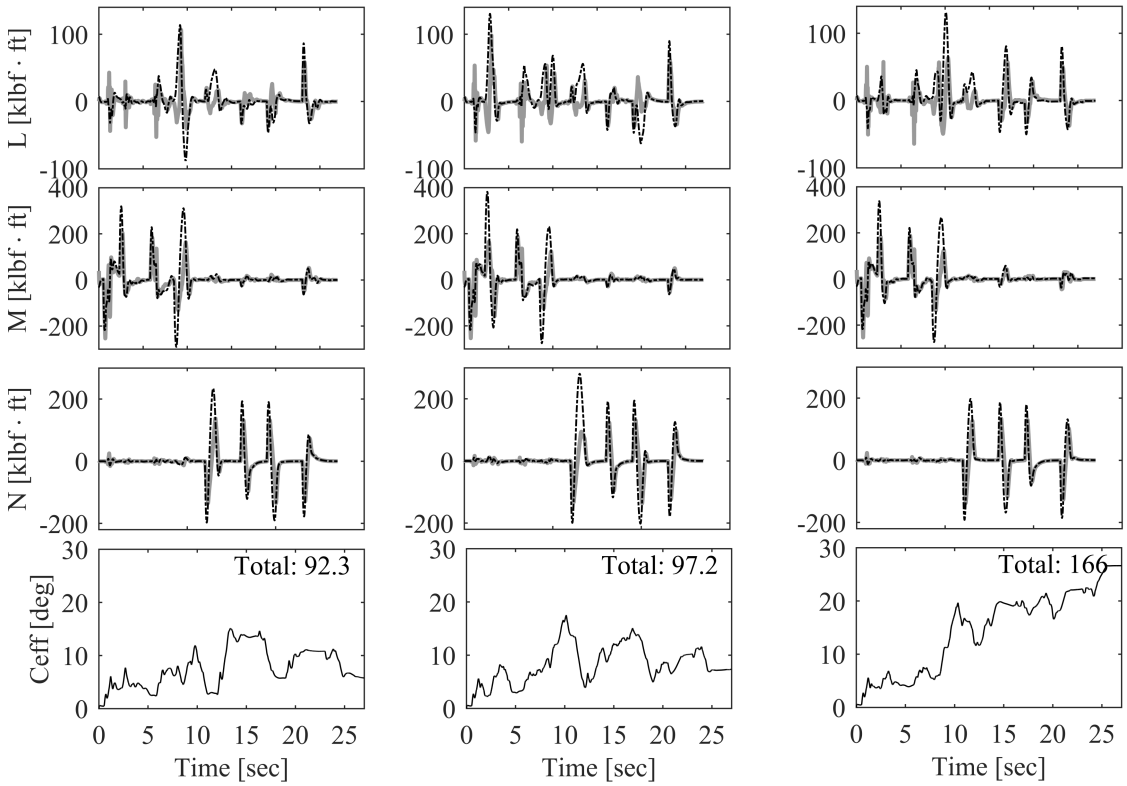

Figure 4.2: Commanded (dot-dashed line) and attained (solid line) control-induced moments and control effort of maneuver D with high failure case for INCA (left), Adaptive-INCA (middle) and VSS-Adaptive-INCA (right).

Table 4.1: Allocation errors for the three controllers for maneuver D.

Controller	INCA		Adaptive-INCA		VSS-Adaptive-INCA	
Failure case	Medium	High	Medium	High	Medium	High
L [klbf · ft]	8.50	20.0	14.6	24.5	13.3	22.7
M [klbf · ft]	29.9	49.2	32.9	50.2	36.3	45.8
N [klbf · ft]	33.9	40.4	40.9	48.4	28.6	35.3
Total	26.6	38.5	31.5	42.7	27.8	35.9

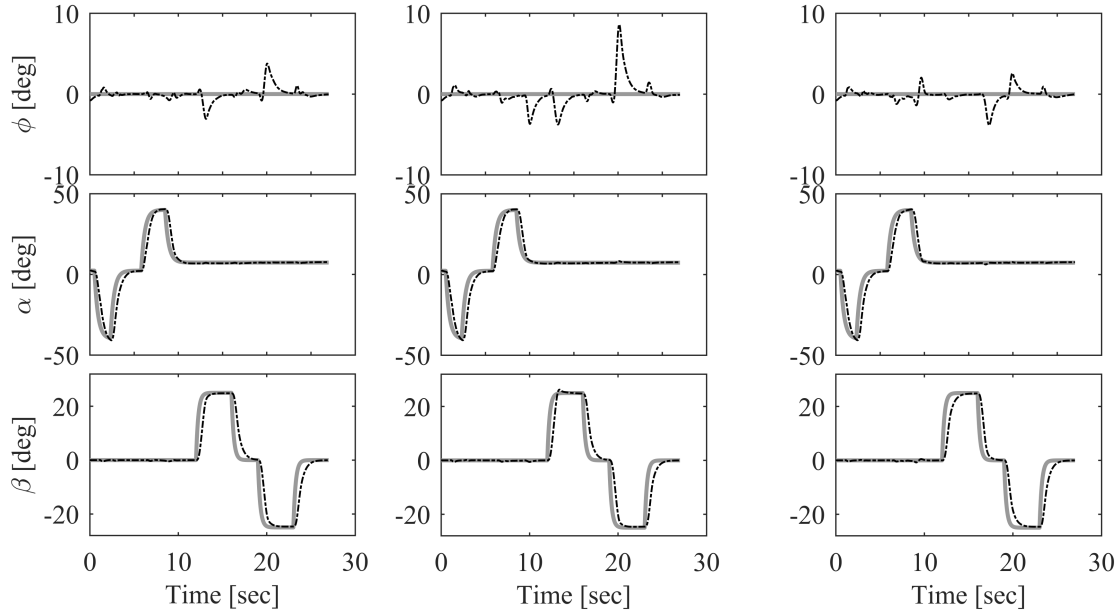

Figure 4.3: Commanded (dot-dashed line) and attained (solid line) control variables of maneuver D with medium failure case for INCA (left), Adaptive-INCA (middle) and VSS-Adaptive-INCA (right).

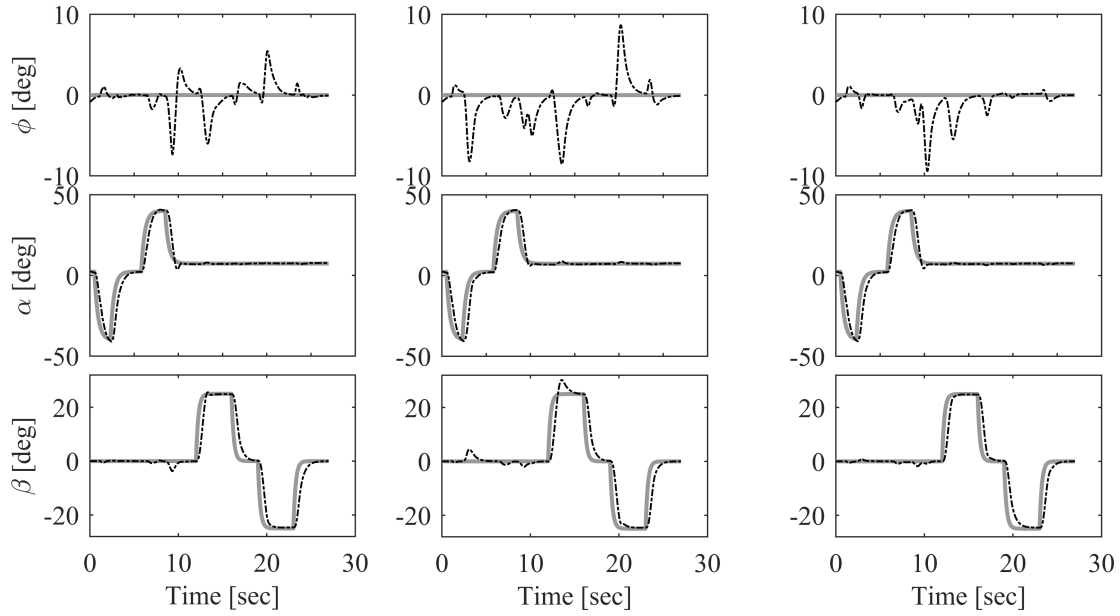

Figure 4.4: Commanded (dot-dashed line) and attained (solid line) control variables of maneuver D with high failure case for INCA (left), Adaptive-INCA (middle) and VSS-Adaptive-INCA (right).

Table 4.2: Tracking errors for the three controllers for maneuver D.

Controller	INCA		Adaptive-INCA		VSS-Adaptive-INCA	
Failure case	Medium	High	Medium	High	Medium	High
ϕ [deg]	0.80	1.72	1.56	2.62	0.80	1.83
α [deg]	5.65	5.80	5.71	5.92	5.72	5.82
β [deg]	4.92	4.91	4.88	5.03	4.85	4.83
Total	4.35	4.50	4.43	4.73	4.35	4.49

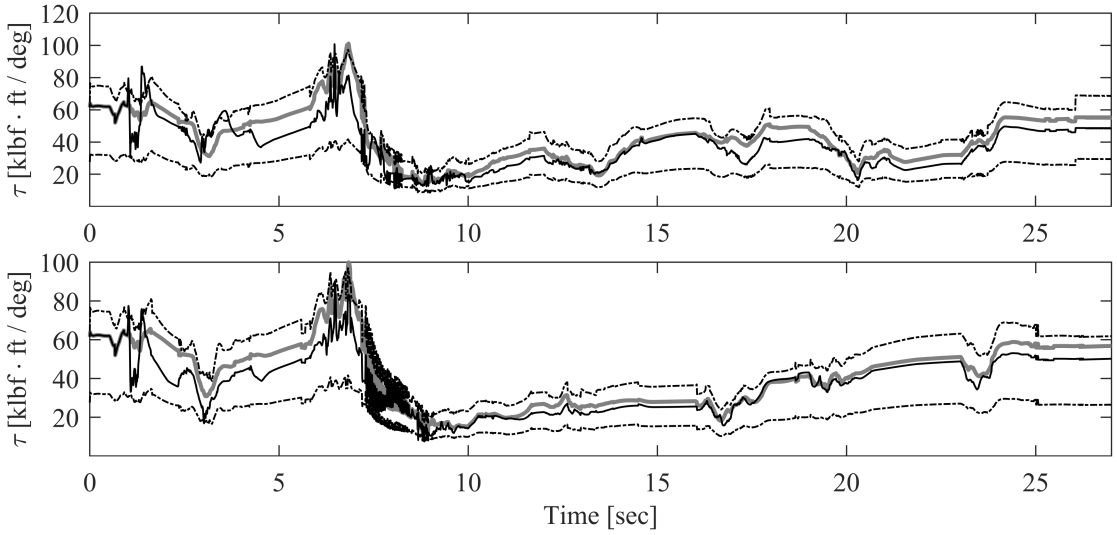

Figure 4.5: Magnitude plot of the CEJ contributions (solid black line) of the Adaptive-INCA (top) and VSS-Adaptive-INCA (bottom) controllers and the original spline (solid grey line), as wel as the ±40% robustness bounds (dot-dashed line) of the INCA controller for maneuver D with medium failure case.

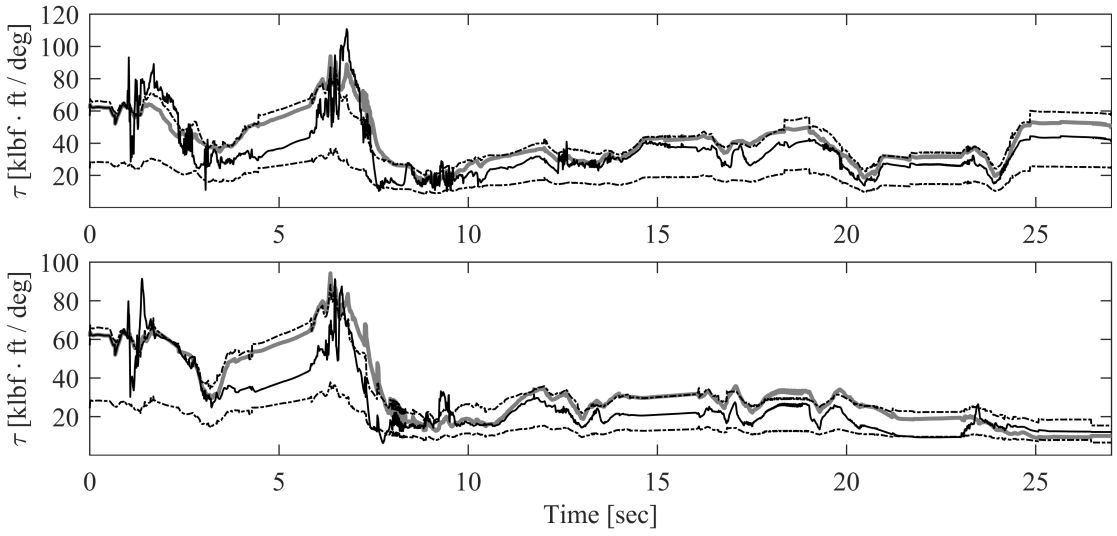

Figure 4.6: Magnitude plot of the CEJ contributions (solid black line) of the Adaptive-INCA (top) and VSS-Adaptive-INCA (bottom) controllers and the original spline (solid grey line), as wel as the ±40% robustness bounds (dot-dashed line) of the INCA controller for maneuver D with high failure case.